# Stretch as a Regulator of Cardiac Contractility: Mechanisms Associated with the Increased Intracellular Calcium Transients

**Xin Shen**

*A thesis submitted in complete fulfilment of the requirements for the degree of Doctor of Philosophy, The University of Auckland, 2014.*

# Abstract

It is well known that stretch is an important regulator of cardiac function, and that an increase in LV diastolic volume increases the subsequent force of contraction. The response to stretch is biphasic, with an initial increase in force that coincides with the stretch attributed to changes in myofilament overlap as well as $Ca^{2+}$ sensitivity. A second phase slowly develops over a period of minutes, known as the slow force response, or SFR, which is accompanied by a concomitant increase in the amplitude of the $Ca^{2+}$ transients. The aim of this thesis was to investigate the mechanisms underlying the SFR. To achieve this, right ventricular trabeculae from adult Wistar rats were used, and measurements of contractile force, intracellular $Ca^{2+}$ and intracellular $pH_i$ were made at a physiological temperature of 37ºC.

Experiments show that the magnitude of the SFR was dependent on the rate of stimulation and $[Ca^{2+}]_o$, such that the stretch response was the greatest at a reduced SR $Ca^{2+}$ content. Furthermore, this study showed, for the first time, that the addition of cross-bridge cycle inhibitors (20 mM BDM or 20 μM blebbistatin) were able to significantly reduce the increased $Ca^{2+}$ transient associated with the SFR. The SFR was blocked by SN-6, a reverse mode $Na^+/Ca^{2+}$-exchange (NCX) inhibitor. Additionally, the SFR was reduced in the presence of $Na^+/H^+$-exchange (NHE) inhibitor HOE642 in $HCO_3^-$-free solutions, but remained unaffected in $HCO_3^-$-buffer solutions. The SFR was increased when $HCO_3^-$ transport was prevented using DIDS. Together, these results suggest a mechanism in which increased metabolic demand from stretch gives rise to increased intracellular $Na^+$ accumulation via NHE and the $Na^+$/ $HCO_3^-$ transporters.

This thesis also explored the possibility of stretch-dependent autocrine/paracrine factors which could contribute to the increased $Ca^{2+}$ transients during the SFR. To do this, a bioassay system was utilised in which the coronary effluent from an 'upstream' stretched, isolated whole heart was collected, and was used to superfuse a separate 'downstream' isolated cardiac trabecula. The 'stretched' coronary effluent exerted a positive inotropic response on the trabecula. Using liquid chromatography-mass spectroscopy (LC/MS), the inotropic factor of interest was identified to be prostaglandin F2α.

# Acknowledgements

First and foremost, I would like to express my sincere gratitude to my supervisor Dr. Marie Ward for providing me the opportunity to undertake this project. The completion of this study would not have been possible without her continued support and guidance throughout the years.

I would like to thank everyone in the Cardiac Functions/Imaging lab for their weekly inputs to my project. In particular, I would like to acknowledge Professor Mark Cannell for his invaluable ideas and solutions whenever I come across a roadblock. Together with Marie, he also helped putting together my first publication as a young scientist, which I am ever so grateful for. I would also like to thank Ms. Vivien Zhang for preparing the coronary effluent samples, and Professor David Greenwood for his help with carrying out LC/MS runs and the subsequent analysis.

This work was made possible with the scholarship provided by the Health Research Council of New Zealand, and I thank them deeply for their generous support. I acknowledge also the financial support of the University of Auckland for travel to a number of international conferences during this project.

Lastly, I would like to thank my loving mother and father for being there when I needed them the most. I love you both very much.

# Table of Contents

# List of Figures

## Chapter 1

# List of Tables

## Chapter 4

# Chapter 1. General Introduction

## 1.1. Chapter Overview

Stretch is an important regulator of normal cardiac function, as well as being implicated as contributing to some pathophysiological conditions such as arrhythmias and the development of hypertrophy. With cardiovascular disease continuing to be the leading cause of mortality world-wide (WHO, 2011), it is imperative to understand the cellular mechanisms that underlie the stretch-mediated responses of the heart.

The contractile response to stretch is biphasic, with an immediate increase in force that coincides with the stretch (the initial inotropic response) that is followed by a more slowly developing phase that occurs over several minutes (the slow force response, or SFR) (Parmley & Chuck, 1973; Allen *et al.*, 1988; Kentish & Wrzosek, 1998; Alvarez *et al.*, 1999; Ward *et al.*, 2008). While the initial inotropic response to stretch has been attributed to the Frank-Starling mechanism, the SFR is known to be associated with an increase in the magnitude of intracellular $Ca^{2+}$ transient. The exact mechanisms underlying the SFR are still being investigated, and will be the focus of my thesis.

The first section of this chapter will provide background information on the structure and function of cardiac myocytes in relation to excitation-contraction (EC) coupling. This will be followed by outlining the Frank-Starling law of the heart. Finally, the last section aims to summarise current proposed mechanisms that are thought to underlie the SFR.

## 1.2. Cardiac Muscle Structure

### 1.2.1. The Cardiac Myocyte

The mammalian heart is a complex, dynamic organ comprised of a number of different cell types including, but not limited to, myocytes, fibroblasts, smooth muscle cells and endothelial cells. Of all of these cell types, myocytes are the fundamental work units of the heart, responsible for the generation of force. Structurally, mammalian cardiac myocytes are frequently described as being 'rod-shaped' following enzymatic isolation, with a relatively conserved length (80-100 µM) to width (10-20 µM) ratio of about 7:1 (Kresh & Chopra, 2011). Individual myocytes are connected with each other through junctional complexes (intercalated discs) which are abundant in gap junctions and desmosomes. Gap junctions facilitate the diffusion of ions between adjacent cells, while desmosomes prevent separation of myocytes during contraction by acting as an anchor. Given this physical and electrical coupling, myocytes form what is known as a syncytium, allowing the heart to contract in a coordinated fashion. Figure 1.1 provides an ultrastructural illustration of cardiac muscle, showing the sarcomeric arrangement that gives myocytes their striated appearance, as well the intercalated discs that connect the individual myocytes.

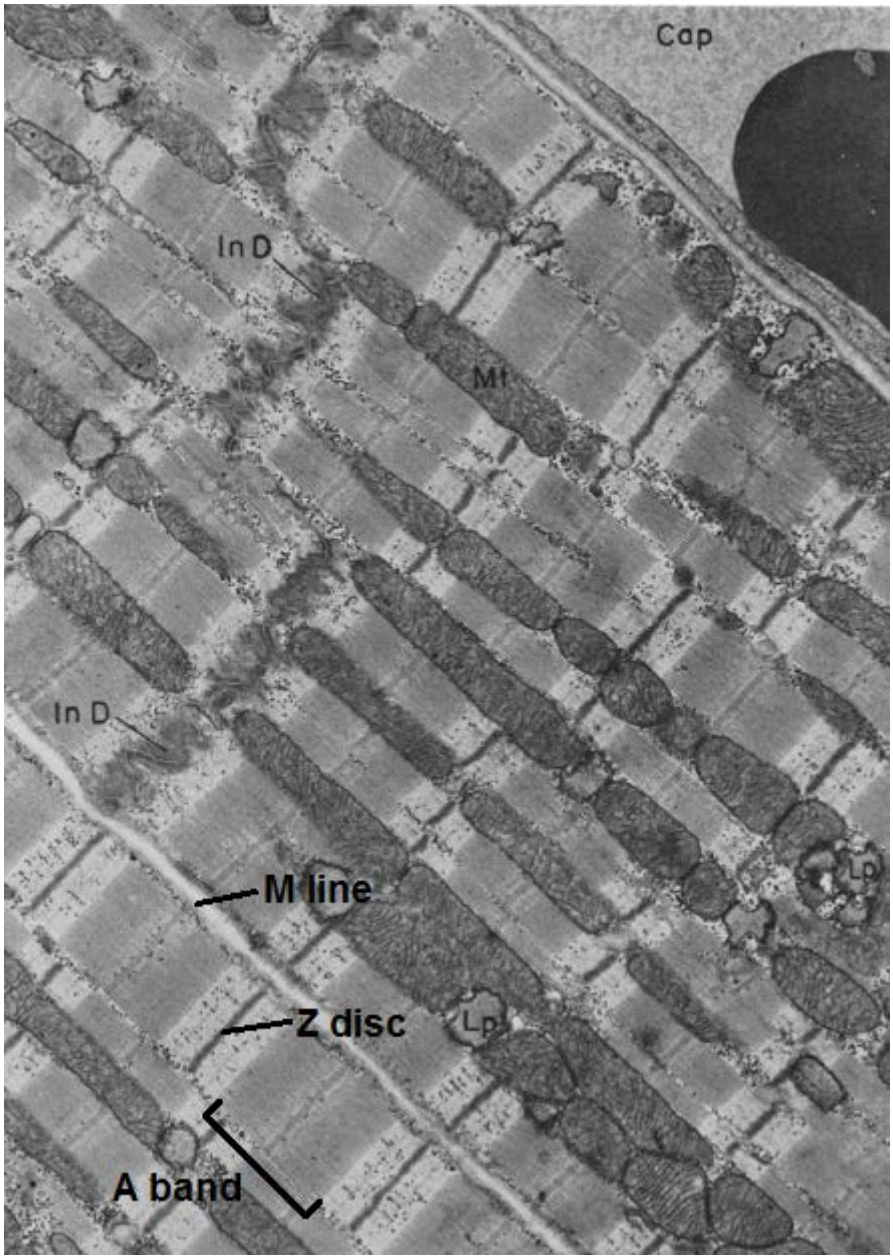


(Fawcett & McNutt, 1969)

Figure 1.1. Electron micrograph of a section of feline ventricular muscle fibres in longitudinal section. The distinct striations are the result of myofibrils being arranged into sarcomeres. Each sarcomere lies between two Z discs, with the M line being in the centre of the A-band. (Mt) represents rows of mitochondria, (Lp) are lipid droplets, while (In D) represents intercalated discs. x 15,000.

### 1.2.2. Transverse Tubules (T-tubules)

The sarcolemma that surrounds mammalian ventricular myocytes is folded into an extensive tubular network known as transverse or "t" -tubules. The t-tubules penetrate deep into muscle fibres, as illustrated in figure 1.2, and account for approximately 30% of the sarcolemma and occur at each Z-line (Brette & Orchard, 2003). In rat myocardium, t-tubules have been shown to occupy as much as 3.6% of the total myocyte volume, with an average reported diameter of around 255 nm (Soeller & Cannell, 1999). Immunohistochemical studies have recorded the localisation of a number key proteins involved in excitation-contraction coupling in the region of t-tubules. These include L-type calcium channels (LTCC), ryanodine receptors (RyR), sodium-calcium exchanger (NCX) and sarco-endoplasmic reticulum calcium ATPase (SERCA) (Brette & Orchard, 2003). From a functional perspective, the presence of the tubular system allows for the rapid propagation of action potentials across the sarcolemma and into the cell (Swift *et al.*, 2006). Electrophysiological studies have shown that a large proportion of the L-type $Ca^{2+}$ current ($I_{Ca}$) (~80%) (Brette & Orchard, 2003) and the NCX $Na^{+}$ current ($I_{Na}$) (~63%) (Despa *et al.*, 2003) occur mostly in t-tubules. For review on the t-tubule system, see (Orchard *et al.*, 2009).

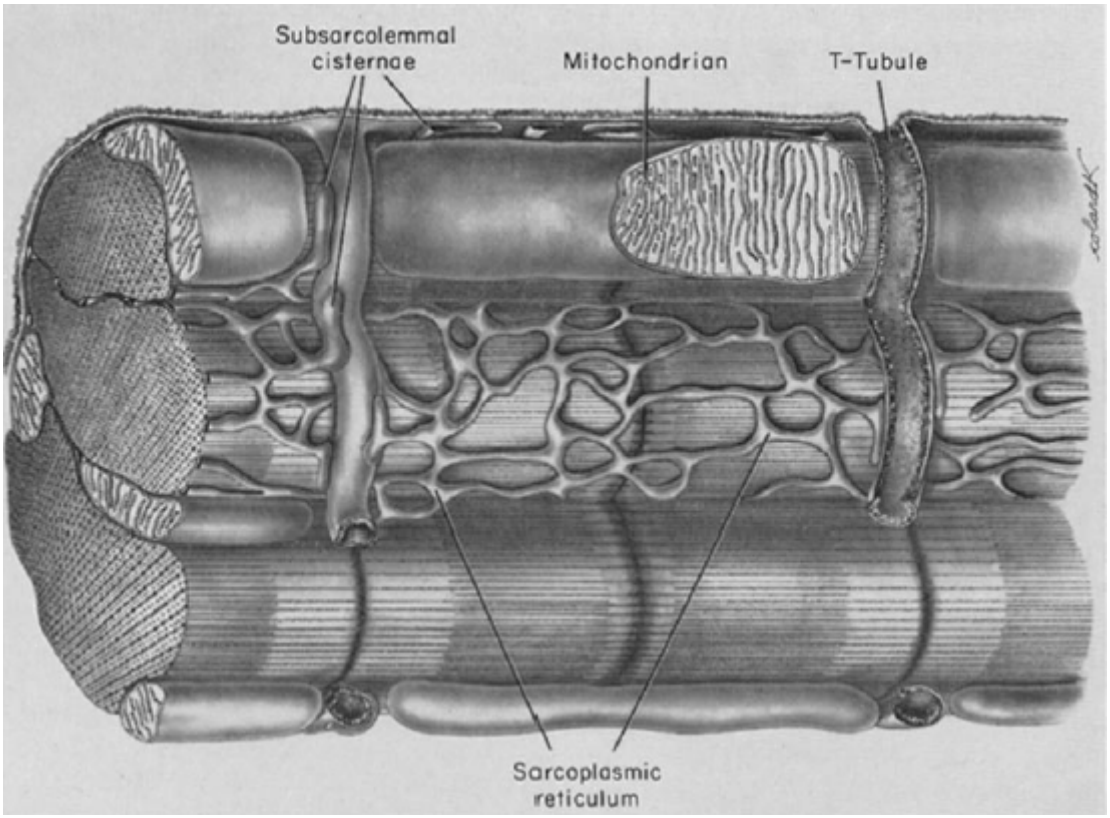


(Fawcett & McNutt, 1969)

Figure 1.2. Illustrative diagram of the transverse tubules (t-tubules), the sarcoplasmic reticulum (SR) and the abundant mitochondria that surrounds the sarcomeres of the mammalian cardiac muscle.

### 1.2.3. The Extracellular Matrix

The extracellular matrix (ECM) is primarily derived from fibroblasts and plays an important part in the maintenance of the overall structural integrity and function of the cardiac muscle. Comprised of fibrous proteins (collagen, elastin), adhesive glycoproteins (fibronectin) and proteogylcans, the ECM provides a physical connection in the form of collagen struts between individual myocytes, as well as linking them to nearby capillaries and nerves to ensure optimal mechanical and electrical coupling (Caulfield *et al.*, 1979). A collection of various focal adhesion proteins including vinculin, talin, α-actinin and dystrophin that make up the connection between the force-generating sarcomeres and the sarcolemma are known as costameres (for review, see (Samarel, 2005)), lying in register with Z-discs (Ervasti, 2003). Figure 1.3 illustrates the position of costameres in relation to Z-discs and the sarcolemma. Functionally, costameres are thought to enable the trans-sarcolemmal transmission of contractile forces in a lateral fashion as a means of ensuring uniform stretch of contiguous cells (Ervasti, 2003).

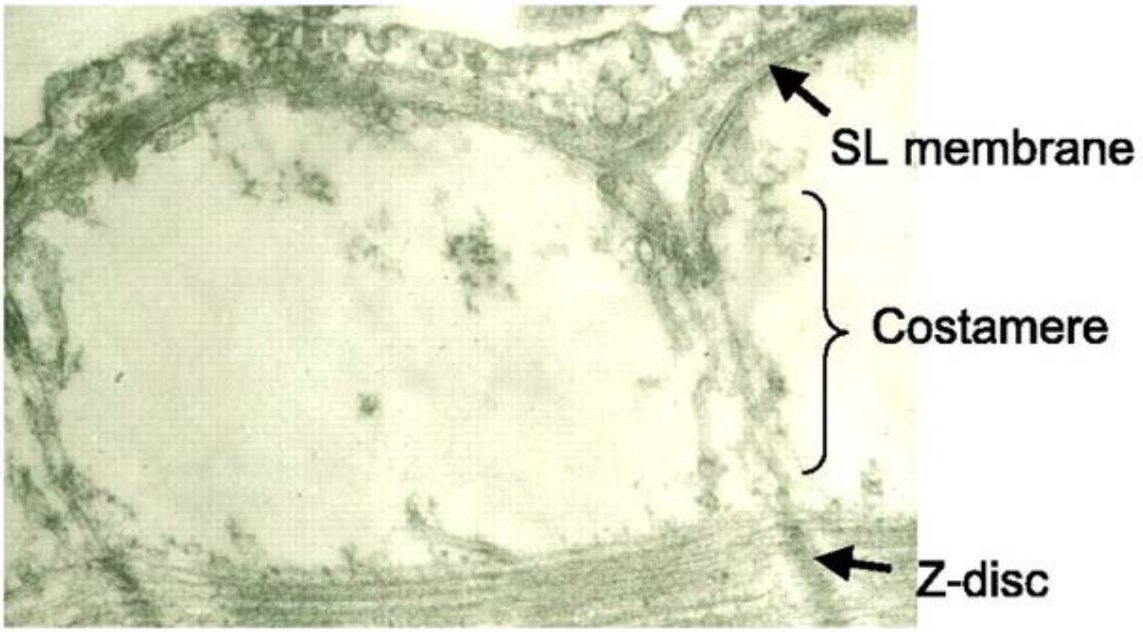


(Samarel, 2005)

Figure 1.3. Structural relationship between the sarcolemma (SL), costamere and Z-disc in the intact ventricular myocardium. Costameres are structurally aligned with the Z-disc, enabling lateral transmission of contractile force across adjacent cells.

The structural linkages between the ECM and the cardiomyocyte cytoskeleton are known as integrins. These integral membrane proteins are comprised of single α- and β-chains, are heterodimeric in structure (Samarel, 2005), and are thought to facilitate the anchoring of myocytes to a common membrane scaffold (Ruoslahti, 1991). Functionally, integrins have been suggested to play an important role in the regulation of mechanotransduction. For example, when the mouse ventricle was subjected to hemodynamic overload, integrin subunits demonstrated altered level of expression that were dependent on the length of the overloading protocol (Babbitt *et al.*, 2002). Additionally, integrins also function as signalling molecules. For example, when integrins bind to ECM proteins, phosphorylation of intracellular targets takes place as a result of activation of kinases including Rho, focal adhesion kinase (FAK) and src kinase (Parker & Ingber, 2007). This subsequently facilitates the transduction of various stretch-mediated signalling cascades which act to promote cell survival and growth (Zamir *et al.*, 2003).

Ultimately, the ECM-integrin-costameric protein complex acts as a highly specialised mechano-sensor which facilitates bidirectional transmission of both externally applied load, as well as intrinsically developed strain.

### 1.2.4. The Endothelium

The entirety of the dense capillary network present in the mammalian myocardium is lined with endothelium. Comprised of endothelial cells, the role of the endothelium has been categorised as being trophic (acting as a selective barrier for metabolites such as glucose and fatty acids), trafficking (governing the passage of leucocytes and macrophages), and tonic (controlling vascular tone through the secretion of various vasodilatory and vasoconstricting peptides such as nitric oxide, NO, and endothelin-1, ET-1, respectively) for review, see (Fishman, 1982; Davidson, 2010). It is well known that the production of NO, an endothelium-derived relaxing factor, increases with increased shear stress on the endothelium (as a result of increased blood flow) (Davies, 1995; Corson *et al.*, 1996; Garcia-Cardena *et al.*, 1998; Balligand *et al.*, 2009). The mechanisms by which NO is produced in response to stretch are less clearly defined, though it could potentially be due to the activation of various mechano-sensing such as cell-ECM adhesion complexes present in the ECM (Balligand *et al.*, 2009). ET-1, another endothelium-derived factor first identified in 1988 by Yanagisawa (Yanagisawa *et al.*, 1988), functions inter-dependently alongside NO in an antagonistic fashion to modulate vascular tone. It has also been reported that ET-1 and its associated receptors are upregulated in response to increased mechanical load as in the case of stretch-induced hypertrophy, (Arai *et al.*, 1995). Given the autocrine/paracrine actions of both NO and ET-1 and their role in mediating stretch-induced responses, the endothelium and its derived factors may contribute to the SFR. The possible involvement of NO and ET-1 on the SFR will be discussed in more detail later in this chapter.

## 1.3. Excitation-Contraction (EC) Coupling

The process which describes the conversion of an electrical stimulus (membrane depolarization) into a mechanical response (muscle contraction) in the myocardium is known as excitation-contraction (EC) coupling, a term first introduced by Alexander Sandow in 1952 (Sandow, 1952). Figure 1.4 provides a diagrammatic overview of EC coupling. Propagation of the cardiac action potential into T-tubules leads to a depolarisation-activated opening of L-type voltage-gated $Ca^{2+}$ channels (LTCC). This in turn gives rise to a small influx of $Ca^{2+}$ as inward $Ca^{2+}$ current, which in turn leads to a much larger $Ca^{2+}$ release from the sarcoplasmic reticulum (SR) via ryanodine receptors, a process better known as $Ca^{2+}$-induced $Ca^{2+}$ release (Endo, 1977; Fabiato, 1983). This increase in intracellular $Ca^{2+}$ binds to the myofilament complex, enables the formation of cross-bridges which ultimately results in the production of force. For relaxation to take place, intracellular $Ca^{2+}$ must unbind from the myofilament complex and be removed from the cytoplasm. This primarily occurs through two pathways, where the unbound $Ca^{2+}$ can either be removed via the Sarco/Endoplasmic Reticulum $Ca^{2+}$-ATPase (SERCA), or be removed via the sarcolemmal $Na^{+}$-$Ca^{2+}$-exchanger (NCX). The remainder of this section will outline a number of key components of the EC coupling process.

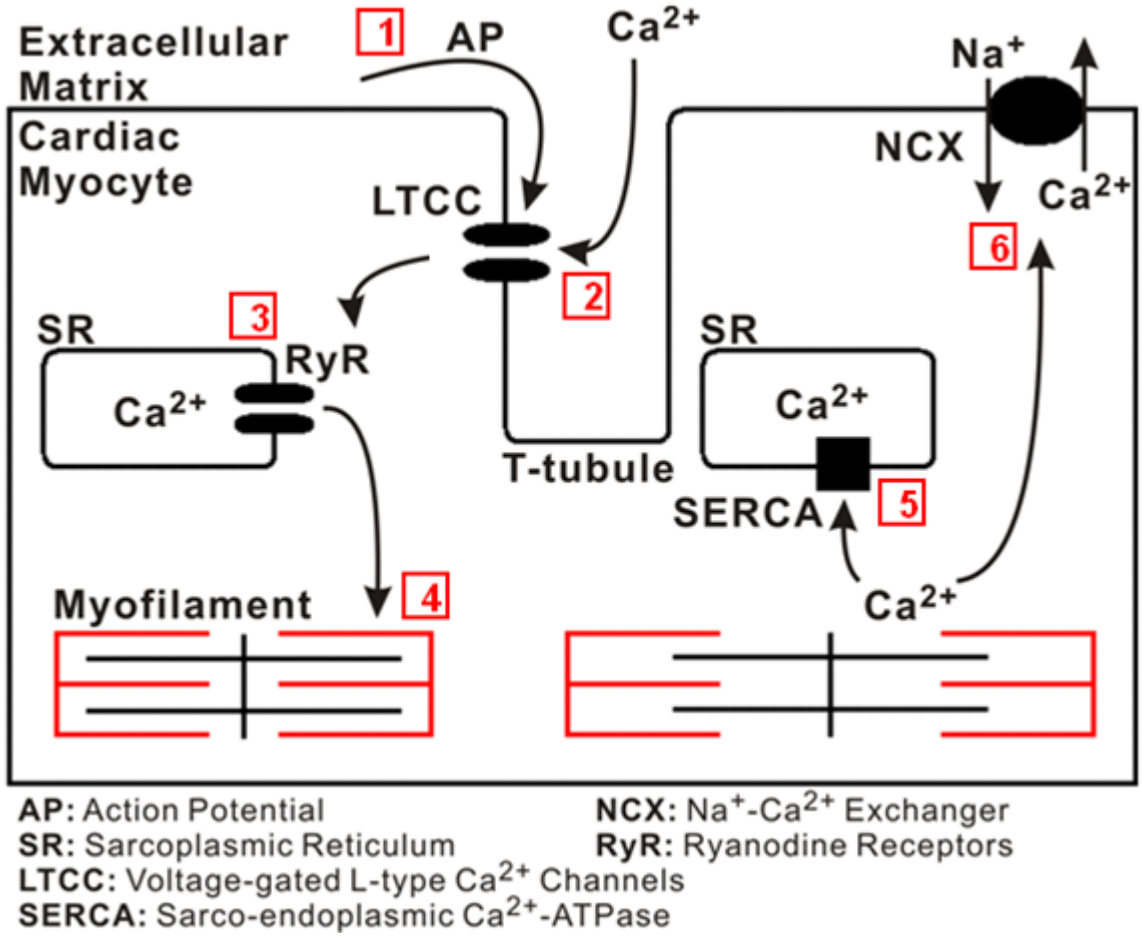


Figure 1.4. Schematic representation of excitation-contraction (EC) coupling in the ventricular cardiac myocyte. Action potential propagates across the cell, triggers an influx of $Ca^{2+}$ through (LTCC) (1) (2). This influx of $Ca^{2+}$ leads to a much larger release of $Ca^{2+}$ from the SR (3). This increase in $Ca^{2+}$ binds to the myofilament complex, results in the generation of force (4). Relaxation occurs when intracellular $Ca^{2+}$ is removed by either SERCA (5), or NCX (6).

### 1.3.1. Ventricular Action Potential

Membrane depolarisation and the propagation of the cardiac action potential (AP) across the cell surface mark the onset of EC coupling. In the intact heart, the AP is first generated by the pacemaker cells located at the sino-atrial (SA) node, which then spreads through the atria, passing through the atrio-ventricular (AV) nodal cells. The AP subsequently propagates further through the bundle of His, down the Purkinje fibres and onto the ventricular myocytes (Katz, 2001). Figure 1.5 shows a typical ventricular action potential and the relative contribution of various ionic currents associated with it. In non-pacemaker cells such as ventricular myocytes, the AP waveform is typically characterised by 5 distinct phases numbered from 0 to 4. Phase 4 is the resting membrane potential at approximately -90 mV. This negative potential is reflective of a high $K^+$ conductance and the resulting $K^+$ current ($I_K$). At phase 0, the arrival of an AP from a neighbouring cell rapidly depolarises the myocyte due to the presence of the inward $Na^+$ current. The opening of these voltage-gated $Na^+$ channels is accompanied by a concomitant reduction in $K^+$ conductance, causing a positive shift in the membrane potential that terminates when $Na^+$ channels inactivates. This brings about early depolarisation or phase 1, which is explained by a fall in $Na^+$ permeability, in conjunction with a rise in a transient outward repolarising $K^+$ current ($I_{to}$) and transient $Ca^{2+}$-activated $Cl^-$ current. Phase 2, or the plateau is unique to the cardiac action potential and determines the duration of the AP. This phase is dependent on the slow inward $Ca^{2+}$ current ($I_{Ca}$) when L-Type $Ca^{2+}$ channels (LTCC) are opened at approximately -40 mV. Phase 3 represents repolarisation carried by delayed rectifier $K^+$ currents, which eventually brings the cell back to its resting membrane potential (Katz, 2001). In the mammalian heart, action potential characteristics have been studied in depth across a number of different species, including pig (Stankovicova *et al.*, 2000), rat (Aimond *et al.*, 1999) mouse (Brunet *et al.*, 2004), canine (Cordeiro *et al.*, 2004) and human (Szabó *et al.*, 2005). Due to the heterogeneous nature of the heart, it is perhaps unsurprising to find regional variations in the mammalian action potential. For example, in the mouse heart, it was shown that $I_{to}$ was significantly higher in myocytes isolated from the right ventricle compared with those isolated from the left ventricle (Brunet *et al.*, 2004). Similarly, regional variations of action potential have also been reported in the rat (Watanabe *et al.*, 1983) and canine (Liu *et al.*, 1993) myocardium, with the general consensus being that this difference is probably due to the differential expression of transient outward $K^+$ currents.

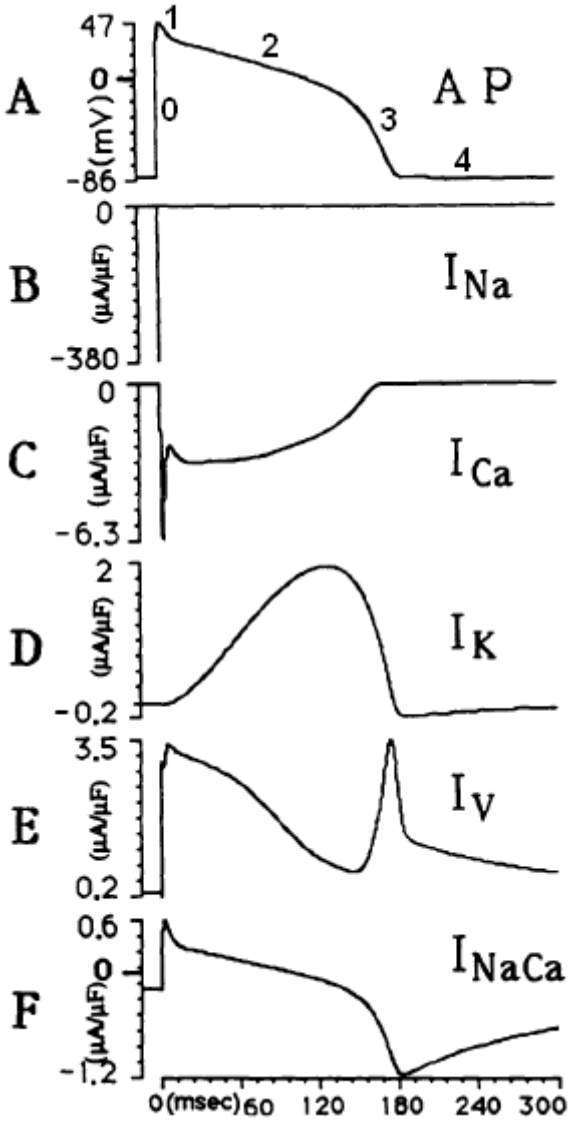


(Luo & Rudy, 1994)

Figure 1.5. Tracings showing a typical cardiac action potential (AP) and major ionic currents associated with it. (A) Four distinct phases (0-4) of an AP. (B-F) Trans-membrane currents during an AP where $I_{Na}$: Inward $Na^+$ current; $I_{Ca}$: Inward L-type $Ca^{2+}$ current; $I_K$ & $I_V$: repolarising $K^+$ currents and $I_{NaCa}$: current through the NCX.

### 1.3.2. Sarcoplasmic Reticulum (SR)

The sarcoplasmic reticulum (SR) is an extensive network of tubules that surrounds the myofilaments and is continuous from one sarcomere to another (Sommer & Johnson, 1970). The principal role of SR is that of an intracellular $Ca^{2+}$ store, responsible for the release and re-uptake of $Ca^{2+}$ during EC coupling. With three disctinct regions, immunofluoresecent and ultrastructural studies have shown that ryanodine receptors, RyR (Specialised intracellular $Ca^{2+}$ release channels) are localised within the corbular and junctional segment of the SR, but not the longitudinal (network) portion (Jorgensen *et al.*, 1993; Franzini-Armstrong *et al.*, 1998). The RyR itself is a large, tetrameric protein with a molecular weight of 565 kDa. They are clustered in close apposition to the LTCC located in the t-tubules, forming what is known as a 'dyad' (Page *et al.*, 1971; Page & Surdyk-Droske, 1979; Orchard & Brette, 2008). Modulation of $Ca^{2+}$ release is managed through complex interactions between RyR and a number of different proteins including calsequestrin, calmodulin, FK-506-binding proteins (FKBP), triadin and junctin (For detailed structural and functional review of these proteins, refer to (Bers, 2004)).

The re-sequestration of $Ca^{2+}$ back into the SR via SERCA is the major pathway in which cytosolic $Ca^{2+}$ is removed. The second major pathway for $Ca^{2+}$ extrusion is out of the cell via NCX. Of the three $Ca^{2+}$-ATPase genes expressed in the sarco- and endoplasmic reticulum (SERCA1, 2 and 3), it is SERCA2a isoform that is present in cardiac muscle (Tada *et al.*, 1998). For every ATP hydrolysed, SERCA pumps 2 $Ca^{2+}$ into the SR, thereby maintaining a substantial $Ca^{2+}$ gradient (approximately 1000 fold) across the SR membrane (Frank *et al.*, 2003). Modulation of SERCA is through its interaction with phospholamban (PLB), a regulatory protein that inhibits SERCA $Ca^{2+}$ uptake in its dephosphorylated state (Orchard & Brette, 2008). Phosphorylation of PLB either by protein kinase A (PKA) or $Ca^{2+}$/calmodulin-dependent protein kinases II (CaMKII) removes its inhibitory effects on SERCA, thereby enhancing $Ca^{2+}$ uptake (Orchard & Brette, 2008).

The extrusion of $Ca^{2+}$ out of the cell is facilitated by NCX, the second of the two major $Ca^{2+}$ removal pathways during relaxation. Molecular studies have identified 3 isoforms of NCX in mammals: NCX1 (Nicoll *et al.*, 1990), NCX2 (Li *et al.*, 1994) and NCX3 (Nicoll *et al.*, 1996), with NCX1 being the most abundantly expressed in the adult mammalian heart. The extrusion of a single $Ca^{2+}$ is electrogenic, driven by the energy acquired from the influx of 3

$Na^+$ (Bers *et al.*, 2003). The NCX can operate in both the forward mode (3 $Na^+$ in, 1 $Ca^{2+}$ out) and the reverse mode (3 $Na^+$ out, 1 $Ca^{2+}$ in). The reversal in the direction of NCX operation depends on the net balance of $[Ca^{2+}]_i$ and $[Na^+]_i$, and given the accepted stoichiometry of 3:1, the reversal potential for NCX is around -40 mV in cardiac myocytes (Bers *et al.*, 2003). With respect to stretch, the NCX plays a pivotal part given the increase in $[Ca^{2+}]_i$ associated with the SFR. This will be discussed in depth later in this chapter.

Together, the overall SR load predominantly depends on the relative contributions of $I_{Ca}$, SERCA and NCX, though sarcolemmal $Ca^{2+}$-ATPase and mitochondrial $Ca^{2+}$ exchange also play a small part (Choi & Eisner, 1999a, b; Orchard & Brette, 2008). It is interesting to note that between different species, there are significant differences in the involvement of SERCA and NCX in the removal of intracellular $Ca^{2+}$. For example, in rabbits, SERCA accounts for approximately 70% of the total $Ca^{2+}$ removal during relaxation, while NCX contributes to around 28%. On the other hand, the bulk (almost 92%) of $Ca^{2+}$ removal in the rat ventricular myocytes is carried out by SERCA, and only 7% are extruded via the NCX (Bers, 2002). This difference has been attributed to the relative difference in the concentration of pump expression (Hove-Madsen & Bers, 1993). Comparison of experimental findings between different species should therefore be treated with certain discretion.

### 1.3.3. Contractile Proteins and the Cross-Bridge Cycle

Cardiac sarcomeres serve to function as the primary force-generating unit of the myocardium. The characteristic array of striations is due to the overlapping arrangement of myofilaments, consisting mostly of thin and thick filaments (Hanson & Huxley, 1953). The thin filament is a double-helical polymer complex containing actin (Hanson & Lowy, 1963), the regulatory complex of troponin (Katz, 1966; Ebashi *et al.*, 1967) and tropomyosin (Bailey, 1946). Figure 1.6 illustrates the spatial arrangement between actin, tropomyosin and the three subunits of troponin. The three subunits of the troponin complex: TnC, TnI and TnT have different roles. TnC serves as a $Ca^{2+}$ sensor and contains binding sites for both $Ca^{2+}$ and $Mg^{2+}$ depending on the contractile state of the cell; TnI inhibits actomyosin ATPase via its linkage with actin, while TnT acts as a structural scaffold that holds the troponin-tropomysin-actin complex together. The thick filaments are largely made up of myosin (MW ~480,000 Da) (Holtzer & Lowey, 1959) that extends from the centre of the sarcomere (M-line) and spans the length of the A-band. The head domain of myosin is known as the cross-bridge that contains binding sites for both actin and adenosine triphosphate (ATP). In addition to myosin, a number of other myosin-associated proteins are found on the thick filament including C, H, X, M proteins as well as the elastic protein titin that contributes to the passive tension in myocytes. (For an extensive structural and functional review, see (Schiaffino & Reggiani, 1996; Gordon *et al.*, 2000)).

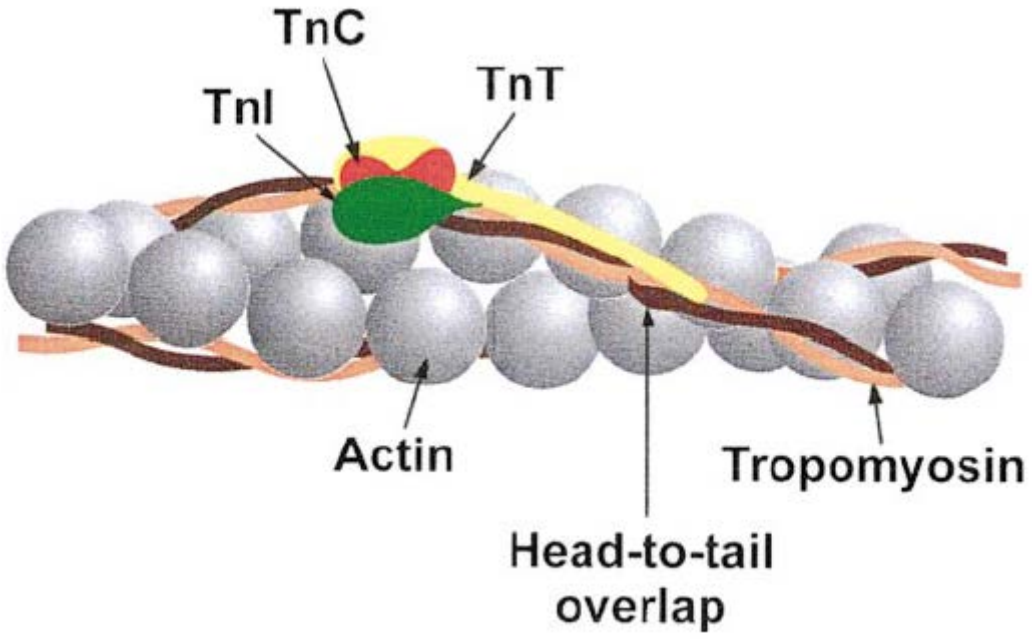


(Gordon *et al.*, 2000)

Figure 1.6. Schematic representation of the spatial orientation between actin, troponin (TnI, TnC and TnT) and tropomyosin. Polymerisation of globular actin, G-actin, forms the helical filamentous F-actin.

The cross-bridge cycle describes the conversion of mechanical energy from chemical energy stored in the form of ATP. Importantly, it underlies what is known as the sliding filament theory which describes the contraction of muscle (Huxley & Niedergerke, 1954; Huxley & Hanson, 1954). At rest, the myofilaments are tightly bound, where the troponin (Tn)-tropomyosin (Tm) complex prevents the binding of myosin heads to their respective binding sites on actin. Following membrane depolarisation, $Ca^{2+}$ released from the SR binds to TnC, inducing a conformational change in the Tn-Tm complex which in turn alleviates the physical blockade between actin and myosin. When ATP binds to the myosin head, myosin dissociates from actin. Hydrolysis of ATP subsequently takes place in order to provide energy for muscle contraction, though hydrolysis products adenosine diphosphate (ADP) and inorganic phosphate ($P_i$) remain bound to myosin. As a result, formation of actin-myosin cross-bridges takes place, and is accompanied by the release of previously hydrolysed product ($P_i$), initiating what is known as a power stroke and leading to the production of force. Figure 1.7 provides an illustration of the above steps.

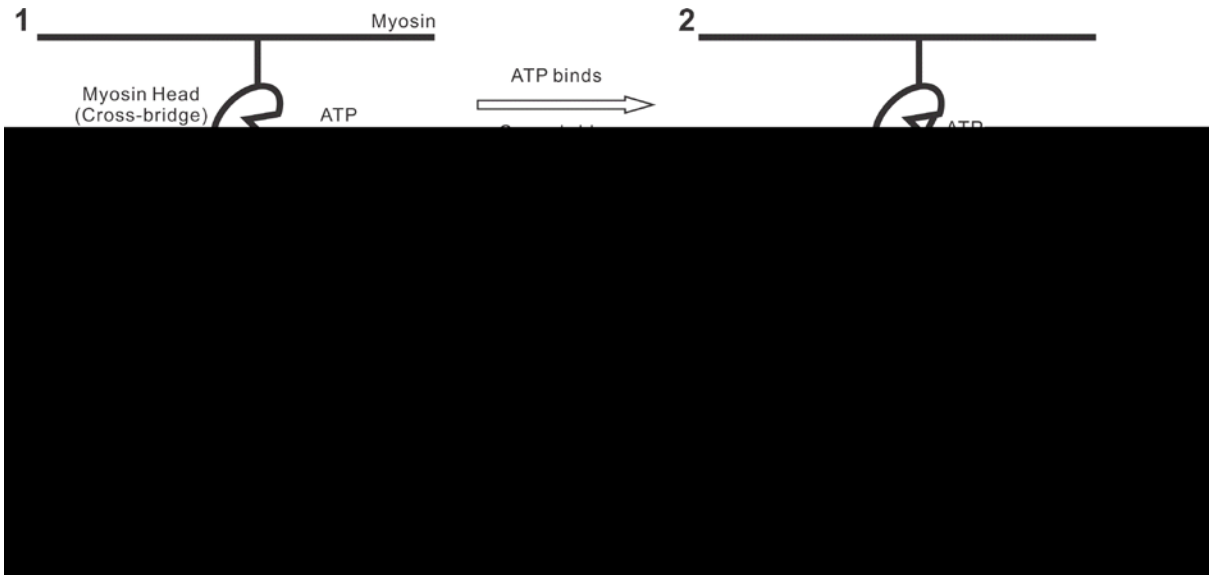


Figure 1.7. A simplified schematic diagram of the cardiac cross-bridge cycle. (1) Cross-bridge is tightly bound in a rigor state to actin. (2) When ATP binds to its binding site on the cross-bridge, myosin dissociates from actin. (3) Hydrolysis of ATP into ADP and $P_i$ follows, causing the cross-bridge to shift along, rebinding to a new actin molecule. (4) The release of $P_i$ initiates the power stroke, causing a conformational change to the cross-bridge, pushing the actin filament towards the M line. (1) Finally, the release of ADP from the ATP binding site returns the cross-bridge to its tightly bound state.

## 1.4. Frank-Starling Mechanism

Near the end of the 19th Century, Otto Frank showed a proportional relationship between the developed pressure and the end-diastolic volume in the frog ventricle contracting at constant volume (Frank, 1895). Later, Ernest Starling observed a related response in which an increase in venous return increased the subsequent cardiac output at a fixed aortic pressure (Patterson & Starling, 1914). Collectively, these two observations have been termed the Frank-Starling mechanism, which describes that under physiological conditions, the proportion of blood pumped into the systemic circulation (as a result of increased force of contraction), is directly dependent on the amount of blood returned to the heart (increased stretch of the myocardium).

Needless to say, the importance of the Frank-Starling mechanism paved the way for decades of extensive investigation into its mechanism. To date, a number of isolated preparations have all been demonstrated to exhibit the Frank-Starling mechanism, including papillary muscles (Parmley & Chuck, 1973), trabeculae (Keurs *et al.*, 1980) and myocytes (Le Guennec *et al.*, 1990). The 'problem' with a cardiac twitch, is that it rapidly rises, then quickly falls, coupled with the fact that the duration of a twitch varies with muscle length (Allen & Kurihara, 1982*a*), this made it very challenging to investigate the steady-state tension at a given external $Ca^{2+}$ concentration. To get around this issue, muscle samples were chemically permeabilised such that experimenters were able to observe the length-tension relationship in an environment where external $Ca^{2+}$ concentration could be precisely controlled. The first of these experiments was done by Fabiato and Fabiato (Fabiato & Fabiato, 1975; 1978), to which they concluded that myofilament overlap alone cannot wholly account for the length-tension relationship. In addition to myofilament overlap, other 'activating' factors such as the binding of $Ca^{2+}$ to the myofilament during contraction could also contribute toward the length-tension relationship. Hibberd and Jewell (Hibberd & Jewell, 1982) showed in permeabilised rat ventricular trabeculae, that the concentration of extracellular $Ca^{2+}$ required to generate half maximal force was lower at longer sarcomere length, suggesting a length-dependent change in the myofilament sensitivity. Indeed, when Allen and Kurihara (Allen & Kurihara, 1982*a*) used aequorin as a measure of intracellular $[Ca^{2+}]$, they found no change in the amplitude of the $Ca^{2+}$ transient when isolated myocytes were subjected to a rapid change in length.

Though it is clear that both physical and activating factors contribute to the length-dependent activation, the underlying mechanism is still being actively investigated. One theory revolves around the fact that when a cardiac cell is subjected to longitudinal stretch, it becomes narrower. This decreases the lattice spacing between the thick and thin filaments, which in turn could increase the binding probability of myosin heads to actin during cross-bridge cycling. McDonald and Moss (McDonald & Moss, 1995) tested this idea in skinned cardiac myocytes immersed in 2.5% dextran as means of compressing the myofilament without altering the sarcomere length. They showed that at short sarcomere length and in the presence of dextran, there was an increase in myofilament sensitivity to levels that was similar to what they observed at long sarcomere length. Interestingly, when Konhilas *et al.* (Konhilas *et al.*, 2002) directly measured the lattice spacing using synchrotron x-ray diffraction, they concluded that $Ca^{2+}$ sensitivity did not significantly change even when up to 6% dextran was applied. Taken together, this suggests that the Frank-Starling mechanism occurs independently of any changes in $Ca^{2+}$ transient. Titin, a large protein that extends from the Z disc toward the M line is traditionally known for its role in maintaining passive tension in sarcomeres. More importantly, it has been shown to contribute to the Frank-Starling mechanism. For example, Lee *et al.* (2010) showed that when the N2B spring element of Titin was genetically knocked out in mouse, there was a subsequent increase in myofilament sensitivity across different sarcomere lengths. For further review of the Frank-Starling mechanism, see (Allen & Kentish, 1985; de Tombe *et al.*, 2010; Campbell, 2011).

## 1.5. The Slow Force Response to Myocardial Stretch

In 1973, experiments by Parmley and Chuck demonstrated a distinct biphasic force response when the isolated cardiac muscle was stretched (Parmley & Chuck, 1973). On stretch, there is an immediate increase in active force (the initial inotropic response –IIR), which accounted for the Frank-Starling mechanism. This was followed by a secondary, slower increase in force over a period of several minutes, typically known now as the "slow force response" (SFR). As evident in figure 1.8, the IIR occurs independent of any changes in the amplitude to the $Ca^{2+}$ transient, while the SFR is associated with an increase in the amplitude of the $Ca^{2+}$ transient. Although the exact mechanism(s) underlying the SFR is yet to be identified, the following section looks at a number of proposed theories that could explain the stretch-mediated phenomenon. In particular, the role of stretch-activated channels, angiotensin II-mediated pathways and the effects of nitric oxide.

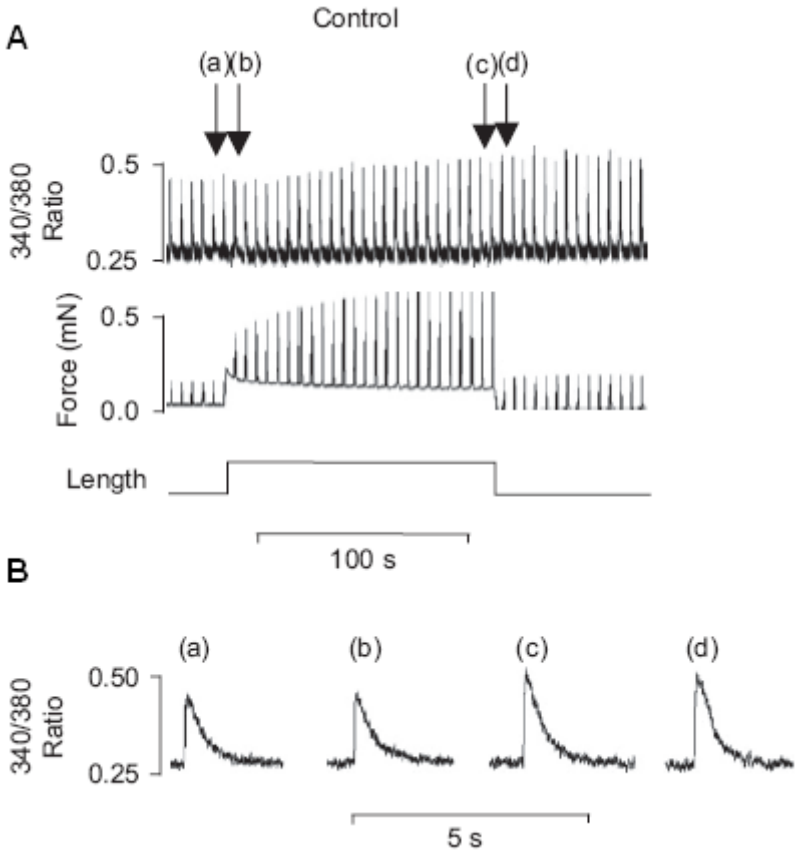


(Ward *et al.*, 2008)

Figure 1.8. The slow force response (SFR) to stretch in an isolated mouse trabecula. A step increase in the length of the preparation leads to an initial, rapid increase in force. This is followed by a much slower, secondary increase in force, known as the SFR. Note the increase in the amplitude of the $Ca^{2+}$ transient (340/380 ratio) during the SFR (from (b) to (c)).

### 1.5.1. Contribution of Non-Selective Stretch-Activated Cation Channels ($SAC_{NSC}$)

Stretch-activated channels act as signal transducing mediators, enabling the transduction of the mechanical stretch into intracellular chemical responses. These mechanosensitive channels exhibits direct non-selective cation conduction, at a reversal potential around -12 to 0 mV (Kamkin *et al.*, 2003). The increase in the magnitude of $Ca^{2+}$ transient that occurs in parallel with the SFR may be due to the direct conduction of $Ca^{2+}$ via these channels, or it may be that the accumulation of intracellular $Na^{+}$ and the subsequent activation of the NCX underlie the aforementioned phenomenon. One recent study demonstrated that, in the rat atrial myocyte, the stretch-activated currents (SAC) primarily consisted of $Na^{+}$, since the inclusion of $Ca^{2+}$ influx produced little effect on the magnitude of the resulting $Ca^{2+}$ transient (Youm *et al.*, 2006). In light of these findings, investigations are underway in search of non-selective, stretch-activated cation channels ($SAC_{NSC}$) which may contribute to the stretch-activated currents. Through liposome reconstitution and patch clamp evaluation, Maroto and colleagues identified a specific channel better known as the transient receptor potential canonical channels, subfamily C, member 1 (TRPC1) which appeared to be a potential candidate for the stretch-activated channels (Maroto *et al.*, 2005). Pharmacologically, Bowman *et al.* (2007) was able to successfully inhibit the SAC by using a specific toxin, GxMTx-4, giving support to the theory that TRPC1 may in fact be accountable for the SAC. In a similar fashion, a number of reports have also identified that a separate isoform, TRPC6, is likely to contribute to the SFR (Spassova *et al.*, 2006).

Currently, there are a number of conflicting reports regarding the potential role of SACs in the development of the SFR. For example, the application of gadolinium, $Gd^{3+}$, failed to block the SFR in rabbit or failing human myocardium (Lewinski *et al.*, 2003; Lewinski *et al.*, 2004). On the other hand, the SFR was found to be significantly reduced in both rat myocytes and intact papillary muscles in the presence of streptomycin (White, 2004). This difference has mostly been attributed to the non-specific nature of the pharmacological inhibitors used (White, 2004; Ward *et al.*, 2008). Recently, Ward *et al.* (2008) demonstrated that not only did both streptomycin and $Gd^{3+}$ reduced the magnitude of the SFR as shown in Figure 1.9, but the application of a more specific inhibitor GxMTx-4 almost completely abolished the SFR. In the same study, immunohistological evidence showed that both TRPC1 and TRPC6 were expressed in mouse ventricles, and that they may be located in close proximity with the T-

tubules (Ward *et al.*, 2008). Together, these results implicate $SAC_{NSC}$ as being one of the potential components in the development of SFR.

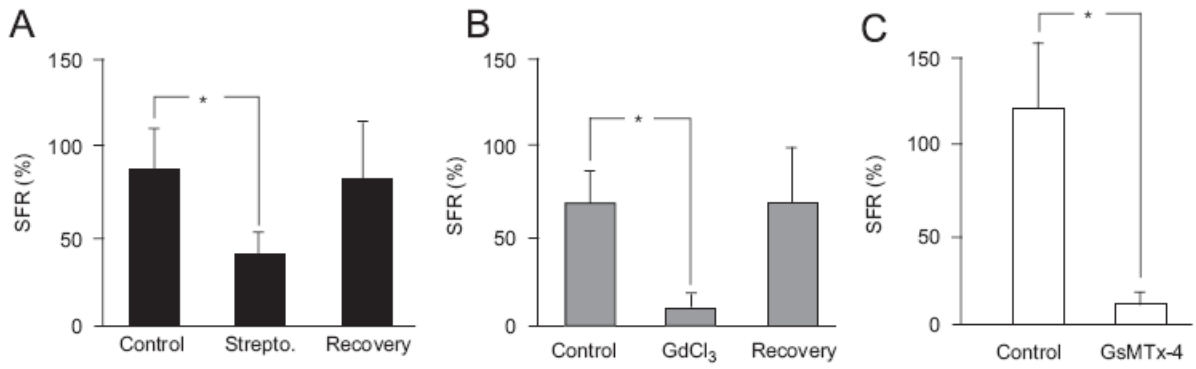


(Ward *et al.*, 2008)

Figure 1.9. The effect of three SAC inhibitors on the SFR to stretch in mouse ventricular trabeculae. A. 400 µM of streptomycin. B. 20 µM of gadolinium chloride. C. 10 µM of GsMTx-4. * indicates a statistic significance of $p < 0.05$.

### 1.5.2. Contribution of Ang II-Mediated Autocrine/Paracrine Pathway

The $Na^+$-$H^+$ exchanger (NHE-1) is a sarcolemmal antiporter protein responsible for the active extrusion of $H^+$ from the cell in exchange for $Na^+$ with a stoichiometric ratio of 1 to 1. For decades, it has been known that cellular acidosis drastically reduces myocardial contractility through mechanisms which are thought to involve calcium delivery as well as myofilament sensitivity to calcium (Orchard & Kentish, 1990). Conversely, when the NHE-1 is stimulated, one would expect an increase in myocardial contractility due to increased intracellular pH. Moreover, the stimulation of NHE-1 must also enhance intracellular $Na^+$ accumulation. This in turn could increase $Na^+/Ca^{2+}$ exchanger activity, leading to an net increase in intracellular $Ca^{2+}$ (Kentish, 1999). As a consequence, the involvement of NHE-1 in the development of the SFR has been extensively investigated.

The mechanism by which myocardial stretch induces NHE-1 activation is presumed to be dependent on local autocrine/paracrine regulation, in particular, the intracardiac renin-angiotensin and the endothelin systems (Kentish, 1999). The exact signal transduction mechanism contributing to stretch-induced Ang II release is not clear, but it could involve integrins as well as various sarcolemmal proteins. Integrins are cell surface receptors that interact with the extracellular matrix (ECM) and the cytoskeleton at regions known as focal adhesion sites (Ruwhof & Laarse, 2000). It is known that in cardiac fibroblasts, stretch-induced signalling cascades behave in an integrin-dependent manner (Ruwhof & Laarse, 2000). It is thought that the deformation of cardiomyocytes is initially perceived by integrins and that this mechanical stress is subsequently transduced into corresponding signals via cytoskeletal (actin microfilaments) reorganisation via a number of intermediate molecules such as α-actinin, talin, vinculin, paxillin, and tensin (Ruwhof & van der Laarse, 2000). Furthermore, integrins may directly influence gene transcription due to sarcomere rearrangement of the desmin-laminin network which may be associated with chromatin (Ruwhof & van der Laarse, 2000). Lastly, the direct modification to the sarcolemma due to mechanical stress can potentially alter the functions of the embedded sarcolemmal proteins such as protein kinase C, which in turn could result in the activation of 'immediate-early' genes such as c-fos in myocardial cells (Ruwhof & van der Laarse, 2000). Interestingly, this activation occurs on a similar time scale as the development of the SFR, indicating a correlation between the two (Kentish, 1999).

Following the initial transduction process, Ang II is formed and proceeds to mediate the production of ET-1. Based on the assumption that NHE-1 activation contributes to the SFR, studies have shown that the pharmacological blockade of either angiotensin receptor type 1 (AT1) or endothelin receptor type A ($ET_A$) in the rat and feline myocardium resulted in significant diminution of the SFR (Alvarez *et al.*, 1999; Pérez *et al.*, 2001). Interestingly, when similar blockade was used in the rabbit (Lewinski *et al.*, 2003), ferret (Calaghan & White, 2001) or the failing human myocardium (Lewinski *et al.*, 2004), the SFR was not notably different than the control protocols, suggesting that the mechanism underlying NHE-1 activation may fundamentally be species-dependent. The order of communication has also been pharmacologically confirmed by a number of studies, whereby the application of exogenous ET-1 in the presence of AT1 blocker failed to abolish the SFR (Pérez *et al.*, 2003), but when $ET_A$ was blocked and Ang II added, the magnitude of the SFR was significantly reduced (Pérez *et al.*, 2003), suggesting that Ang II formation must in some ways be a prerequisite for the subsequent actions of ET-1. Originally, it was hypothesised that the stretch-induced formation of Ang II would facilitate the direct release of pre-formed ET-1 from cardiomyocytes (Yamazaki *et al.*, 1996). However, when endothelin-converting enzyme (ECE), an enzyme responsible for the catalytic formation of ET-1 from 'big' ET-1, was inhibited, the subsequent SFR was almost completely abolished (Pérez *et al.*, 2001). This suggests that the primary source of ET-1 could be attributable to the activation of ECE, which is mediated by Ang II.

Currently, the final sequence in this chain of events leading up to the activation of NHE-1 appears to be dependent on the Ang II/ET-1-mediated formation of reactive oxygen species (ROS). The mechanism of ROS formation is believed to operate in a 'ROS-induced-ROS-release' manner, whereby a small amount of intracellular ROS generates a much larger ROS release from the mitochondria (Kimura *et al.*, 2005). In the context of NHE-1 activation, studies have demonstrated that Ang II and the subsequent formation of ET-1 is capable of activating the sarcolemmal enzyme NADPH oxidase (NOX), which results in the production of a small amount of superoxide radical ($\cdot O_2^-$) (Kimura *et al.*, 2005; Caldiz *et al.*, 2007). This in turn leads to a substantial release of mitochondrial $\cdot O_2^-$ via the mitochondrial ATP-sensitive potassium ($mK_{ATP}$) channels, which may ultimately be responsible for the activation of NHE-1 and the subsequent development of the SFR (Caldiz *et al.*, 2007). More accurately, it is the dismutated product of $\cdot O_2^-$, hydrogen peroxide ($H_2O_2$), that facilitates NHE-1 activation, given that NOX-generated $\cdot O_2^-$ is highly unstable and potentially lethal (Caldiz *et*

*al.*, 2007). In the myocardium, the dismutation of $\cdot O_2^-$ to $H_2O_2$ is catalysed by the enzyme superoxide dismutase (SOD), which exists both extracellularly as a membrane bound protein as well as intracellularly as cytoplasmic and mitochondrial isoforms (Caldiz *et al.*, 2007). Although the exact molecular mechanism by which $H_2O_2$ activates NHE-1 remains to be elucidated, it is likely to involve the phosphorylation of the carboxyl tail of the NHE-1 mediated by various kinases (Rothstein *et al.*, 2002). For example, $H_2O_2$ leads to the activation of ERK kinase (MEK), which in turn activates the extracellular signal-regulated kinase 1/2 (ERK1/2). This in turn facilitates the formation of $p90^{rsk}$ which ultimately results in the phosphorylation of $Ser^{703}$ residue in the cytosolic tail of NHE-1 (Rothstein *et al.*, 2002). There is recent evidence to suggest that the transactivation of epidermal growth factor receptor (EGFR) is required for Ang II-mediated cardiac hypertrophy (Kagiyama *et al.*, 2002; Zhai *et al.*, 2006). Villa-abrille *et al.* (2010) demonstrated that in the presence of EGFR inhibitors, the resulting SFR as well as Ang II/ ET-1 mediated increase in $\cdot O_2^-$ were abolished. The same group of researchers also confirmed a potential cross interaction between Ang II and mineralcorticoid receptors (MR), as SFR was completely blocked when the rat papillary muscles were pre-incubated with the MR inhibitor, eplerenone (Caldiz *et al.*, 2011). The following flow diagram summarises the cascade discussed this far:

**Stretch → Transactivation of EGFR/MR → Ang II → ET-1 → H2O2 synthesis → NHE-1 activation**

The activation of NHE-1 results in two potential pathways which may be associated with the development of the SFR: either by increasing intracellular pH or by enhancing intracellular $Na^+$ accumulation (Alvarez *et al.*, 1999). Although an increase in pH may partly account for the SFR, a growing body of evidence suggests that, under physiological conditions, it is the enhanced cellular $Na^+$ accumulation and the subsequent activity of the NCX which contributes to the aforementioned phenomenon. First, one study demonstrated that the consequent rise in pH due to NHE-1 activation is counteracted by the activation of a bicarbonate ($HCO_3$)-dependent acid loading mechanism, such that the extrusion of $H^+$ is matched by a parallel efflux of $HCO_3$ from the cell (Cingolani *et al.*, 2003). This compensatory mechanism is probably facilitated by the $Na^+$-independent $Cl^-$-$HCO_3^-$ exchanger (AE3c and AE3fl in the cardiac muscle), given that its inhibition in a bicarbonate-

free condition failed to recover the increased pH upon NHE-1 activation (Cingolani *et al.*, 2003). However, under certain pathophysiological conditions where the acid loading mechanism is compromised or when the cellular concentration of $HCO_3$ is greatly reduced, the NHE-1-mediated increase in pH can become the predominant contributing factor in the development of the SFR (Cingolani *et al.*, 2003). The NCX is a membrane exchanger protein that can function either in a forward (3 $Na^+$ in, 1 $Ca^{2+}$ out) or a reverse (3 $Na^+$ out, 1 $Ca^{2+}$ in) mode (Pitts, 1979; Kimura *et al.*, 1986; Crespo *et al.*, 1990), and has been implicated in the development of the SFR in the rat (Alvarez *et al.*, 1999), feline (Perez *et al.*, 2001), rabbit (von Lewinski *et al.*, 2003) as well as the failing human myocardium (Lewinski *et al.*, 2004). In essence, the accumulation of $Na^+$ is thought to thermodynamically favour the NCX to operate in the reverse mode (Blaustein & Lederer, 1999). The NCX in turn actively exchanges the elevated $Na^+$ for $Ca^{2+}$, which may ultimately underlie the $Ca^{2+}$ transient associated with the SFR. Indeed, Selective inhibition of the NCX in reverse mode with KB-R7943 was able to significantly reduce the SFR upon stretching the myocardium (Lewinski *et al.*, 2003). Additionally, when intracellular $Na^+$ was raised via the inhibition of the $Na^+$-$K^+$-ATPase, the magnitude of the SFR was significantly increased (von Lewinski *et al.*, 2003). Figure 1.10 illustrates one proposed mechanism leading up to the SFR in rat and feline myocardium. Collectively, these results support the idea that the SFR is very much dependent on intracellular $Na^+$ accumulation and that NHE-1 activation is likely to contribute to this.

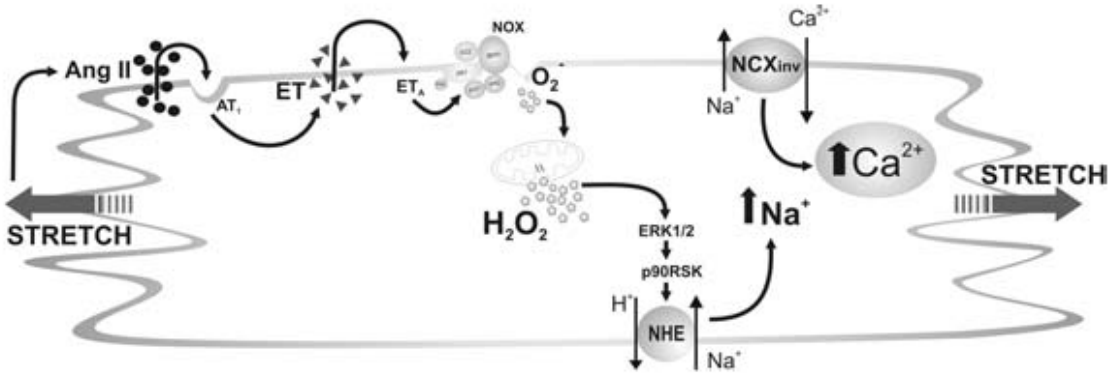


(Caldiz *et al.*, 2007)

Figure 1.10. One proposed mechanism of the SFR upon stretching rat or feline myocardium. The initial stretch leads to the release of Ang II and ET-1. NHE-1 then becomes activated, presumably due to the generation of $H_2O_2$. The activation of NHE-1 causes intracellular $Na^+$ to accumulate, which in turn increases $[Ca^{2+}]_i$ via reverse-mode NCX.

### 1.5.3. Contribution of Nitric Oxide

Nitric oxide (NO) is regarded as one of the more important endothelium-derived signalling factors responsible for the regulatory effects on endothelial smooth muscle. Recently, the effects of endogenous NO have been considered to underlie the slow force response for a number of reasons. First, myocardial stretch was shown to elicit an increase in NO production (Petroff *et al.*, 2001). Second, endothelial nitric oxide synthase (eNOS) is located in close proximity to the SR-T-tubule junctions, which may be the site of mechanical coupling between stretch and cellular responses (Levin & Page, 1980). Third, NO-mediated S-nitrosylation of the regulatory thiols of the ryanodine receptors has been shown to significantly enhance $Ca^{2+}$ release from the SR (Stoyanovsky *et al.*, 1997), which might account for the increased $Ca^{2+}$ transients during the SFR.

Petroff *et al.* (2001) observed that, in the rat cardiac myocyte, the application of a NOS inhibitor L-NAME was able to significantly abolish the increase in $Ca^{2+}$ spark frequency underlying the potentiated $Ca^{2+}$ transient associated with the mechanically stretched cardiomyocyte (Fig 1.11) (Petroff *et al.*, 2001). In addition, direct fluorescent labelling of endogenous NO using 4,5-diaminofluorescein (DAF-2) revealed a significant increase in fluorescence when the cardiac myocyte was subjected to stretch (Petroff *et al.*, 2001). Moreover, when potential secondary pathways following NO secretion such as cGMP and PKG were inhibited, the NO-dependent stretch response remained unaffected (Levin & Page, 1980), suggesting that endogenous NO could directly target the cellular mediating effector such as ryanodine receptors. The molecular basis for this cascade of events is critically dependent on Phosphatidylinositol kinase (PI(3)K), given that its inhibition produced a significantly less pronounced increase in $Ca^{2+}$ transient upon stretch as well as reduced phosphorylation of its downstream targets; protein kinase B and eNOS (Petroff *et al.*, 2001). Interestingly, the time course of this cascade corresponds closely to the rise in $Ca^{2+}$ transient following stretch (Petroff *et al.*, 2001), further strengthening the theory that NO may underlie the SFR. The mechanism underlying the initial increase in PI(3)K in the myocardium was thought to mirror a similar pathway observed in endothelial cells (Dimmeler *et al.*, 1999), though no direct experimental evidence has been provided thus far to corroborate this hypothesis. Based on previous observations and their experiment, Petroff *et al.* proposed that the colocalisation of eNOS and the junctional dyad (T-tubule coupled to the SR) is able to release sufficient NO (~0.5 to <1 mM) (Petroff *et al.*, 2001), to activate both type 1 and type

2 ryanodine receptors to trigger an increased $Ca^{2+}$ release rate, without significantly affecting other regions of the cell. Interestingly, when Calaghan and colleagues repeated the experiment following a similar protocol, they failed to notice any NO-mediated responses in rat cardiomyocytes (Calaghan & White, 2004). A noteworthy difference between the two experiments was in the preparation of the myocyte, where Petroff's group encased the cells in agarose such that shear stress may potentially trigger NO release. Furthermore, this theory depends absolutely on a functional SR, and since there is some doubt that the SR is involved in the development of SFR (Kentish & Wrzosek, 1998), the role of NO requires further investigation.

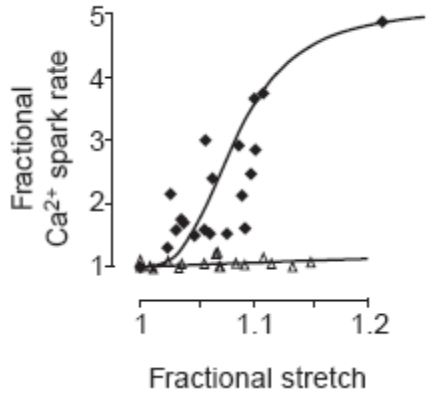


(Petroff *et al.*, 2001)

Figure 1.11. A comparison of the $Ca^{2+}$ spark rate to stretch between control (filled shapes) and L-NAME treated (hollow shapes) rat myocytes. Myocytes were embedded in 1.5% low-melting agarose in HEPES-buffered solution and drawn into a polyethylene tube for stretch ($p < 0.05$, n = 20).

### 1.5.4. The role of L-type $Ca^{2+}$ Channels and Sarcoplasmic Reticulum in the SFR

One simple explanation for the SFR would be a stretch-induced increase in the influx of $Ca^{2+}$ through sarcolemmal L-type $Ca^{2+}$ channels. However, this idea remains largely inconclusive, as one study had shown that in the presence of LTCC antagonist diltiazem, the magnitude of the SFR changes very little (von Lewinski *et al.*, 2004). In addition, the voltage-dependent $Ca^{2+}$ current following stretch does not differ significantly with those prior to stretch (Hongo *et al.*, 1996; Lewinski *et al.*, 2004). Moreover, investigators have found that, in the ferret papillary muscles, the SFR was still present during diastole, indicating that systolic involvement of L-type $Ca^{2+}$ channels is unlikely be the major contributor to the SFR (Allen *et al.*, 1988).

The SR contributes significantly toward the E-C coupling process in the mammalian cardiac muscle. It has been hypothesised that the SFR may be due to the enhanced SR loading of $Ca^{2+}$ as a result of increased intracellular $Ca^{2+}$ (Bluhm & Lew, 1995). Studies have evaluated this hypothesis through the application of SR inhibitors ryanodine and cyclopiazonic acid (CPA) (Bluhm & Lew, 1995; Kentish & Wrzosek, 1998). At the nano-molar range, ryanodine is known to lock the RyRs at a semi-conducting state, leading to enhanced leakage of $Ca^{2+}$ from the SR (Bluhm & Lew, 1995). CPA, a SERCA antagonist, was used to prevent the uptake of $Ca^{2+}$ from the cytoplasm by the SR. Even though the combined application of ryanodine and CPA resulted in substantial depletion of $Ca^{2+}$ from the SR stores, the magnitude of the SFR was not significantly affected as shown in Fig. 1.12 (Bluhm & Lew, 1995). This conclusion was later confirmed by Kentish & Wrzosek (1998). In contrast, Lewinski *et al.* (2004) found that, after using SR inhibitors, the SFR was significantly reduced. These results indicate that, under physiological conditions, the development of SFR in most mammals may not critically depend on the SR, though it would require further investigation.

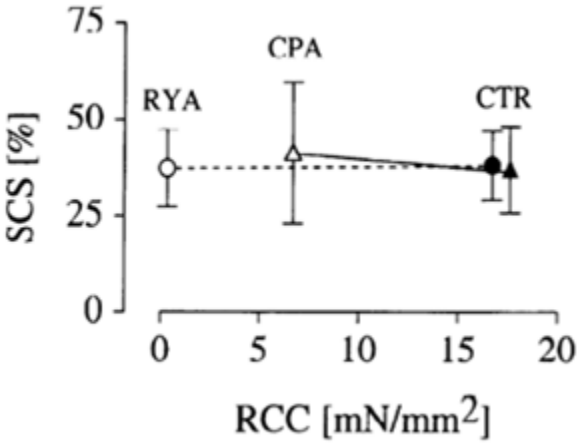


(Bluhm & Lew, 1995)

Figure 1.12. Slow changes in stress (SCS) of papillary muscle as a function of rapid cooling contractures (indication of SR $Ca^{2+}$ Content). Although the application of ryanodine (RYA) and cyclopiazonic acid (CPA) reduced the SR $Ca^{2+}$ content by 97% and 63%, respectively, the magnitude of the slow force response did not change significantly.

### 1.5.5. The Role of Cyclic AMP

Cyclic AMP (cAMP), an intracellular second messenger, is synthesized by adenylate cyclase and is involved in a number of localised phosphorylatory signaling cascades inside the cell (For review, see (Cooper *et al.*, 1995; Mika *et al.*, 2012)). Functional and ultrastructural studies reveal the points of $Ca^{2+}$ entry into the cell are often located in close proximity with adenylate cyclises (Cooper *et al.*, 1995). Given that the magnitude of intracellular $Ca^{2+}$ transient increases in parallel with the development of the SFR, a possible mechanism may involve the activation of the phosphorylation pathway by cAMP. In the intact canine heart, Todaka *et al.* (1998) demonstrated that when the left ventricular volume was progressively increased via a piston pump operated water-filled balloon placed within the ventricle, a parallel increase in intracellular cAMP was observed (Fig 1.13). More importantly, the cAMP concentration rose in concert with the changing calcium transient, indicating a potential role for cAMP in the development of the SFR. Intracellular cAMP is also known to mediate the phosphorylation of numerous intracellular regulatory processes which enhances $Ca^{2+}$ handling.

The exact mechanism contributing to the rise in cAMP following stretch is largely unknown. Todaka *et al.* (1998) showed that the application of β-agonist to the heart resulted in the abolition of the SFR to stretch as well as altering the underlying cAMP concentration. They proposed that when the heart is subjected to stretch, certain components of this particular signalling cascade such as the β-receptors, adenylate cyclase and the associated G-proteins, may change their functional properties in a stretch-dependent fashion. Indeed, a number of studies reported the activation of adenylate cyclase and the subsequent rise of intracellular cAMP upon cell deformation through either hyposmotic swelling (Watson, 1990) or via airway pressure inflation (Russo *et al.*, 1989), though these observations may not be representative of the events in the cardiac muscle as the cells studied were mice lymphoma (Watson, 1990) and lung cells (Russo *et al.*, 1989). Not surprisingly, as these components are large membrane-spanning proteins, they are expected to be coupled to cytoskeletal structural proteins such as actin filaments to allow the direct transmission of mechanical force into chemical stimuli (Watson, 1990). On the other hand, studies have also demonstrated a reduction in cytosolic cAMP in response to stretch (Hilal-Dandan & Brunton, 1995). Discrepancies in these data are likely to be the result of tissue-dependent stretch activation, or variations in procedural protocols such as the method of stretch induction. Taken together,

these findings suggest that intracellular cAMP may, at least in part, contribute to the SFR to stretch.

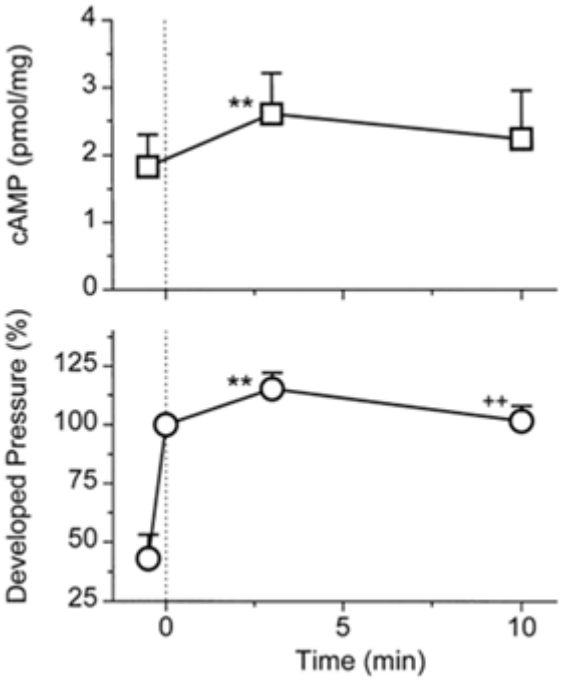


(Todaka *et al.*, 1998)

Figure 1.13. A comparison of intracellular cAMP content and the developed force in response to stretch over a period of 10 minutes. The slow force response to stretch is mirrored by parallel changes in cAMP concentration over a period of 3 minutes.

## 1.6. Thesis Objectives

To date, SFR has been observed in isolated myocytes (White *et al.*, 1995; White, 2004), papillary muscle (Allen & Kurihara, 1982; Cingolani *et al.*, 2003; Caldiz *et al.*, 2007), ventricular trabeculae (Alvarez *et al.*, 1999; Kockskamper *et al.*, 2008a; Ward *et al.*, 2008) as well as isolated blood-perfused hearts (Tucci *et al.*, 1984), suggesting that it is likely to be an intrinsic response exhibited by individual myocytes. However, it is interesting to note that despite contributing to nearly 70% of the total myocardial mass, myocytes roughly account for only around 30% of the total cardiac cell number. It is not unlikely then, that contributions from the external environment (e.g. endothelial cells) could potentially augment the SFR.

From a physiological perspective, changes in intracellular ionic concentration associated with stretching the myocardium can have a number of implications, especially when one considers the intricate coupling of mechanical to electrical activities in the heart. Such is the case when, under certain pathophysiological conditions, myocardial stretch induces an intracellular ionic imbalance ($Ca^{2+}$ and/or $Na^{+}$), which can in turn become arrhythmogenic (stretch-induced arrhythmias) (Hansen *et al.*, 1995). In Duchenne Muscular Dystrophy (DMD), the cytoskeletal protein dystrophin becomes severely downregulated as a result of a mutation. The absence of dystrophin gives rise to dilated cardiomyopathy, as various $Ca^{2+}$ entry pathways are thought to be disrupted in response to mechanical stress (Yeung & Allen, 2004; Fanchaouy *et al.*, 2009). These are but two examples that are associated with a high mortality risk. A better understanding of pathways involved in the SFR and the associated changes in $[Ca^{2+}]_i$ may give us the necessary insights to combat these detrimental aspects of myocardial stretch.

The thesis aims to add to our understanding of the mechanisms underlying the SFR by exploring intrinsic and extrinsic factors that may influence the SFR. The next chapter looks to describe, and to explain the experimental models and protocol used to achieve this goal.

# Chapter 2. General Methodology

## 2.1. Chapter Overview

Investigating the SFR required a number tools and techniques. These include a live muscle preparation that can be subjected to repetitive stretch, a way to measure force changes on a milli-Newton (mN) scale, and a way to observe and quantify changes in intracellular [$Ca^{2+}$] in the specimen. For this project, intracellular pH during stretch was also investigated. Furthermore, to determine whether potential extra-humoral factors are released in response to stretch, a bioassay system was developed, consisting of two principal components: an 'upstream' whole heart in Langendorff configuration, and a 'downstream', isolated trabecula superfused with the venous effluent obtained from the coronary circulation of the whole heart. The following chapter looks to outline the various tools and techniques used to study the SFR.

## 2.2. Ethical Approval

This study was carried out in strict accordance with the recommendations in the Guide for the Care and Use of Laboratory Animals of the National Institutes of Health. The experimental protocol was approved by the Animal Ethics Committee of The University of Auckland, permit number AEC R665.

## 2.3. The Cardiac Trabecula

Cardiac trabeculae obtained from the right ventricle of adult Wistar rats were used throughout the experiment. As shown in figure 2.1A, the rat RV trabeculae are intact, multicellular ventricular muscle strips typically located just beneath the atrio-ventricular ring, with one end attached to the valve tissue and the other fixed to the right ventricular free wall. There are a number of characteristics that make trabeculae ideal cardiac preparations for studying the SFR. First, myocytes within each trabecula are longitudinally aligned (as shown in figure 2.1B), which when stretched, allows for a more or less uniform distribution of strain across the entirety of the preparation. Trabeculae therefore have an advantage as an experimental preparation over samples such as ventricular wall tissue, where muscle fiber orientation show region-dependent variations (Greenbaum *et al.*, 1981; LeGrice *et al.*, 1995). One of the problems with isolated cardiac muscle preparations is ensuring the delivery of sufficient oxygen to the core of the tissue. In vitro, the absence of the capillary network means that oxygen transport can only be achieved through diffusion, a process hugely dependent on the radius of the preparation. It has been documented that in the rat trabecula, a diameter of less than 200 µm is preferable to ensure adequate diffusion of oxygen to the core of the muscle at room temperature (Schouten & Keurs, 1986). Under physiological conditions (37 °C, ~5 Hz stimulation, for rat) where oxygen consumption is further increased, the diameter of trabeculae would need to be even smaller (~150 µm) to ensure adequate delivery of oxygen throughout the tissue (Raman *et al.*, 2006). Compare this with papillary muscles which typically have a diameter of over 300 µm. It is therefore easy to see the benefit of using cardiac trabeculae as an experimental muscle preparation.

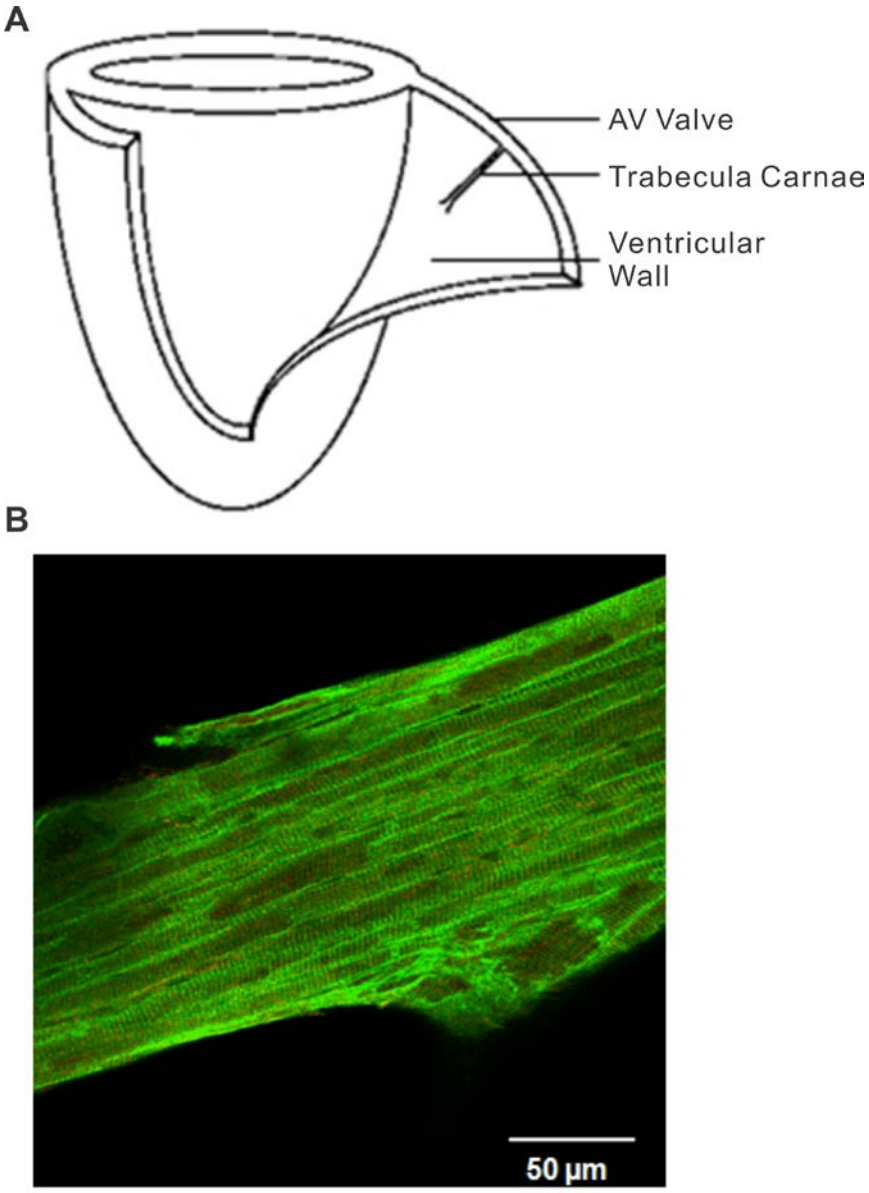


Images from (Hanley & Loiselle, 1998) (top) and Dr. Marie Ward (bottom).

Figure 2.1. The right ventricular trabecula. (A) Schematic diagram of the cardiac trabecula showing its relative position within the ventricular wall. (B) A mouse trabecula labelled for caveolin-3, a surface membrane protein (in green), and anti-TRPC6 (in red) showing that each muscle fiber is aligned longitudinally.

## 2.4. Isolation, Dissection and Mounting of Trabeculae

A total of 35 trabeculae (cross-sectional area: 0.032 ± 0.003 $mm^2$) were used in this study. The rats were anaesthetised with isofluorane using 100% $O_2$ as carrier gas prior to decapitation using a bench-top guillotine. The hearts were quickly excised and submerged in chilled physiological solution (see later) before being transferred to the dissection setup shown in figure 2.2. The aorta was cannulated and retrograde perfusion of the coronary vasculature commenced during dissection of a trabecula. The heart was oriented in the dissection chamber with the right ventricular free wall uppermost. An initial cut was made across the right atrium, followed by a cut perpendicular to the apex along the septal wall. This exposed the ventricular wall shown in figure 2.1A, which was then held in place using insect pins.

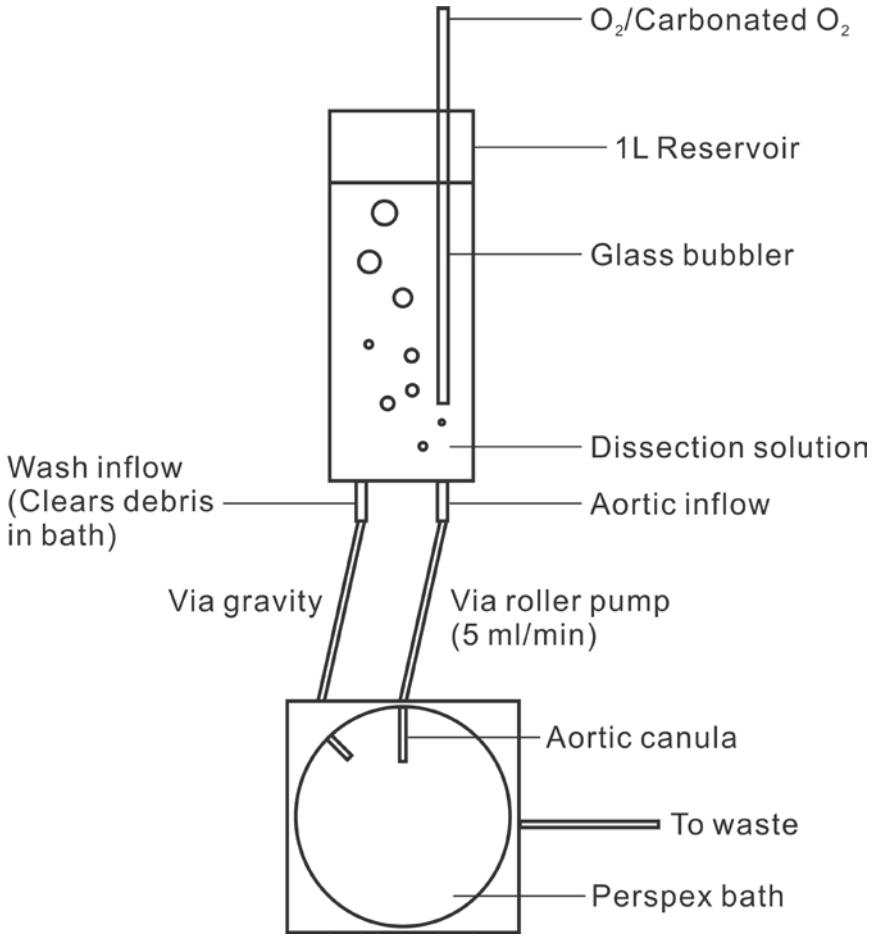


Figure 2.2. Schematic diagram of the micro-dissection setup. The heart is transferred to the Perspex® bath and cannulated after being excised from the rat. Dissection solution is bubbled with either 100% $O_2$ or 95% $O_2$/5% $CO_2$ and used to perfuse the heart via a roller pump.

Un-branched trabeculae were micro-dissected from the right ventricle (RV) of adult Wistar rats (weight: 287 ± 6 g) with small blocks of ventricular wall tissue at each end. Dissected trabeculae were transferred to a custom made Perspex® bath (450 µl) on the stage of an inverted light microscope (Nikon Eclipse TE2000-U, Japan). Muscles were continuously superfused with recirculating, oxygenated physiological solution (see later) using a roller pump (Minipuls 2, Gilson, France) with a flow rate set at 10 ml/min. Given that the force generated by trabeculae is in the milli-Newton range, the pulsatile nature of the pump can potentially increase baseline 'noise' to the force measurements. To minimise the pulsation, the bath was designed with modifications as shown in figure 2.3. First, the removal of the superfusate was made through a second Perspex® reservoir separated from the main bath by a weir. Second, the outflow needle was positioned just above the meniscus of the bath such that a mixture of solution and air was continuously drawn away.

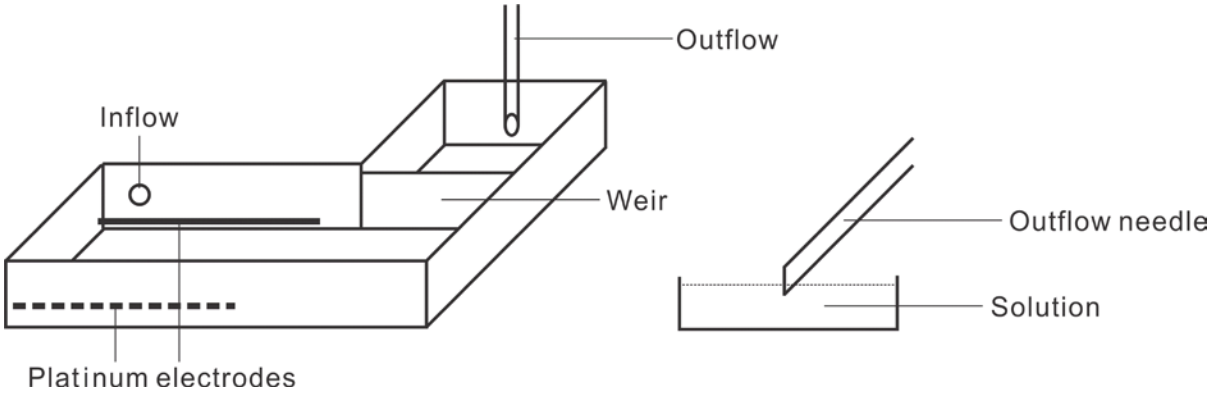


Figure 2.3. Schematic diagram of the Perspex® muscle bath. A weir was put in place to regulate the flow of superfusate into the separate outflow chamber. A 18 gauge needle was positioned level with the top of the weird for aspiration of solution and air from the muscle chamber and to reduce pulsatility.

Figure 2.4 shows how the trabecula was mounted following dissection. The block of tissue at one end of the trabecula was placed into a wire cradle extending from the beam of a force transducer (KX801 Micro Force Sensor, Kronex Technologies), while the small tissue block at the other end was held within a nylon loop attached to a three-axis micromanipulator to allow for length changes.

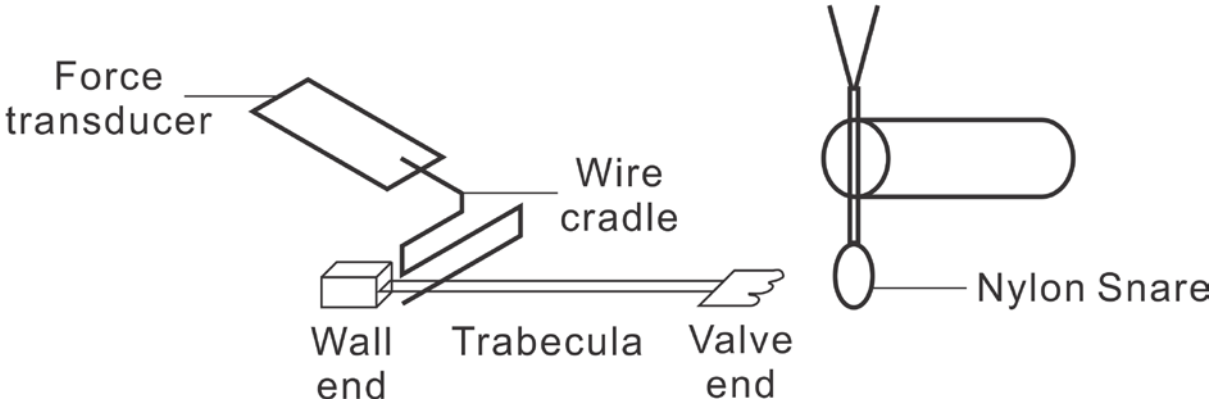


Figure 2.4. Schematic diagram showing the mounting of a trabecula between a custom-made wire cradle and a nylon snare.

## 2.5. Chemicals and Solutions

Trabeculae were primarily superfused with Krebs-Henseleit (K-H) solution containing (in mM): 118 NaCl; 4.75 KCl; 1.18 $MgSO_4$; 1.18 $KH_2PO_4$; 24.8 $NaHCO_3$ and 10 D-Glucose. The superfusate was bubbled continuously with 95% $O_2$ and 5% $CO_2$ to maintain pH of 7.4. For some experiments, a $HCO_3^-$-free Tyrode's solution bubbled with 100% $O_2$ was used, containing (in mM): 141.8 NaCl; 6 KCl; 1.2 $MgSO_4$; 1.2 $Na_2HPO_4$; 10 HEPES and 10 D-Glucose. For both solutions, extracellular calcium ($[Ca^{2+}]_o$) was adjusted by adding $CaCl_2$ from a 1 M stock solution. The dissection and the initial mounting solutions contained 0.25 mM $[Ca^{2+}]_o$, and 20 mM 2,3-butanedione monoxime (BDM). BDM served a cardioprotective purpose by reversibly suspending contractile activity via a reduction in the rate of cross-bridge formation, minimising energy expenditure and potential cutting injuries to the heart during dissection (Backx *et al.*, 1994). Where fluorescent indicators were used at 37 ºC, 1 mM probenecid, an anionic transport blocker, was added to the superfusate to minimise the loss of de-esterified dye (Di Virgilio *et al.*, 1988; Virgilio *et al.*, 1989).

## 2.6. Force Measurement

Figure 2.4 shows that the wire cradle holding the trabecula extends from a force transducer. More specifically, it is super-glued (Quick Fix, Selleys, Australia) to the silicon beam of a strain gauge force transducer (KX801 Micro Force Sensor, Kronex Technologies, USA) with a detection range down to as low as 1 μN. Figure 2.5 shows an example of one such force transducer. A two-point calibration was performed with 0 mg, and a 100 mg weight suspended from the wire cradle, from which a calibration factor was then generated.

The mounted trabecula was flanked by a pair of platinum electrodes running down either side of the muscle chamber as shown in figure 2.4. The electrodes were coupled to a stimulator (model D100, Digitimer™, UK), with repeating electrical pulses of 5 ms duration at a voltage adjusted to 10% above threshold. Stimulation frequency of 0.2 Hz and 2 Hz were applied at room temperature and at 37 °C, respectively, unless otherwise stated.

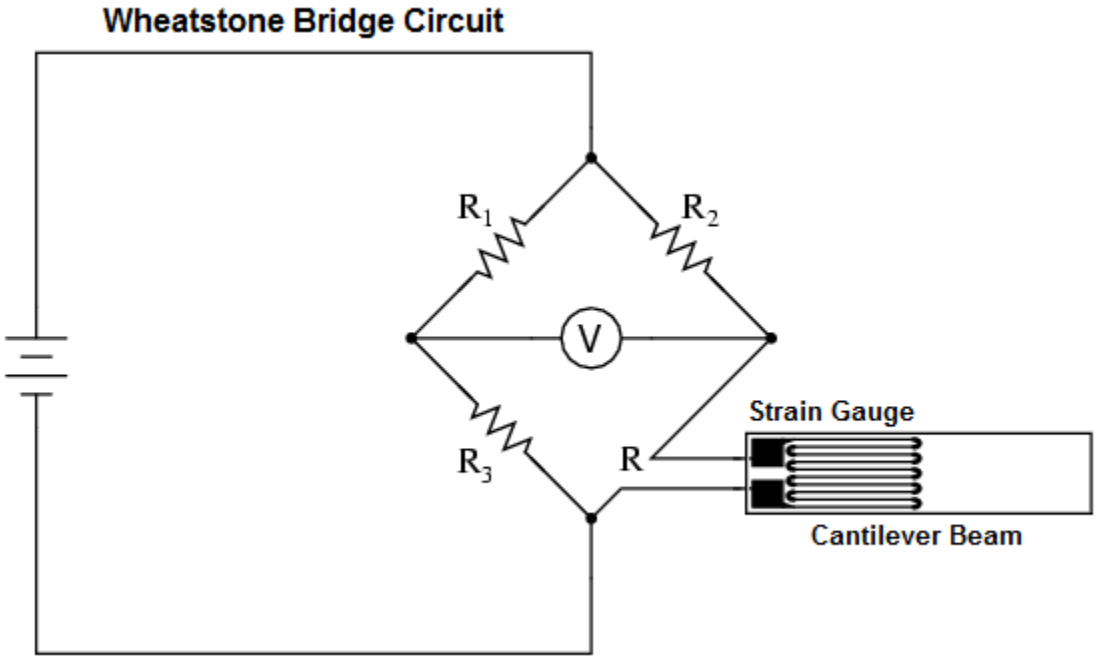


(Modified from: http://www.eng.cam.ac.uk/DesignOffice/mdp/electric_web/DC/DC_8.html)

Figure 2.5. A standard configuration of a Wheatstone Bridge Circuit. Four resistors are connected such that $R_1/R_3$ are arranged in parallel with $R_2/R_{gauge}$. $R_1/R_3$ is known as the ratio arm of the setup and is of equal value. Similarly, $R_2$/Rgauge or the rheostat arm is equal to each other at zero force. As a result, when the net force is zero, the two arms of the bridge are balanced, giving a voltage output of zero. However, when a positive force is exerted on the strain gauge (stretched), an increase in $R_{gauge}$ will be observed, which in turn disrupts the total resistance balance of the rheostat arm, providing a voltage read out from the voltmeter.

## 2.7. Stretch protocol

Once mounted in the muscle chamber and contracting regularly in response to field stimulation, trabeculae were gradually lengthened to determine optimal muscle length ($L_o$), defined as the length at which there is no longer any increase in active force (peak minus passive force) in response to further increase in muscle length. An example of this process is illustrated in figure 2.6. Trabeculae were then shortened to 90% of $L_o$ and allowed to reach steady state. Approximation of sarcomere length (SL) was made at a magnification of 40x by counting the number of straiations per 20 µM in order to determine SL at $L_o$. In this study, the average sarcomere length of trabeculae at $L_o$ was 2.1 ± 0.02 µm, n = 35.

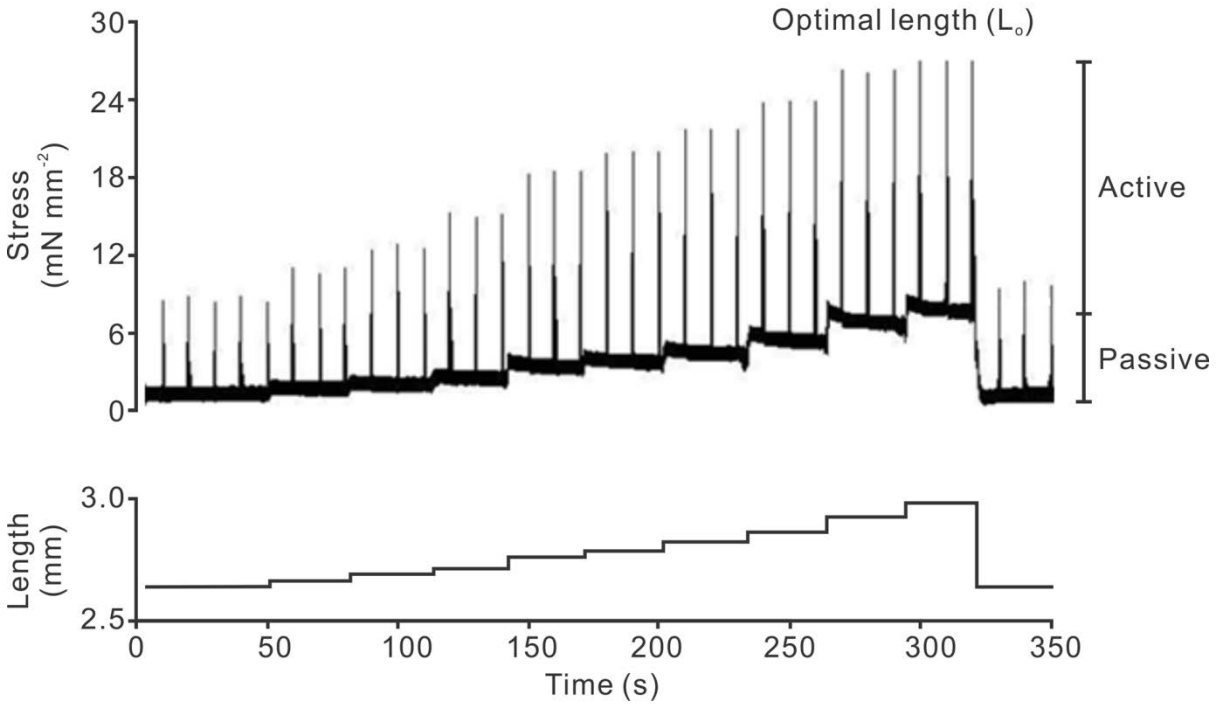


Figure 2.6. Determination of optimal length ($L_o$) in trabecula. Both passive and active force of contraction increases in response to increased muscle length (due to the Frank-Starling law of the heart). Lo is the point at which further stretching the muscle no longer causes the active force to increase.

To examine the SFR, muscles were subject to uniaxial stretch from 90% $L_o$ to 100% $L_o$ for 3 minutes before returning again to 90% $L_o$. Figure 2.7 shows a representative force recording of a rat trabecula at 2 Hz stimulation. The SFR was measured following 3 minutes of stretch and expressed as a percentage of the initial inotropic response to stretch. All experiments were carried out at 37 °C and with 1.5 mM $[Ca^{2+}]_o$, unless otherwise stated. Stability of the preparation was generally assured by the reversible and stable nature of the responses.

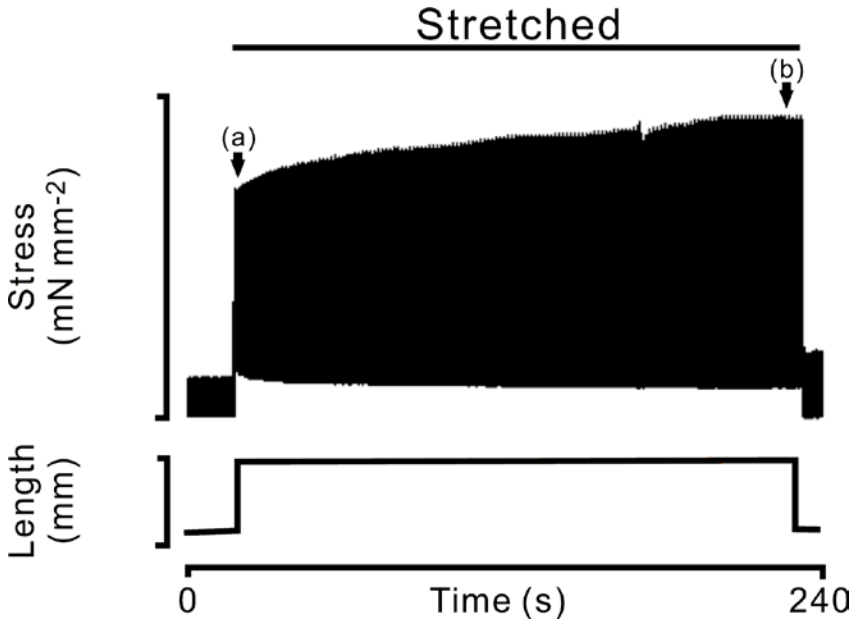


Figure 2.7. A typical SFR from a rat trabecula after its length was increased from 90% $L_o$ to 100% $L_o$ for 3 minutes. SFR is quantified with the equation: SFR = ((b-a)/a)*100.

## 2.8. Measurement of $[Ca^{2+}]_i$ using Fura-2/AM

In order to observe intracellular ionic changes associated with the SFR, fluorescent indicators were used. The principle intracellular ion of interest in this project was $Ca^{2+}$. The ratiometric fluorescent indicator fura-2 in its acetoxymethyl (AM) ester form (membrane permeable) was used and emitted fluorescence recorded.

In this study, two fluorescence measurement systems were used. System I utilised a spectrophotometer (Cairn Research, Faversham, Kent, UK) coupled to an inverted light microscope (Nikon Diaphot 300, Japan) was used to record the fura-2 signal. The system uses a six-filter wheel (3 x 340 nm, 1 x 360 nm, 2 x 380 nm) operating at a frequency of 43 Hz in order to provide rapidly changing excitation wavelengths. System II used the Optoscan monochromator system (Cairn Research, Faversham, Kent, UK) which was also coupled to an inverted light microscope (Nikon Eclipse TE2000-U, Japan). Both systems use a 75 W Xenon arc lamp as the source of illumination focused onto the muscle through a 20x fluor objective (Nikon). Fluorescence was recorded from the middle of the central portion of the trabecula via a 'window' approximately 100 µm x 200 µm.

Intracellular $Ca^{2+}$ measurements were made as described previously (Ward *et al.*, 2003). Specifically, 2x 50 µg ampules of fura-2/AM (Teflabs, TX, USA) were each dissolved in 20 µl of warmed anhydrous dimethyl sulfoxide (DMSO) with 5% wt/vol of Pluronic F-127 (Teflabs, TX, USA). Such mixture of Pluronic F-127/DMSO has been used to facilitate the loading of the otherwise poorly soluble AM form of fluorescent indicators (Takahashi *et al.*, 1999). Each ampule was gently shaken and was given 5 minute to allow the dye to fully dissolve. The contents of each vial were subsequently transferred to 10 ml of physiological superfusate to make up a final dye concentration of 10 µM. As pluronic F-127 is a surfactant, 10 µl of antifoam A (Sigma Aldritch, Australia) was added to the final loading solution to prevent perturbations to flow from the formation of excess foam with continuous bubbling of the solution. Loading of the indicator into the myocytes was carried out at room temperature to minimise dye leakage. The duration of loading was 2 hours, at a stimulation frequency of 0.2 Hz and with 1.5 mM $[Ca^{2+}]_o$. It should be noted that calibration of Fura-2 was not performed in this study. This was because we were primarily concerned with the relative change in the $Ca^{2+}$ transients between different treatment groups, rather than the absolute $[Ca^{2+}]_i$ *per se*.

## 2.9. Data Acquisition and Statistical Analysis

Raw data from System I were acquired using LabVIEW SignalExpress (National Instruments, Austin, USA). Raw data from System II were acquired using Acquisition Engine (Cairn Research, Faversham, Kent, UK). In experiments recorded using SignalExpress, an analogue form of the data was also stored using a conventional chart recorder (Graphtek Linearcorder Mark VII, Leatham Electronic Limited, Wellington).

Recorded force and fluorescence data were sampled at 400 Hz and sections of interest were exported as text files for off-line analysis using a custom-written program (IDL Research Systems Inc., Boulder, CO, USA). Analysis of $Ca^{2+}$ transients was performed using a five parameter exponential function shown below (eq. 1)Individual transients across 6 cardiac cycles were fitted using the equation, and the parameters were subsequently averaged to give the final $Ca^{2+}$ transients (Ward *et al.*, 2003).

$$\mathbf{y = A_0 exp(-t/A1)/(1 + exp(-(t + A_2)/A_3)) + A_4 \ (eq.\ 1)}$$

where $A_0$ represents the maximum change in the fluorescence ratio, $A_1$ is the time constant of exponential decay during the relaxation phase of the transient, $A_2$ is the time difference between the rising phase and the decay phase of the transient, $A_3$ is the transient's time constant of rise and $A_4$ is the diastolic or minimum fluorescence. From the above equation (eq. 3), diastolic fluorescence, systolic fluorescence, time constant of fluorescence decay and the maximum rate of rise of fluorescence was calculated. In addition, averaged force parameters from the analysis included time to peak force, time to half relaxation and maximum rate of rise of force. The gradual incremental increase in force and $Ca^{2+}$ with each successive contraction during the SFR explains the relatively low of number of cardiac cycles averaged in the analysis.

Statistical analysis was performed using either the Excel Data Analysis Toolpak (Microsoft Corporation, USA) or IBM SPSS Statistics 20 (IBM Corporation, USA). All results were expressed as mean ± SEM. Paired or unpaired Student's t-tests, as well as One-Way Analysis of Variance (ANOVA) were used depending on the experimental protocol. Tukey's HSD post-hoc test was performed where necessary. $p = 0.05$ was considered to be the upper limit of statistical confidence.

# Chapter 3. Cellular Mechanisms Underlying the Slow Force Response

## 3.1. Chapter Overview

The slow force response has generally been characterised as an intrinsic property of cardiac myocytes (Tucci *et al.*, 1984). Over the past couple of decades, potential subcellular pathways underlying the SFR have been the subject of extensive investigation. Although the exact mechanism is still unclear, a number of different mechanisms have been implicated. These include the release of autocrine/paracrine factors such as Angiotensin II (Ang II) (Cingolani *et al.*, 1998; Alvarez *et al.*, 1999; Perez *et al.*, 2011), influx of $Ca^{2+}$ and/or $Na^{+}$ via stretch-activated non-selective cation channels (White, 2004; Ward *et al.*, 2008) and enhanced $Ca^{2+}$ spark rate due to stretch-mediated production of nitric oxide (Petroff *et al.*, 2001). Nevertheless, there is good evidence that the SFR is linked to increased sarcolemmal (SL) $Na^{+}$ entry which reduces net $Ca^{2+}$ efflux via $Na^{+}/Ca^{2+}$-exchange (NCX) (Alvarez *et al.*, 1999; Pérez *et al.*, 2001; Lewinski *et al.*, 2003).

The primary aim of this chapter looks to explore novel intrinsic mechanisms which contribute to the development of the SFR. Experiments described in this chapter were all performed in the rat RV trabecula at physiological temperature. Experimental protocol for each section will also be described if it has yet to be mentioned in Chapter 2.

## 3.2. The SFR in Rat RV Trabeculae

Figure 3.1A shows a typical SFR and the corresponding increase in the magnitude of $Ca^{2+}$ transient in this series of experiments. The trabeculae were subjected to stretch from 90% to 100% $L_o$ at 37 °C, 2 Hz stimulation frequency and 1.5 mM $[Ca^{2+}]_o$. An immediate increase in both passive and active force was seen on stretching the trabecula, followed by a much slower increase in active force which developed over several minutes (the SFR). Figure 3.1B shows individual twitches on the (left hand panel) and $Ca^{2+}$ transients (right hand panel) from Figure 3.1A for the initial inotropic response (a) and the SFR following 3 min of stretch (b). The increase in the amplitude of the $Ca^{2+}$ transient associated with the SFR can also be seen in Figure 3.1B. Under these experimental conditions, the initial inotropic response increased stress ($mN.mm^{-2}$) from 6.23 ± 1.15 at 90% $L_o$ to 17.85 ± 2.62 at 100% $L_o$, and the SFR that developed over the following 3 min was 23.6 ± 4.1 % above the initial inotropic response (*n* = 6). As measured by the fura-2 340/380 fluorescence ratios, the magnitude of $[Ca^{2+}]_i$ during the SFR increased from 0.98 ± 0.15 at 90% $L_o$ to 1.07 ± 0.16 at 100% $L_o$. The time constant of fluorescence decay was not changed during the SFR, being 0.324 ± 0.070 s immediately after stretch, and 0.336 ± 0.066 s after 3 min of stretch ($p$ = 0.90, $n$ = 6).

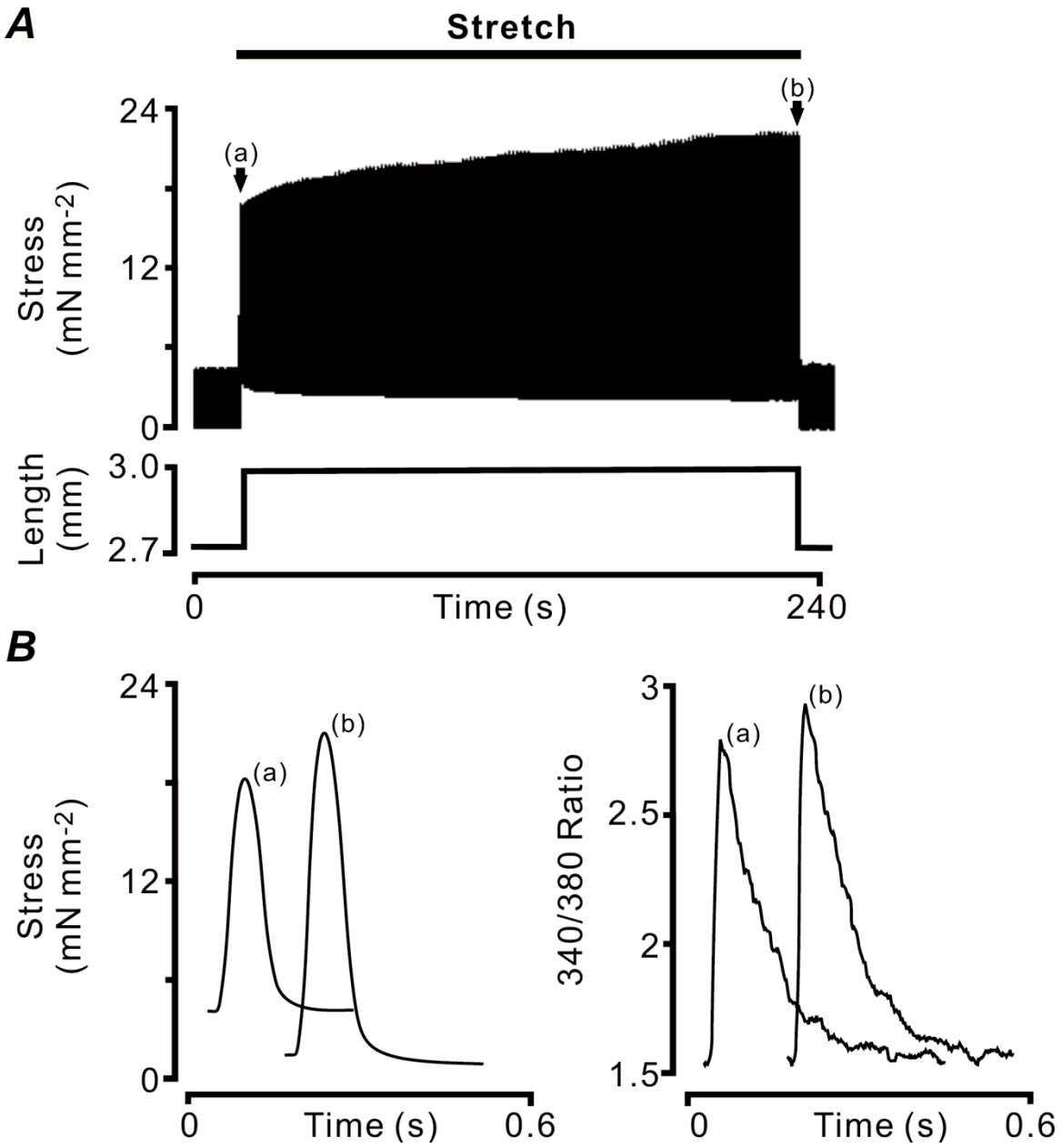


Figure 3.1. The SFR in the rat RV trabecula. A, shows a representative force recording of the SFR (2 Hz stimulation frequency, 1.5 mM $[Ca^{2+}]_o$ and 37ºC) in response to a 3 minute stretch protocol described in Chapter 2. B shows exemplar data from a trabecula, with the left panel showing the average of 6 consecutive contractions from points (a) and (b), while the right panel shows the average of 6 $Ca^{2+}$ transients from those same points.

## 3.4. The Effect of Extracellular [$Ca^{2+}$] on the SFR

Dissection of the cardiac trabecula is not without technical complications. There were instances where the only available trabecula from a particular animal was branched, and the removal of these branches usually leads to a preparation that exhibited $Ca^{2+}$ overload once superfused with the physiological solution. $Ca^{2+}$ overload is usually characterised by an under-shoot in the twitch force shown in figure 3.2, as well as physical 'writhing' of the preparation due to widespread propagation of $Ca^{2+}$ waves. Interestingly, when these 'damaged' muscles were subjected to a stretch, the SFR was absent.

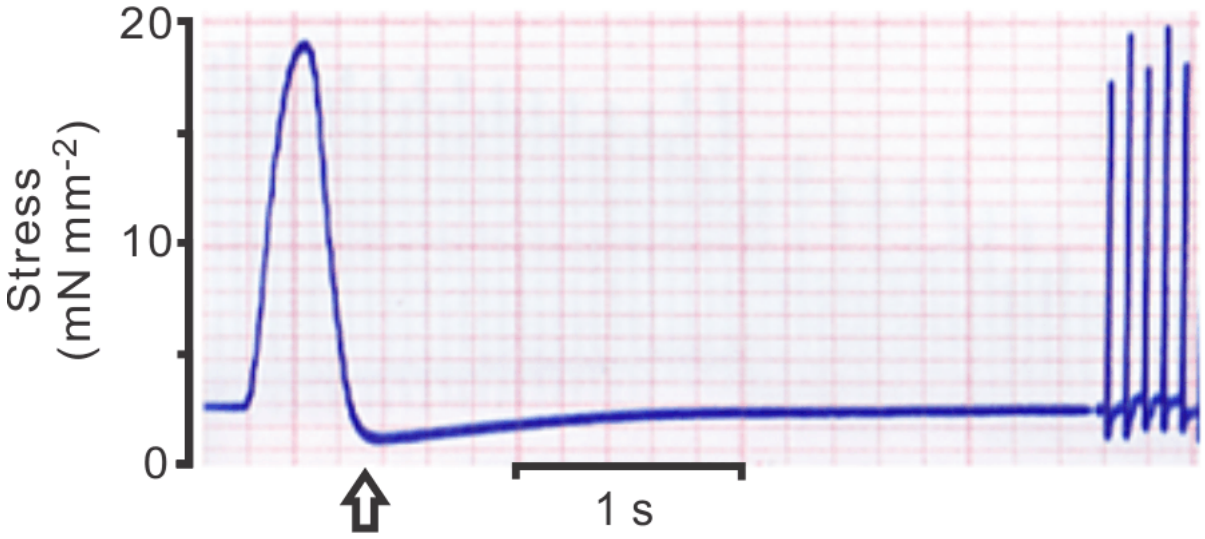


Figure 3.2. Force recording of a trabecula that was 'damaged' during dissection. The arrow points out the under-shoot in the trace that is typical of such preparations.

This particular observation pointed to a role for SR $Ca^{2+}$ content and fractional release of SR $Ca^{2+}$ as likely modulators of the SFR (Bassani *et al.*, 1995; Trafford *et al.*, 2001). In addition, there have been reports that decreasing (Allen *et al.*, 1988) or increasing (Ward *et al.*, 2008) resting muscle length in isolated muscle preparations can decrease or increase resting $Ca^{2+}$, respectively, suggesting that the SL $Ca^{2+}$ regulation is directly involved in the SFR. A role for SL $Ca^{2+}$ regulation appeared to be confirmed by Kentish and Wrzosek (1998), who showed that the magnitude of the SFR remained unchanged after the SR was blocked, although the time taken for the SFR to develop was increased (Kentish & Wrzosek, 1998). However, it should be noted that no slow change in diastolic $Ca^{2+}$ following stretch was detected by Kentish and Wrzosek. In contrast, Lewinski et al. (2004) found that the SFR was accompanied by an increase in the SR $Ca^{2+}$ content that was significantly reduced when SR inhibitors were applied.

To investigate the possibility that the SFR could be a SR $Ca^{2+}$-dependent process, extracellular $Ca^{2+}$ concentration was changed to alter the SR $Ca^{2+}$ fluxes (Trafford *et al.*, 2001; Bassani *et al.*, 2012). Figure 3.3A and figure 3.3B show a typical force and $Ca^{2+}$ transient record of a trabecula after being stretched in 1 mM $[Ca^{2+}]_o$ and 3 mM $[Ca^{2+}]_o$, respectively. Note the absence of the SFR of the trabecula stretched in the 3 mM $[Ca^{2+}]_o$ as well as the lack of increase in $Ca^{2+}$ transient typically associated with the SFR. Figure 3.3C summarises mean data from trabeculae superfused with four different $[Ca^{2+}]_o$ (in mM: 0.5, 1, 1.5 and 3). An increase in $[Ca^{2+}]_o$ from 0.5 mM to 1.5 mM decreased the overall magnitude of the SFR from 50.9 ± 9.1 % to 23.2 ± 6.6 % and at 3 mM $[Ca^{2+}]_o$ the SFR was essentially abolished. As might be expected from the central role of changes in the amplitude of the $Ca^{2+}$ transient in the SFR, there was no detectable change in the fura-2 fluorescence transient associated with stretch in 3 mM $[Ca^{2+}]_o$ ($p = 0.5$, $n = 3$).

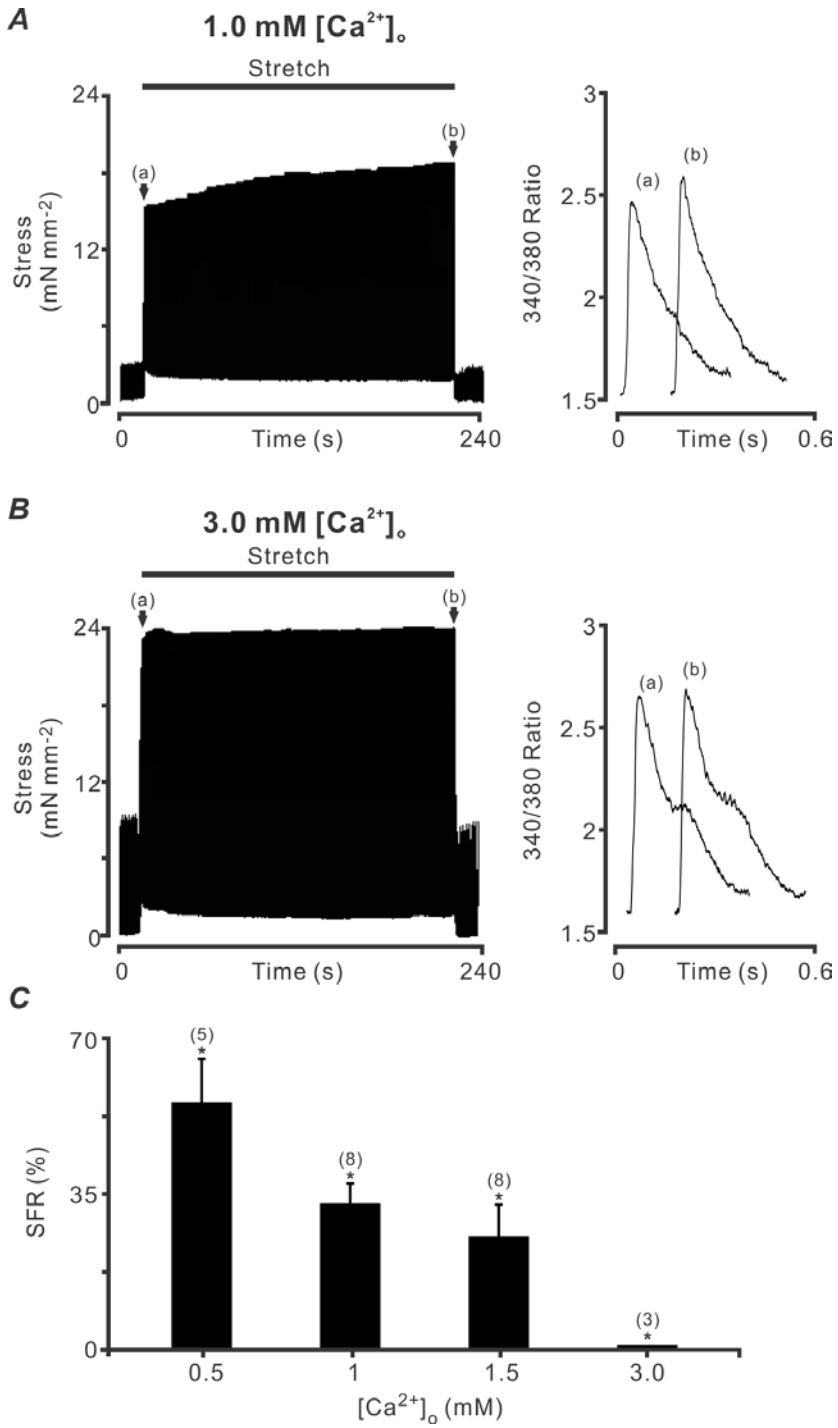


Figure 3.3. Effect of $[Ca^{2+}]_o$ on the SFR. A and B, shows representative force and $Ca^{2+}$ transient response of a trabecula being stretch in 1 mM and 3 mM $[Ca^{2+}]_o$ superfusate, respectively. C, shows the pooled data in mean ± SEM. The magnitude of the SFR decreased as $[Ca^{2+}]_o$ was increased from 0.5 to 1.5 mM. At 3 mM $[Ca^{2+}]_o$, the SFR was completely abolished. *$p < 0.05$ between groups (ANOVA), with the number of trabeculae shown in brackets.

While the lack of change in the $Ca^{2+}$ transient suggests that the SFR was blocked by high $[Ca^{2+}]_o$, it is possible that an SFR would not be seen if the $Ca^{2+}$ levels were already sufficiently high to saturate the contractile machinery. However, figure 3.4 shows that under our experimental conditions, it was still possible to increase force by delivering paired stimulation pulses (King & Taylor, 1968; Ward *et al.*, 2010) to increase SR $Ca^{2+}$ release, so that the lack of force response is not simply explained by saturation of the contractile machinery. Note that there is a greater potentiation of stress following paired-pulse stimulation in 1 mM $[Ca^{2+}]_o$ compared with that in 3 mM $[Ca^{2+}]_o$, pointing to a possible difference in the extent of SR $Ca^{2+}$ load (further examined in section 3.5).

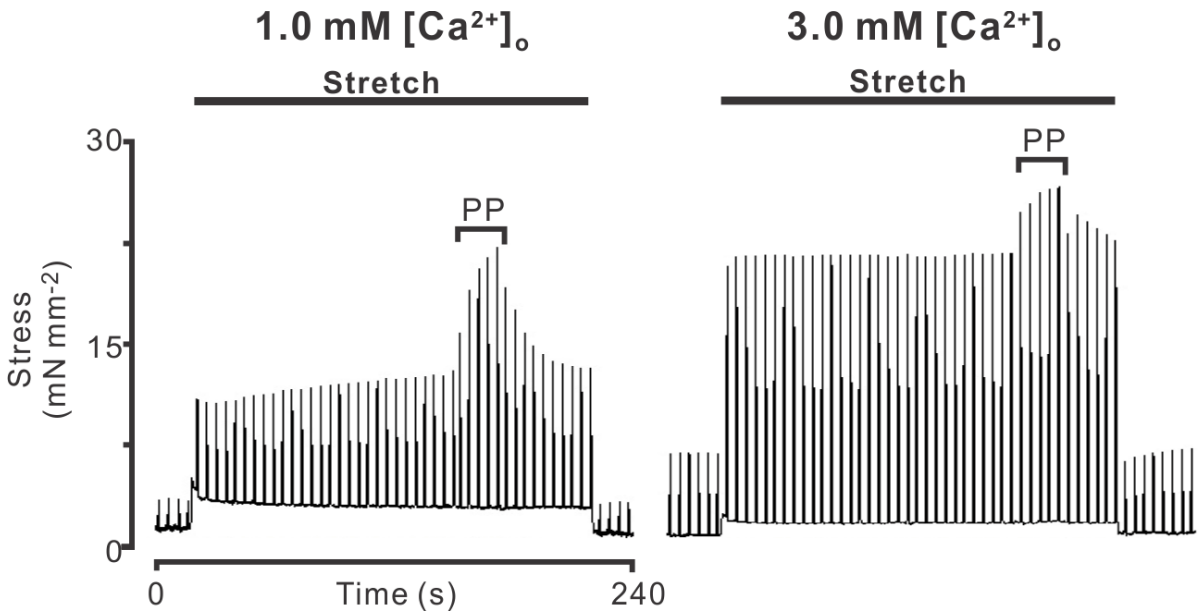


Figure 3.4. Effect of paired-pulse stimulation during the SFR at 1 mM $[Ca^{2+}]_o$ (left) and 3 mM $[Ca^{2+}]_o$ (right). 5 paired-pulses were delivered at a frequency of 0.2 Hz, with 80 ms delay between pulses.

## 3.5. Effects of Stimulation Frequency on the SFR

The force-frequency relationship in rat myocardium has been variously described as negative (Baudet *et al.*, 1996), positive (Layland & Kentish, 1999) or biphasic (Kassiri *et al.*, 2000; Endoh, 2004). As shown in figure 3.5C, the force-frequency relationship for rat trabeculae at short length (90% $L_o$) is biphasic under our experimental conditions, with minimum force being developed at 1 Hz. However, it is generally agreed that the force-frequency relationship reflects the state of SR $Ca^{2+}$ load within the preparation (for review see (Endoh, 2004)).

To further examine the idea that the SFR is dependent on the degree of SR loading, stimulation frequency was altered from 0.1 to 4 Hz at 1.5 mM $[Ca^{2+}]_o$ while the standard stretch protocol was carried out. Figure 3.5A illustrates the effect of stimulus frequency on the SFR. As expected from the biphasic force-frequency relationship, the active force immediately following stretch was lower at 1 Hz when compared to both 0.2 and 2 Hz. However, the relative increase in the SFR was much larger at 1Hz than at the other frequencies. Pooled data (mean ± SEM) from 10 trabeculae are shown in figure 3.5B, with an average SFR (%) of 26.4 ± 5.0, 55.9 ± 7.4 and 31.5 ± 4.3 at 0.2, 1 and 2 Hz, respectively ($p$ = 0.002).

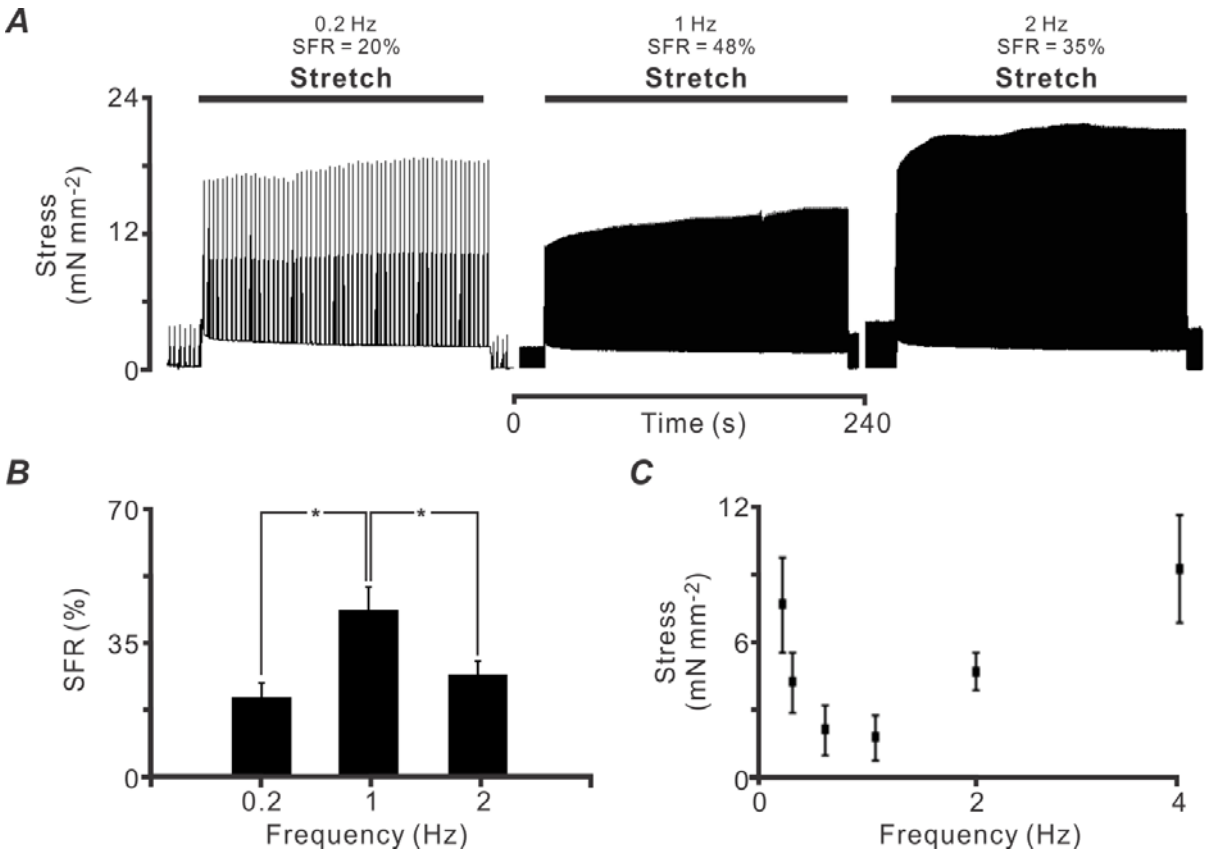


Figure 3.5. Effects of stimulation frequency on the SFR. A, shows examples of the SFR from a single trabecula at stimulation frequencies of 0.2, 1 and 2 Hz, with averaged data from 10 preparations graphed in B (mean ± SEM), $*p < 0.05$. A clear biphasic force relationship was seen, where the SFR was largest at 1 Hz. C, shows the force-frequency relationship for trabeculae held at 90% $L_o$. A negative relationship was observed at low stimulation frequencies (0.1 to 1 Hz), while a positive relationship was observed at frequencies above 1 Hz ($n = 6$).

The next step was to show that these changes were related to changing SR load. In order to directly assess the SR $Ca^{2+}$ content at each stimulation frequency, trabeculae were superfused with 20 mM caffeine immediately after stopping stimulation. Caffeine has been used extensively as a tool in uncovering the role of SR in EC coupling and cellular $Ca^{2+}$ modulation. Its addition to cardiac muscle leads to a site-specific interaction on the ryanodine receptors, which in turn increases the open probability of channel (Rousseau & Meissner, 1989; Sitsapesan & Williams, 1990). The subsequent release of $Ca^{2+}$ from the SR can be recorded as a rapid increase in intracellular fluorescence intensity, which in this case, is represented by an increase in the fura-2 340/380 ratio. The area under the increased fura-2 signal is therefore reflective of the total SR $Ca^{2+}$ content. It is worth noting that in multicellular preparations, the magnitude of caffeine-induced transients depends heavily on

the diffusion of caffeine itself through the muscle and its synchronised arrival at the cells. For this reason, each trabecula served as its own control, and the area under the caffeine-induced $Ca^{2+}$ transients within individual trabeculae was compared at each of the 3 stimulation frequencies (0.2 Hz, 1 Hz and 2 Hz).

Figure 3.6A illustrates caffeine-induced transients from a representative trabecula. Note that the area under the caffeine transient was smaller at 1 Hz than at either 0.2 or 2 Hz. Figure 3.6B shows mean ± SEM data from 6 trabeculae. The SR $Ca^{2+}$ content was clearly lower at 1 Hz than at either the lower or higher stimulation frequencies tested ($p = 0.016$). It is notable that these data mirror the force-frequency relationship shown in figure 3.5C. These results show that the SFR has a biphasic dependence on stimulation frequency, but is inversely related to both twitch force and SR $Ca^{2+}$ content so that the SFR is largest when the SR has the greatest capacity to increase its $Ca^{2+}$ content.

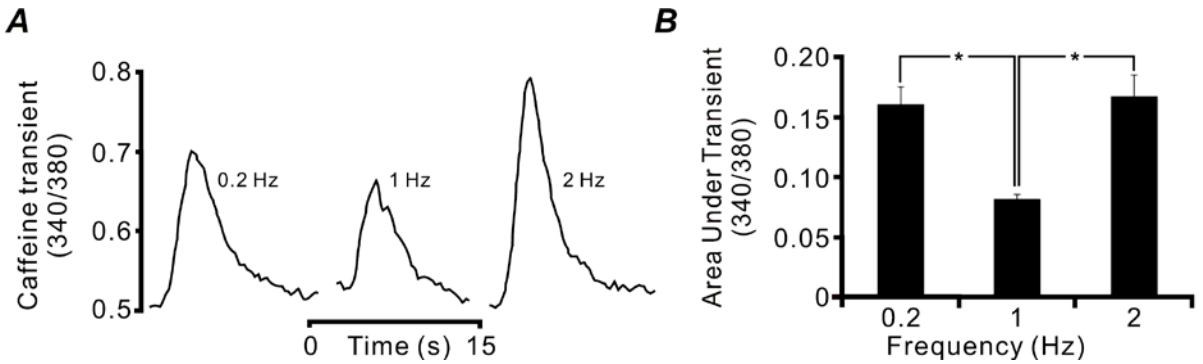


Figure 3.6. SR $Ca^{2+}$ load at different stimulation frequencies as measured by caffeine-induced transients. A, shows caffeine-induced $Ca^{2+}$ transients from a representative trabecula at 0.2, 1 and 2 Hz stimulation frequency (dashed lines indicate the amplitude of the caffeine transients). B, shows averaged caffeine transient data ($n = 6$). The amplitude of the caffeine transients provided a qualitative measure of SR $Ca^{2+}$ load, which also changed with stimulation frequency in a biphasic manner. *$p < 0.05$.

## 3.6. Sarcolemmal $Ca^{2+}$ efflux is slowed during stretch

The previous experiments support the idea that the magnitude of the SFR is dependent on the SR $Ca^{2+}$ load, and that a partially filled SR results in trabeculae having a greater capacity to respond to stretch (in comparison to an SR that is better loaded), suggesting that the increase in the $Ca^{2+}$ transient amplitude during the SFR is dependent on trans-sarcolemmal $Ca^{2+}$ entry, rather than SR $Ca^{2+}$ load *per se*. Previous studies have implicated NCX as a mechanism for increasing $[Ca^{2+}]_i$ during the SFR. We therefore examined the SL $Ca^{2+}$ flux between unstretched and stretched trabeculae using a combination of caffeine (20 mM) and 2',5'-di(tert-butyl)-1,4-benzohydroquinone (TBQ) (30 µM) added to the superfusate to functionally eliminate SR $Ca^{2+}$ storage (Spencer & Berlin, 1995; Kabbara & Stephenson, 1997). To compare changes in SL flux between stretched and un-stretched trabeculae, $[Ca^{2+}]_o$ was stepped between 1.5 mM and 0 mM. Figure 3.7A illustrates the experimental protocol in a representative trabecula. The SL $Ca^{2+}$ flux following the change in $[Ca^{2+}]_o$ was quantified by measuring the gradient created by $Ca^{2+}$ efflux and influx over a 20 s period. Figure 3.7B, shows that the rate of $Ca^{2+}$ efflux was significantly reduced in the stretched preparation ($0.004 \pm 0.001$ ratio units $s^{-1}$) when compared with the unstretched muscle ($0.008 \pm 0.002$ ratio units $s^{-1}$, $n = 6$). On the other hand, $Ca^{2+}$ influx on re-introduction of 1.5 mM $[Ca^{2+}]_o$ did not differ appreciably between stretched and unstretched trabeculae (data not shown). The dependence of the SL $Ca^{2+}$ flux on NCX was confirmed by the addition of $NiCl_2$, an NCX antagonist. Figure 3.7C shows that both the $Ca^{2+}$ efflux and influx on stepping from 1.5 mM to 0 mM $[Ca^{2+}]_o$ were completely abolished by 5 mM $NiCl_2$ in stretched and un-stretched trabeculae.

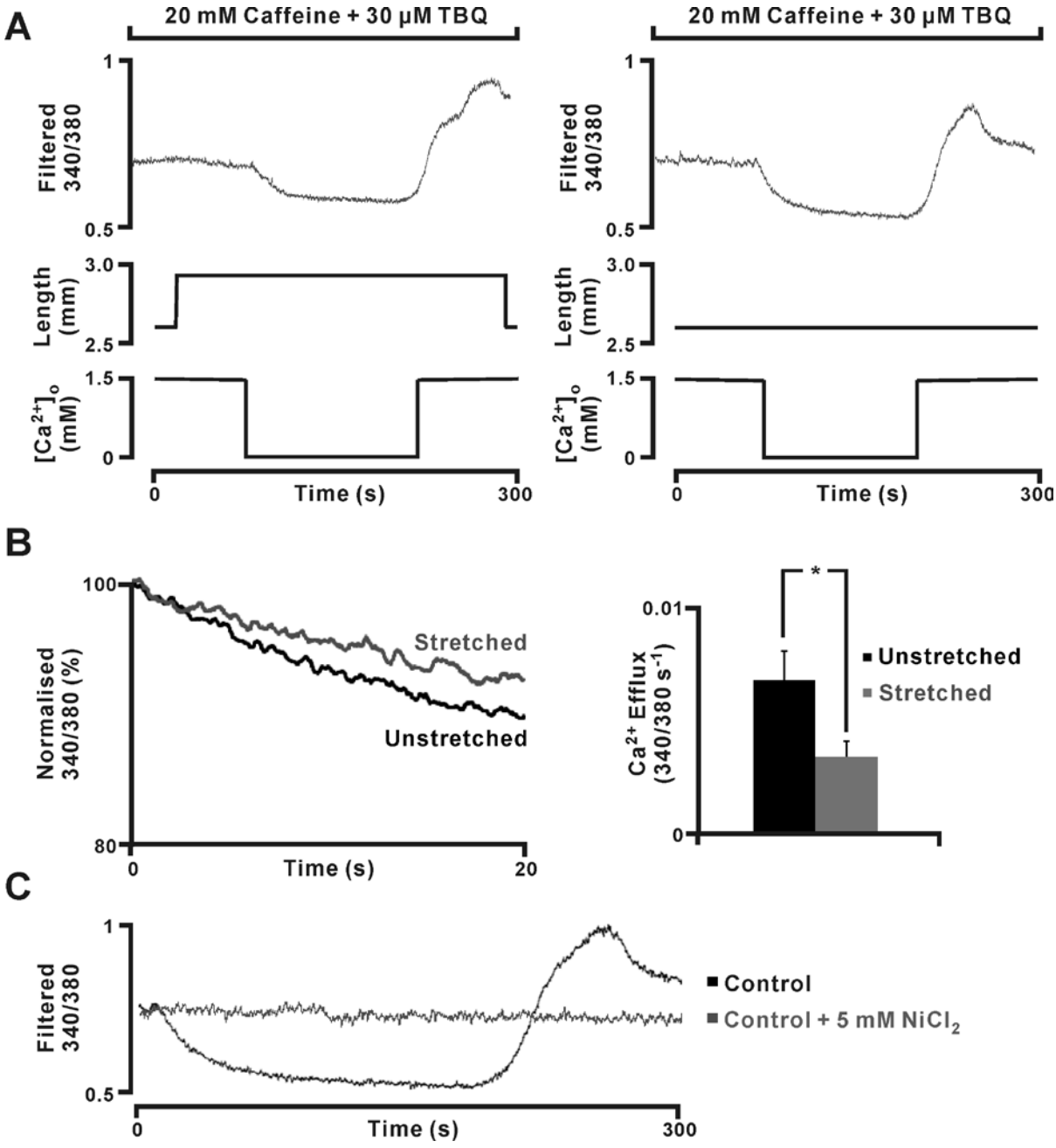


Figure 3.7. Effect of stretch on sarcolemmal $Ca^{2+}$ efflux A, shows the protocol used to assess sarcolemmal $Ca^{2+}$ flux in stretched and unstretched trabeculae. Electrical stimulation of trabeculae was stopped and 20 mM caffeine in conjunction with 30 µM TBQ was added to the superfusate to eliminate the accumulation of $Ca^{2+}$ by the SR, while $[Ca^{2+}]_o$ was subsequently changed from 1.5 mM and 0 mM to observe SL $Ca^{2+}$ efflux. B, shows normalised $Ca^{2+}$ efflux from 6 trabeculae over a period of 20 seconds on the left, while the mean data are graphed on the right. $Ca^{2+}$ efflux in stretched trabeculae was slower than for unstretched trabeculae. C, SL $Ca^{2+}$ flux was completely blocked by addition of 5 mM NiCl, indicating an NCX-dependent mechanism. $*p < 0.05$ between groups, $n = 6$.

## 3.7. Modulation of the SFR by energy consumption

One mechanism that can increase $Na^+$ entry is the NHE, and Cingolani and colleagues have presented considerable evidence for increased activity of the NHE in response to stretch, mediated either directly or via autocrine/paracrine pathways (for reviews see (Kentish, 1999; Cingolani *et al.*, 2013). However, simply increasing NHE activity alone cannot produce a steady state increase in $Na^+$ influx without a concomitant increase in proton supply. This problem prompted an investigation into possible links between pH regulation and metabolic demand during the SFR.

Since it is well known that $H^+$ (along with $CO_2$) is a major by-product of cellular energy metabolism (Vaughan-Jones *et al.*, 2009), we hypothesised that the initial inotropic response to stretch should increase $H^+$ production. This would activate homeostatic mechanisms that maintain intracellular $[H^+]$ and subsequently lead to increased $[Na^+]_i$ influx via NHE-mediated proton extrusion and/or via $Na^+$-$HCO_3^-$ co-transport (NBC) (the latter being acid-equivalent extrusion (Vaughan-Jones *et al.*, 2009)). The subsequent increase in $[Na^+]_i$ would then increase $Ca^{2+}$ via NCX, initiating a force/metabolism-dependent positive feedback that could contribute to the increased $Ca^{2+}$ influx during the SFR. Figure 3.8 displays a simplified schematic of the proposed positive feedback loop.

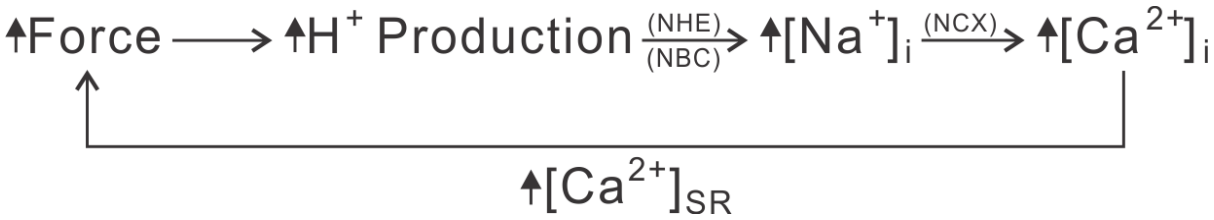


Figure 3.8. Myocardial stretch immediately increases force production in cardiac muscle, which, in turn, increases proton production as a result of increased cross-bridge cycling and metabolic demand. The subsequent increase in $[H^+]_i$ leads to increased accumulation of $[Na^+]_i$ via NHE and/or NBC, which then increases $[Ca^{2+}]_i$ via the reverse-mode NCX. Ultimately, this results in a net increase in SR $Ca^{2+}$ load.

To test this hypothesis, we used two cross-bridge cycling inhibitors, BDM (20 mM) (Backx *et al.*, 1994) and blebbistatin (20 μM) (Farman *et al.*, 2008), at concentrations that abolished twitch force by preventing cross bridge cycling, eliminating the associated metabolic $[H^+]_i$ and $CO_2$ production. Although the SFR *per se* would be eliminated when the twitch was blocked, we know that the SFR is due to the increase in the amplitude of the $Ca^{2+}$ transient after stretch (Allen & Kurihara, 1982). Therefore changes in the amplitude of the $Ca^{2+}$ transient in these conditions would have produced a SFR, were cross-bridge cycling not inhibited. Put another way, changes in the $Ca^{2+}$ transient amplitude could be used as a reliable proxy for force production, which is acceptable because length is constant after the stretch.

Figure 3.9 shows the increase in $Ca^{2+}$ transient amplitude (% initial response) 3 minutes after stretch before (control) and during cross-bridge inhibition. Examples of $Ca^{2+}$ transients from representative trabeculae are shown on the right hand panel immediately on stretching the trabeculae (a) and following 3 min of stretch (b) for both of the inhibitors used. Figure 3.9A shows that BDM reduced the stretch-dependent increase in the $Ca^{2+}$ transient amplitude associated with the SFR from 8.8 ± 0.9% in control to 2.5 ± 1.1% in BDM ($p = 0.002$, $n = 6$). As shown in figure 3.9B, the more selective cross-bridge cycling inhibitor blebbistatin blocked the SFR-linked change in $Ca^{2+}$ even more effectively. The stretch-dependent increase in $Ca^{2+}$ transient during the SFR was reduced by blebbistatin to 1.3 ± 1% compared to 9.2 ± 2.1% in control ($p = 0.004$, $n = 5$). It should be noted that neither of these agents appeared to affect SR $Ca^{2+}$ cycling as both diastolic $Ca^{2+}$ and the decay time-course of $Ca^{2+}$ transients were not significantly affected by their application.

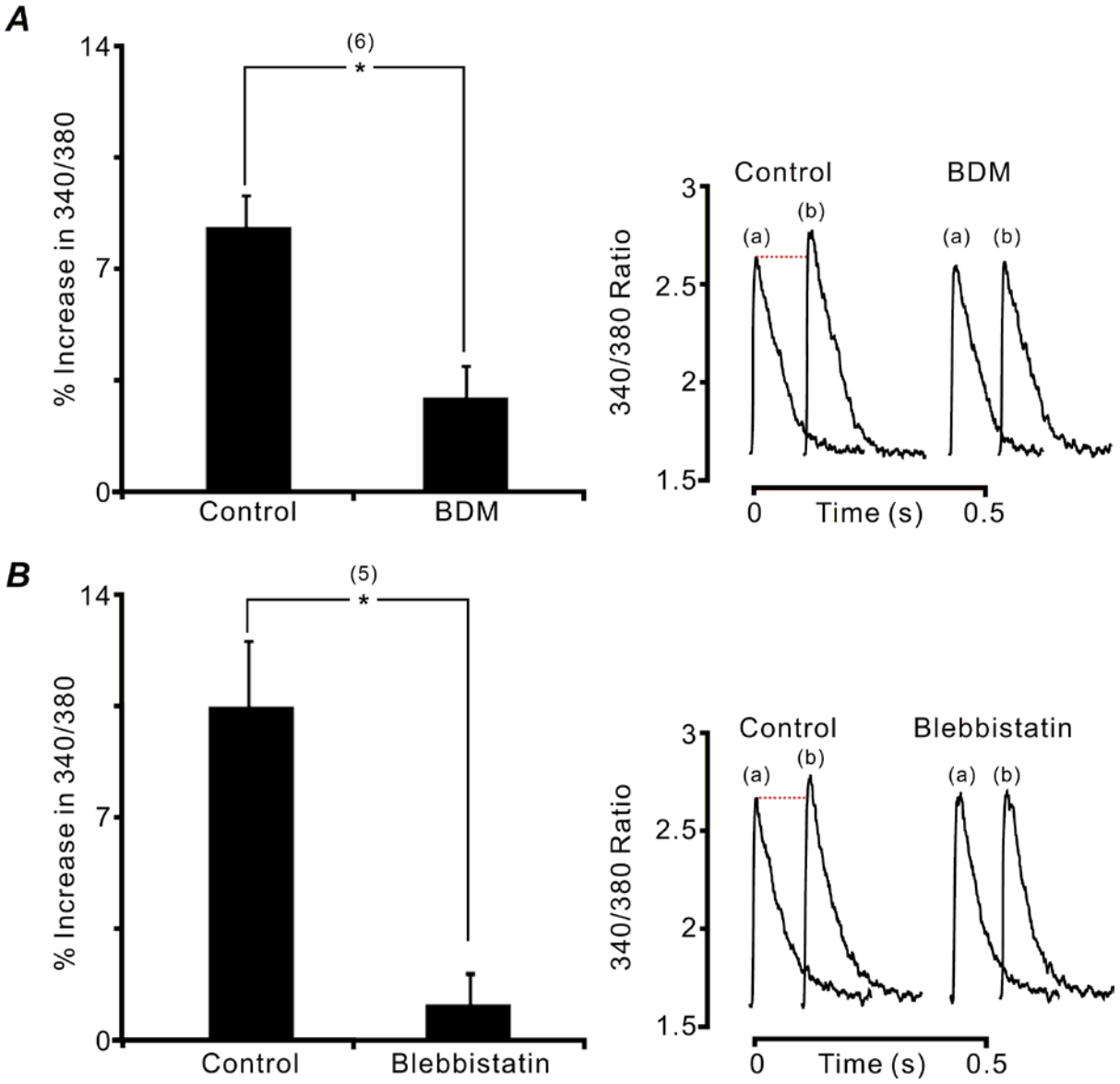


Figure 3.9. Inhibition of force production reduces the stretch-dependent increase in $[Ca^{2+}]_i$. Trabeculae stimulated at 2 Hz were exposed to inhibitors of cross-bridge cycling at concentrations that abolished twitch force. They were then subjected to a 3 min step increase in length from 90% to 100% $L_o$. The mean ± SEM change in $Ca^{2+}$ transient amplitude (340/380 ratio) after 3 min of stretch is shown (% initial response), with exemplar $Ca^{2+}$ transients for the initial response (a) and following 3 minutes (b) stretch shown to the right for control and during inhibition of cross-bridge cycling. Both BDM (20 mM), A, and blebbistatin (20 µM), B, reduced the stretch-dependent increase in $[Ca^{2+}]_i$ associated with the SFR. $*p < 0.05$ against control, with the number of trabeculae shown in brackets.

To directly assess changes in intracellular $H^+$ production associated with the SFR, the ratiometric fluorescence indicator 2',7'-Bis-(2-Carboxyethyl)-5-(and-6)-Carboxyfluorescein (BCECF) was used. BCECF was first introduced by Tsien and colleagues in 1982 (Rink *et al.*, 1982), and has been used extensively in cardiac preparations (Alvarez *et al.*, 1999; Kockskamper *et al.*, 2008a; De Giusti *et al.*, 2009), and a number of other cells types (Cho *et al.*, 1998; Taylor *et al.*, 2006; Carraro-Lacroix *et al.*, 2009) as a determinant of intracellular pH.

The loading protocol for BCECF was similar to that used for fura-2/AM loading described in Chapter 2. Briefly, 10 µM BCECF/AM (Teflabs, TX, USA) was dissolved in 20 µl of warmed anhydrous dimethyl sulfoxide (DMSO) with 5% wt/vol of pluronic F-127. The loading duration was 2 hours at room temperature, 1 mM $[Ca^{2+}]_o$ and 0.2 Hz stimulation. Emitted fluorescence intensity at 535 nm (excited at 490 nm and 440 nm) was acquired using the Optoscan monochromator system (Cairn Research, Faversham, Kent, UK). The ratio of 490 nm to the isosbestic wavelength 440 nm (after being subtracted from autofluoresence) was used as a measure of intracellular pH. On average, the fluorescence of 490 nm increased from 0.89 ± 0.02 to 2.81 ± 0.01 after a 2 hour loading, while the fluorescence of 440 nm increased from 0.21 ± 0.01 to 0.44 ± 0.01 for the same duration, $n = 3$.

The validity of BCECF loading was further assessed by delivering an ammonium choloride, $NH_4Cl$, prepulse to the trabecula and observing the subsequent change in BCECF fluorescence intensity (Boron & De Weer, 1976; Kim & Smith, 1988; Wallert & Frohlich, 1989). The idea is that the uncharged base $NH_3$ is formed upon dissociation of $NH_4Cl$ in solution. Its entry into the cell causes rapid alkalinisation as it takes up a free intracellular protons, leading to an increase in $pH_i$. Figure 3.10 shows a representative recording of the fluorescence response of 490 nm and 440 nm during the acid loading protocol. As expected, there was an immediate rise in 490 nm fluorescence following the addition of 20 mM $NH_4Cl$. This initial increase is not maintained, and undergoes a re-acidification process that is thought to be due to a slow entry of $NH_4^+$ (Boron & De Weer, 1976). Upon removal of $NH_4Cl$, pH begins to recover, albeit at a very slow pace. Throughout this procedure, the 440 nm fluorescence intensity remain effectively unchanged.

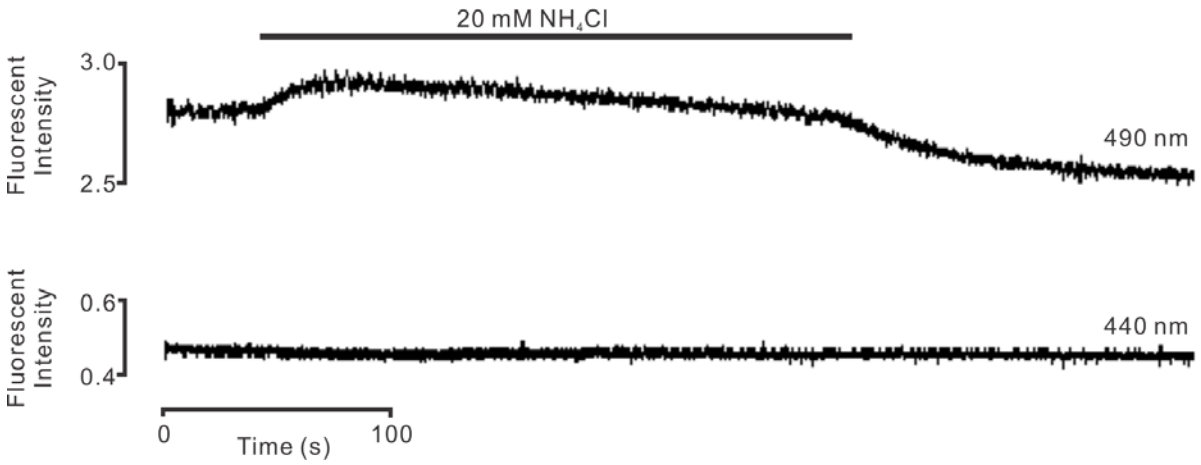


Figure 3.10. Changes in $pH_i$ in one rat RV trabecula as measured by BCECF fluorescence before, during and after the addition of $NH_4Cl$. Field stimulation was switched off during protocol.

Calibration of BCECF was performed using the High $K^+$/nigericin method described previously (Thomas *et al.*, 1979), where nigericin, a $K^+$-$H^+$ ionophore, is used in the presence of high extracellular $K^+$ to manipulate intracellular $H^+$ concentration. The calibration solution contained (in mM): 140 KCl, 1.2 MgSO4, 1.2 KH2PO4, 10 HEPES, 0.01 nigericin, 10 Glucose and 1 $CaCl_2$. The calibration buffers were adjusted with NaOH in order to obtain 4 different values of pH: 6.145, 7.098, 7.805 and 8.534. At the end of an experiment, the trabecula was superfused with each calibration buffer for a period of 10 minutes until new steady state fluorescence intensity was reached. A calibration curve of fluorescence ratio (490/440) as a function of pH was constructed (figure. 3.11) from 4 separate experiments. This curve was used for comparison with experimental data. Here, the mean ± SEM pH at diastolic steady-state was 7.04 ± 0.014, $n$ = 4.

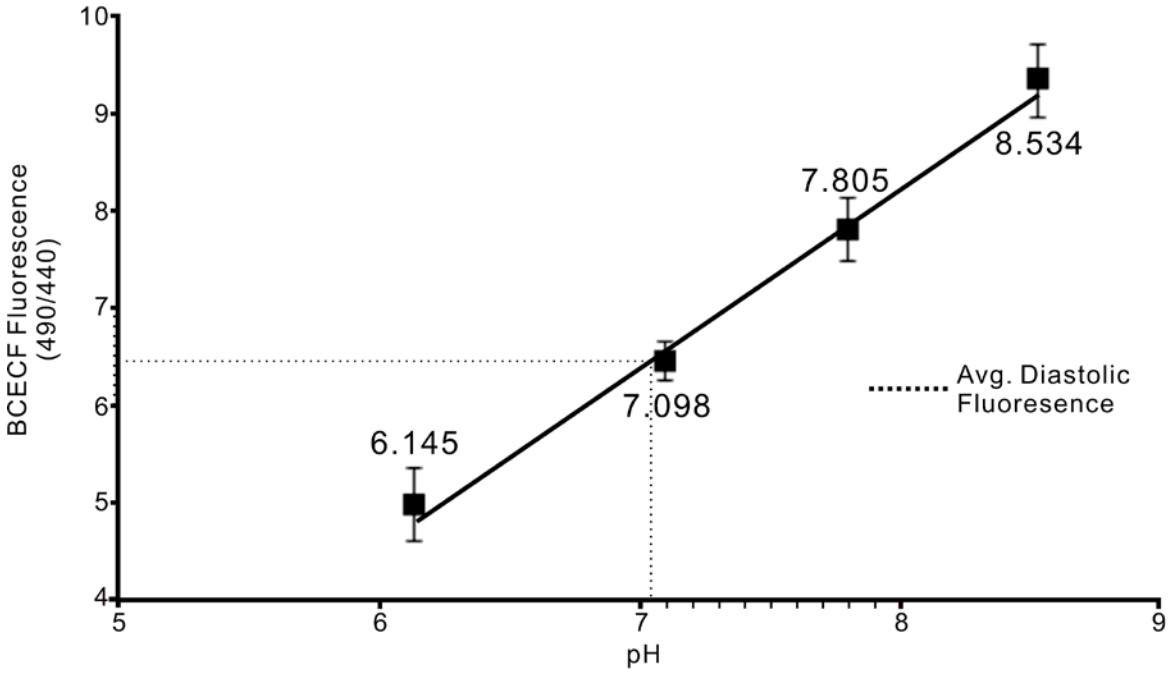


Figure 3.11. In vivo calibration of BCECF in rat RV trabeculae. BCECF fluorescence intensity correlates linearly with intracellular pH in the range of pH examined. Dashed line indicate the mean diastolic fluorescence, $n = 4$.

The SFR and the change in intracellular $H^+$ associated with it was examined in a $HCO_3^-$-free environment (HEPES buffered solution). If the hypothetical pathway suggested in figure 3.8 proves to be accurate, one would expect a reduction in $pH_i$ to accompany the SFR. As shown by figure 3.12A, stretch under current conditions was associated with a slow acidification in BCECF-loaded trabeculae as the SFR developed. In 5 trabeculae, the average SFR (in %) was 23.1 ± 2.7 and was accompanied by a reduction in $pH_i$ (in %) of 3.3 ± 0.01, $p = 0.003$, $n = 5$. Consistent with the previous finding, figure 3.12B shows that both stress and the stretch-dependent acidification were inhibited by BDM. Here, the average observed decrease in pH (in %) was 0.7 ± 0.001, though this was not significantly different from the pH recorded at diastolic steady state, $p = 0.194$, $n = 4$. To ensure that the absence of this stretch-dependent acidification is not due to non-specific effects of BDM, trabeculae were also subjected to a period of quiescent stretch. Figure 3.12C shows a pH response to stretch very similar to what was observed in BDM-treated trabeculae. The reduction in pH here (in %) from baseline was 0.018 ± 0.003, though again, this change was not statistically significant, $p = 0.225$, $n = 3$.

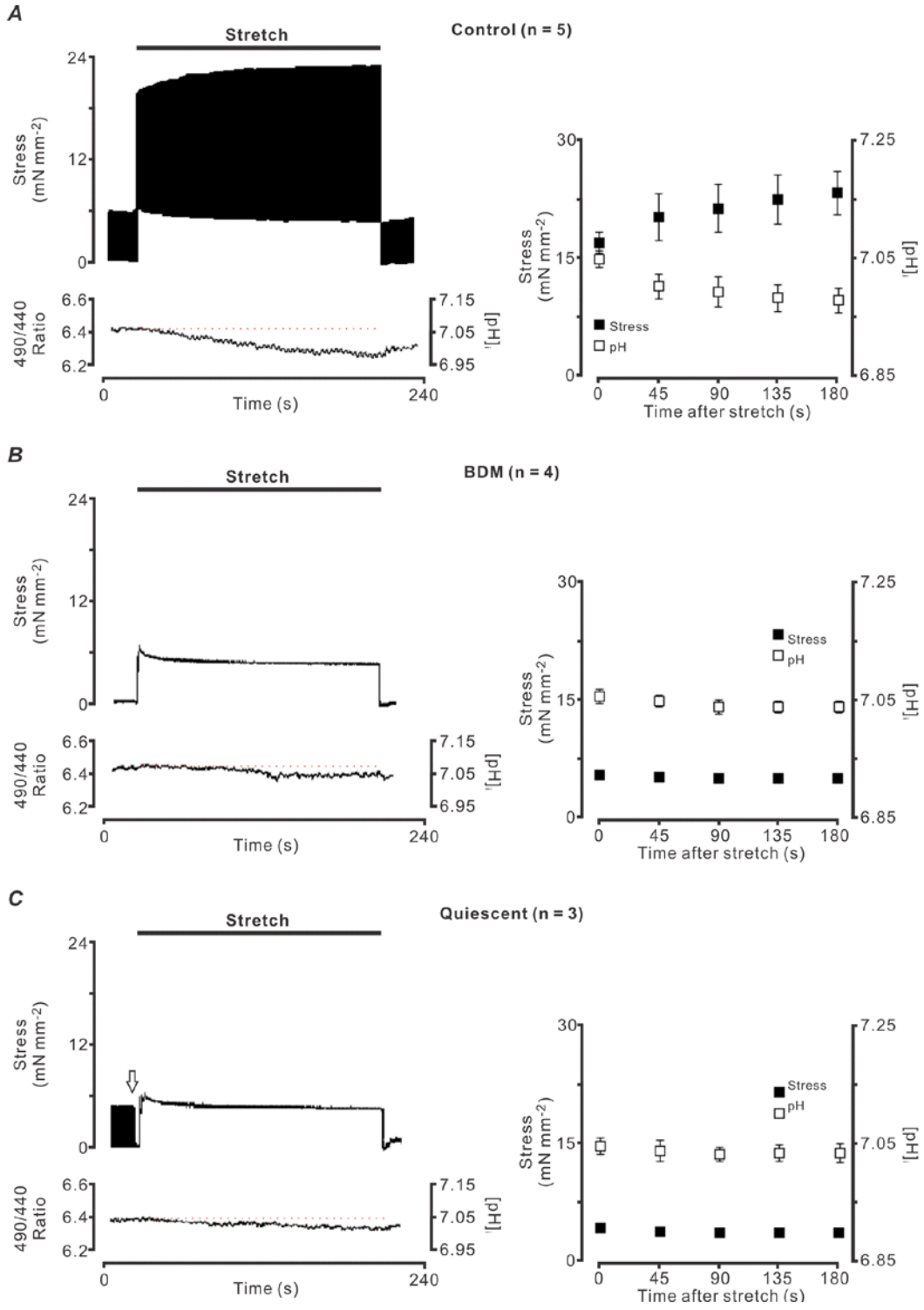


Figure 3.12. Stretch-mediated decrease in intracellular $H^+$ concentration. Left hand panels show representative traces of stress and pHi responses following stretch. Right hand panels display pooled data in mean ± SEM stress (black squares) and intracellular pH changes (open squares) during the SFR in HEPES-buffered solution. A, B and C represent responses in control, during 20 mM BDM superfusion and quiescent stretch, respectively. The arrow in C, denotes the point at which field stimulation was switched off. Inhibition of the cross-bridge cycle greatly reduced the change in $[pH]_i$ associated with stretch, as did quiescent stretch where force of contraction was completely absent.

## 3.8. Role of sodium-hydrogen exchange and bicarbonate transport

To further test the idea that the increased metabolic demand associated with the initial inotropic response was related to increased proton supply and hence to $Na^+$ entry via NHE and NBC, we used HOE642 to inhibit NHE, and either 4,4'-Diisothiocyano-2,2'-stilbenedisulfonic acid (DIDS) to inhibit $HCO_3^-$ transport or removal of $HCO_3^-$ from the superfusate. In $HCO_3^-$-containing solutions (K-H), inhibition of NHE with HOE642 did not affect the magnitude of the SFR, while inhibition of the $Na^+$-$HCO_3^-$ transport with DIDS increased the magnitude of the SFR (figure 3.13, $p$ = 0.001). However, simultaneous application of DIDS and HOE642 caused a marked decrease in the SFR. Removal of $HCO_3^-$ from the extracellular solution (labelled 'control' figure 3.13) produced a SFR similar to that seen in $HCO_3^-$-containing solutions in the presence of DIDS. In the absence of extracellular $HCO_3^-$, application of HOE642 caused a decrease in the SFR ($p$ = 0.01) to a level similar to that seen in the presence of DIDS and HOE642 in $HCO_3^-$-containing solutions. SN-6 (an inhibitor of NCX) was able to prevent most of the SFR, confirming that NCX is involved in the generation of the SFR (figure 3.13). However, we note that SN-6 is a rather poor blocker of forward mode exchange (Iwamoto *et al.*, 2004), which might explain the incomplete block of the SFR, although it is notable that neither blocking SL acid transport nor NCX eliminated the SFR completely.

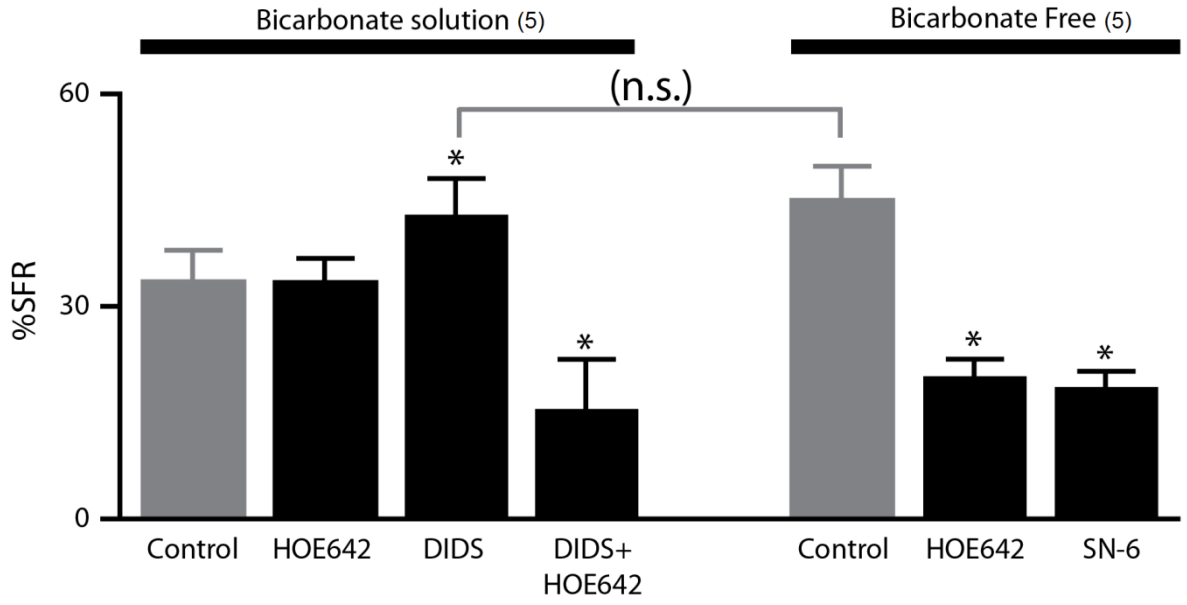


Figure 3.13. Effects of acid transport inhibition on the SFR. The magnitude of the SFR in bicarbonate-buffered (K-H) and HEPES-buffered solutions is shown, together with inhibitors of NHE (1 µM HOE642) and sarcolemmal $HCO_3^-$ transport (0.5 mM DIDS). In K-H buffered solution, application of HOE642 did not affect the SFR, whereas DIDS (0.5 mM) significantly increased SFR magnitude. Application of DIDS (0.5 mM) in conjunction with NHE inhibition significantly reduced the SFR. In bicarbonate-free HEPES buffer, HOE642 significantly reduced the SFR. Application of SN-6 (10 µM), a reverse-mode NCX inhibitor, significantly reduced the SFR. $*p < 0.05$ against control in bicarbonate and bicarbonate-free solutions, with the number of trabeculae shown in brackets. There was no significant (n.s.) difference between DIDS in bicarbonate solution, and the bicarbonate-free control solution.

## 3.9. The role of Angiotensin II and Endothelin in the SFR

A critical step in the NHE-mediated pathway previously described involves the increased release of angiotensin II (Ang II) following stretch, which in turn increases intracellular $Ca^{2+}$ via reduced NCX $Ca^{2+}$ extrusion (Cingolani *et al.*, 1998; Alvarez *et al.*, 1999). Figure 3.14A shows that the application of 1 μM Ang II produced a slow increase in force in rat trabeculae held at fixed length ($L_o$). In addition, figure 3.14B reveals that this increase in force was blocked by 1 μM losartan, an angiotensin II type 1 ($AT_1$) receptor blocker, in agreement with previous reports (Feolde *et al.*, 1993). Interestingly, figure 3.14C shows that when trabeculae were subjected to our stretch protocol (from 90% to 100% $L_o$) in the presence of losartan, there was no change in the magnitude of the SFR ($p = 0.15$, $n = 6$). Another important part of this pathway is thought to involve an increase in ET-1release that occurs downstream of Ang II after stretch (Alvarez *et al.*, 1999). However, the application of the selective $ET_A$ receptor antagonist BQ-123 (0.5 μM) was unable to block the SFR as summarised in figure 3.14C ($p = 0.21$, $n = 4$). These results suggest that the SFR in our preparation is mediated by neither stretch-dependent Ang II nor ET-1 secretion.

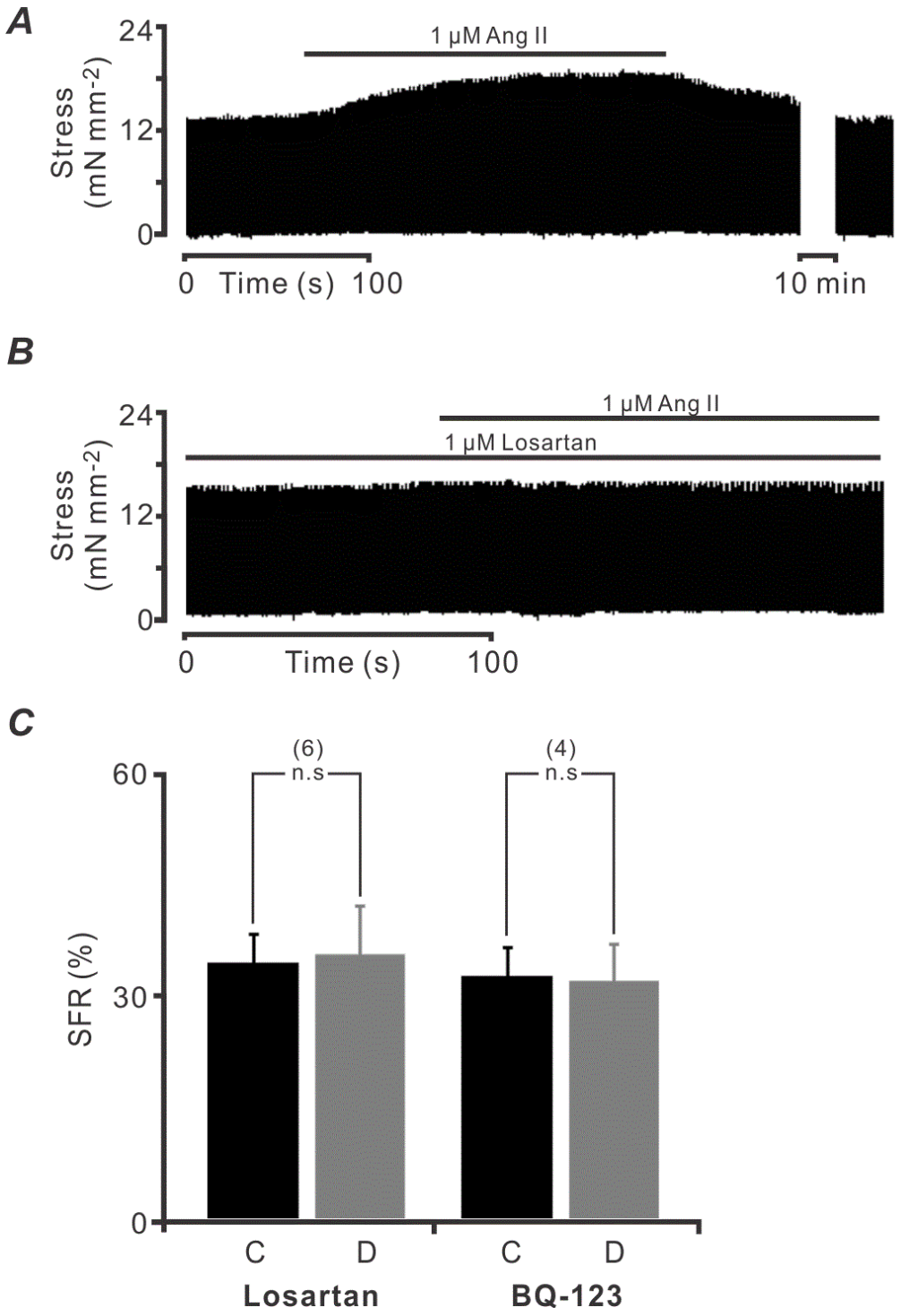


Figure 3.14. Trabeculae response to angiotensin and the absence of a losartan-sensitive component in the SFR. A, shows the positive inotropic response to 1 µM angiotensin in a representative trabecula, which was blocked completely by addition of 1 µM losartan, as shown in B. (2 Hz stimulation frequency 1.5 mM $[Ca^{2+}]_o$ and 37ºC.) Blocking the angiotensin II receptors with losartan had no effect on the magnitude of the SFR (n.s). C, shows mean ± SEM SFR for trabeculae subjected to stretch when either 1 µM losartan or 0.5 µM BQ-123 was present in the superfusate ($p$ = 0.15, $n$ = 5 trabeculae).

## 3.10. The role of reactive oxygen species in the SFR

Previously, it was shown that during the SFR, there is a NAPDH oxidase-mediated increase in mitochondrial reactive oxygen species (ROS) (Caldiz *et al.*, 2007). The increase in ROS occurs as a response to stretch-induced Ang II release and acts via NHE. The effects of two ROS scavengers N-2-mercaptopropionylglycine (MPG) and 4,5-dihydroxy-1,3-benzenedisulfonic acid (Tiron) were separately investigated. Figure 3.15 shows the mean ± SEM data of the two ROS scavengers. In 2 mM MPG, the magnitude of the SFR (in %) was 35.8 ± 2.2 vs. 35.5 ± 2.7 in control, $p > 0.05$, $n = 4$. In 10 mM Tiron, the SFR was 36.5 ± 3.5 vs. 35.5 ± 2.7 in control, $p > 0.05$, $n = 4$.

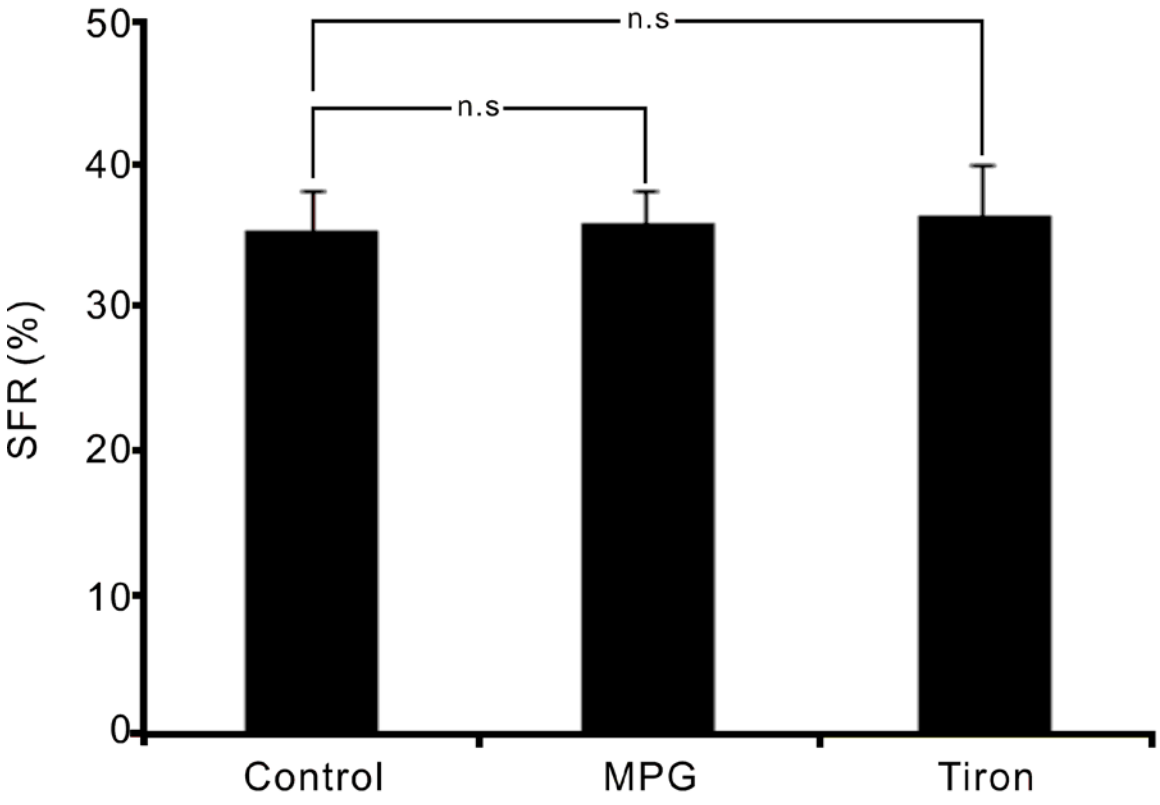


Figure 3.15. Effects of reactive oxygen scavengers on the SFR. Neither MPG (2 mM, $n = 4$) nor Tiron (10 mM, $n = 4$) were able to reduce the magnitude of the SFR at 2 Hz stimulation frequency, 1.5 mM $[Ca^{2+}]_o$ and 37ºC.

## 3.11. The role of microtubules in the SFR

There is evidence to suggest that microtubule formation plays a critical role in the stretch-mediated increase in $Ca^{2+}$ spark rate in rat myocytes (Iribe *et al.*, 2009). This response did not appear to be dependent on nitric oxide or stretch-activated channels and was relatively short lived. Incubation of trabeculae with 20 µM colchicine, an inhibitor of microtubule polymerisation, for a period 2 hours was unable to abolish the SFR. Figure 3.16 compares the mean ± SEM SFR between control and colchicine-treated preparation. In control, the magnitude of the SFR (in %) was 36.7 ± 5.6, whereas the SFR post colchicine treatment was 38.9 ± 5.8 ($p < 0.05$, $n = 3$).

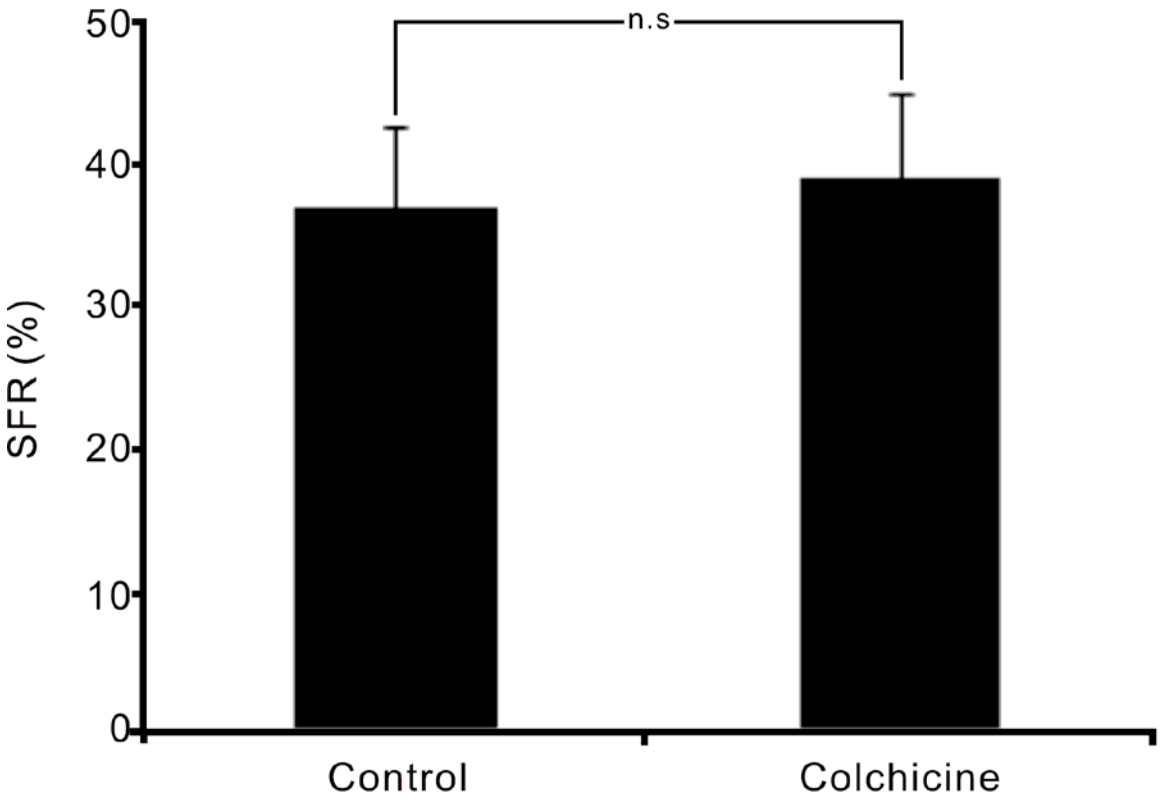


Figure 3.16. Effects of microtubule inhibition on the SFR. 2 hour incubation of colchicine (20 µM, $n = 3$) did not reduce the magnitude of the SFR at 2 Hz stimulation frequency, 1.5 mM $[Ca^{2+}]_o$ and 37ºC.

## 3.12. Chapter Summary and Discussion

The stretch-dependent increase in the intracellular $Ca^{2+}$ transients underlying the SFR was first shown by Allen and Kurihara in 1982 (Allen & Kurihara, 1982) and there is good evidence that the increase in $Ca^{2+}$ is linked to an increase in $Na^{+}$ via NCX. The source of the $Na^{+}$ appears highly preparation dependent with NHE and/or stretch activated channels being implicated. The role of NHE has been extensively studied, although simply increasing NHE activity cannot increase $Na^{+}$ influx in steady state as it is limited by proton supply (production rate). It appears that this point has been previously overlooked by workers in the field. Results presented in the current chapter are generally in agreement with a role for NCX and NHE in the SFR, but extend previous work by examining the roles of cross-bridge cycling and $HCO_3^-$ transport. Here, for the first time, I have shown that when cross-bridges are inhibited, the increase in $Ca^{2+}$ transient amplitude (that underlies the SFR) is also inhibited. This immediately suggests that force and/or metabolic demand contribute to the SFR in our preparation. Since stretch produces an immediate increase in force, it seems highly plausible that this should lead to increased metabolic proton production, without excluding contributions to the SFR from other possible mechanisms. Others have shown that the initial inotropic response to stretch is accompanied by an increase in myofilament sensitivity to $Ca^{2+}$ (Allen & Kentish, 1985; Monasky *et al.*, 2010), which may continue in part during the SFR. However, a possible slow increase in myofilament sensitivity to $Ca^{2+}$ does not explain the increase in $Ca^{2+}$ transient amplitude during the SFR, which is sufficient to explain the SFR by itself. In any case, without other changes, increased $Ca^{2+}$ binding to troponin C should *decrease* $Ca^{2+}$ transient amplitude.

The ability of the SR to increase $Ca^{2+}$ cycling during the SFR was also critical to the magnitude of the SFR, since modulating SR content via rate or external $Ca^{2+}$ also modulated the SFR. These results are reminiscent of the previously reported ability of β-adrenergic stimulation to abolish the SFR (Todaka *et al.*, 1998) since β-adrenergic stimulation also increases SR $Ca^{2+}$ content via enhanced SR $Ca^{2+}$ uptake.

### 3.12.1. Metabolic links to the SFR

The results presented here confirm that the SL acid extrusion systems (acid-equivalent $HCO_3^-$ transporters and NHE) contribute to the SFR. It is well known that metabolic demand is increased by inotropic interventions (Bountra *et al.*, 1988; Vaughan-Jones *et al.*, 2009). The results obtained in this study with inhibitors of acid extrusion can be explained by the relative roles of the acid regulation systems under conditions of increased metabolic demand produced by the initial inotropic response to stretch. Figure 3.17 shows a schematic diagram of how the SFR may be modulated by the acid extrusion systems. Both NHE and $Na^+$-independent $Cl^-$-$HCO_3^-$ exchanger (CBE) have been implicated in the SFR (Alvarez *et al.*, 1999; Pérez *et al.*, 2001; Cingolani *et al.*, 2003; Lewinski *et al.*, 2003; White, 2004). The importance of NHE in the SFR is supported by siRNA NHE-1 down regulation inhibiting the SFR (Perez *et al.*, 2011). However, in $HCO_3^-$ containing solutions, proton regulation is assisted by the $HCO_3^-$ transporters that can neutralize acid with the assistance of intracellular carbonic anhydrases (Scheibe *et al.*, 2006). The combination of these mechanisms limit pH changes associated with increased work (Vaughan-Jones *et al.*, 2006), but do so by increasing $Na^+$ influx and (via NCX) $Ca^{2+}$. Note that changes in $[Na^+]_i$ following stretch were not directly measured in this study, despite it being a crucial component in the proposed pathway. There were two reasons for this: (i) The $[Na^+]_i$ indicator SBFI yields a very noisy signal at physiological temperature, making it difficult to detect very small changes in $[Na^+]_i$ in our hands, and at room temperature, a 10 mM change in $[Na^+]_i$ results in a change of only 0.1 ratio units (unpublished data M. Ward). Previous studies have demonstrated an increase in $[Na^+]_i$ with stretch, which ranges between 1 mM and 2 mM (Cingolani *et al.*, 2003; Kockskamper *et al.*, 2008a). (ii) Changes in activity of $Na^+$ transporters and exchangers do not necessarily result in large changes in $[Na^+]_i$, unless they are blocked using pharmacological agents.

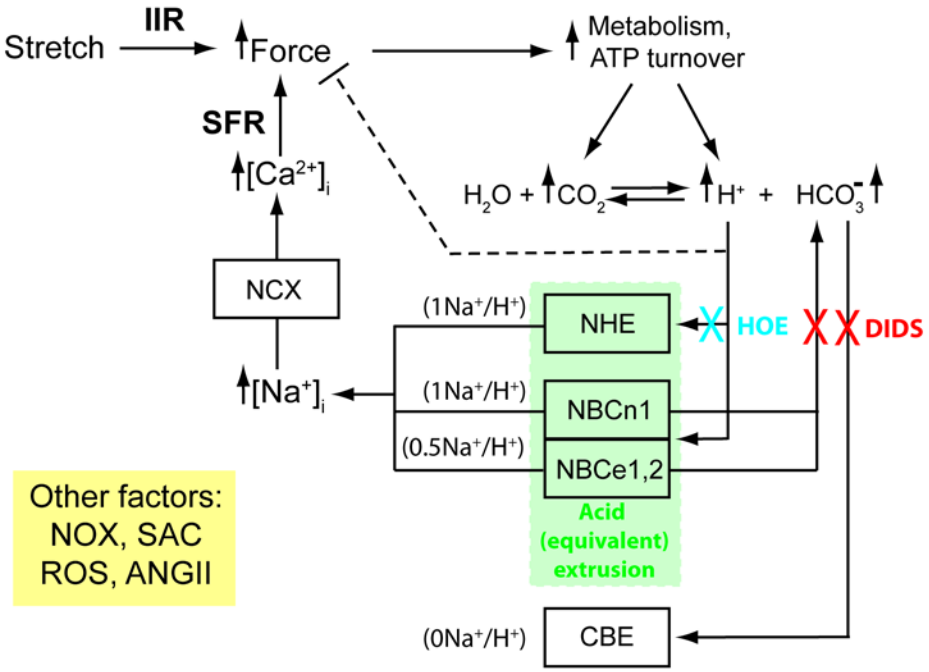


Figure 3.17. Proposed positive feedback mechanism within the SFR. Myocardial stretch immediately increases force production in cardiac muscle (the initial inotropic response, IIR) due mainly to increased myofilament $Ca^{2+}$ sensitivity. This in turn increases proton production as a result of increased cross-bridge cycling and metabolic demand. The subsequent increase in $[H^+]_i$ leads to increased $Na^+$ entry and $[Na^+]_i$ via sarcolemmal NHE and NBC (green filled rectangle, with the relative stoichiometries for $Na^+$ and $H^+$ shown in brackets to the left), which then increases $[Ca^{2+}]_i$ via NCX. In $HCO_3^-$-buffered solution, the increase in $[Na^+]_i$ results from the activity of both NHE and NBC, with the relative contribution of NBC dependent on the stoichiometry of the isoforms present (NBCn1: NBCe1,2). Ultimately, the increase in $[Na^+]_i$ (which is limited by the $Na^+$-dependence of $Na^+$ extrusion by the $Na^+/K^+$ ATPase) results in a net increase in SR $Ca^{2+}$ content and twitch force, which in turn increases cross-bridge cycling and metabolic demand. The acid-equivalent extrusion pathways inhibited by HOE642 (blue X), and $HCO_3^-$-free solution or DIDS (red X), are indicated. Other factors that are thought to contribute to the SFR are shown in the yellow rectangle (NOX, sarcolemmal NADPH oxidase; SAC, stretch-activated channels; ROS, reactive oxygen species; ANGII, angiotensin II).

A key feature of the pathways shown in figure 3.17 is that NBC, NHE and CBE are not equivalent in terms of $Na^+$ entry per proton extruded. In the heart there are both electro-neutral (NBCn1) and electrogenic (NBCe1,2) NBC isoforms expressed (for review see (Vaughan-Jones *et al.*, 2009)), which means the net $Na^+$ entry per proton extruded by the NBC isoforms will be less than that associated with NHE which has a 1:1 stoichiometry. The similar increase in the magnitude of the SFR in $HCO_3^-$-free solutions and when $HCO_3^-$ transport is blocked with DIDS can therefore be explained by acid extrusion being mediated (in these conditions) solely by NHE whose 1:1 stoichiometry implies a greater net $Na^+$ influx than when the NBC isoforms are active (Vaughan-Jones *et al.*, 2006). The slow acidification that develops with stretch when $HCO_3^-$ transport is blocked would tend to decrease the inotropy associated with the SFR by inhibiting cross-bridges, but is clearly insufficient to counteract the acid-dependent increase in $[Na^+]_i$ that subsequently increases SR $Ca^{2+}$ content and $Ca^{2+}$ transient amplitude.

In support of the proposed feedback mechanism outlined in figure. 3.17, current experimental data have shown that cross-bridge cycle inhibitors can block a large fraction of the increased $Ca^{2+}$ transients that accompany the SFR, consistent with the idea that the increased metabolic demand from the initial inotropic response leads to increased $Na^+$ entry. Together, these results suggest that up to ~50% of the SFR may be attributed to the metabolic linkage proposed. It is worth noting that the variable stoichiometry of the NBC system provides a novel way for the heart to respond to increased work; when proton flux increases, so does $Na^+$ entry, which leads to an increase in intracellular $Na^+$ (which is ultimately limited by $Na^+/K^+$ ATPase activity) and intracellular $Ca^{2+}$. The latter is cycled via the SR to increase the force of contraction, offsetting any negative inotropic effects that might arise from acidification. Therefore, by altering the relative expression of electroneutral and electrogenic NBC isoforms, the cell may tune the relative inotropy produced by this system. This may provide an explanation for the benefit of expressing multiple forms of NBC and, in connection with this point, we note that the expression of the electrogenic NBC isoform is reduced in a myopathic model (Khandoudi *et al.*, 2001).

Since increasing extracellular $Ca^{2+}$ increases inotropy (and therefore metabolic demand), one might expect the mechanism described above to be activated by this intervention. However, the SFR is dependent on $Ca^{2+}$ cycling via the SR (Lewinski *et al.*, 2004), and, as shown via the rate-dependence of the magnitude of the SFR and force in section 3.5, high SR $Ca^{2+}$ content limits the magnitude of the SFR (figure 3.6). Therefore, increasing metabolic demand

by increasing extracellular $Ca^{2+}$ would not be expected to show a large SFR because the SR would be maximally filled in this condition (Bassani *et al.*, 1995). In connection with this point, since the SFR provides a significant inotropy within the Frank-Starling mechanism, failing hearts with increased sympathetic drive may be less able to raise force when stretched which would lead to increased ventricular dilation.

### 3.12.2. Other mechanisms in the SFR

It is apparent that under the current experimental protocol, a significant fraction of the SFR is mediated by a pathway that is not linked to proton-dependent $Na^+$ entry. One pathway that has been proposed is an Ang II-mediated increase in NHE activity (Alvarez *et al.*, 1999) (for a review, see (Cingolani *et al.*, 2011)). Although the current preparation responded to Ang II, losartan did not block the SFR, which immediately suggested that this pathway is not a significant contributor to the SFR in this study (see also (Calaghan & White, 2001; Lewinski *et al.*, 2003; Kockskamper *et al.*, 2008b)). Furthermore, some groups (Pérez *et al.*, 2001; Luers *et al.*, 2005) have reported cellular alkalinisation during the SFR (albeit at a much longer time period after the initial stretch than investigated in our study). This contrasting observation could potentially be explained by the proposed activation of $HCO_3^-/Cl^-$-exchange by an Ang II-dependent mechanism (Pérez *et al.*, 2001), although this did not appear to be the case here since there was no increase in intracellular pH when cross-bridge cycling was inhibited.

Previously, the SFR was linked to increased mitochondrial ROS production (Caldiz *et al.*, 2007). However, the application of ROS scavengers in this study was unable to abolish the SFR. The increase in ROS appears to be secondary to the initial release of Ang II following stretch (Caldiz *et al.*, 2007). Given that Ang II is not the primary component underlying the SFR in the current study, it is probably not surprising to find that inhibition of ROS does not alter the magnitude of the SFR in our experiments.

One study using isolated rat cardiomyocytes gave evidence for a microtubule-mediated regulation of stretch-induced increase in $Ca^{2+}$ spark rate (Iribe *et al.*, 2009). At present, pre-incubating rat trabeculae with colchicine was unable to modulate the SFR. It is worth noting that the increase in $Ca^{2+}$ spark rate in response to myocyte stretch is relatively short-lived (peaking within 5 seconds before dropping back to basal rates within a minute), the SFR typically takes 10 to 15 minutes to fully develop. Therefore, it is unlikely that such a transient increase in $Ca^{2+}$ can significantly alter the SFR.

There is pharmacological evidence for a stretch-activated ion channel being involved in the SFR (White, 2004; Ward *et al.*, 2008), possibly activated by cytoskeletal linked NOX production (for review see (Prosser *et al.*, 2013)). This pathway could provide a straight-forward explanation for the observation that diastolic length changes can produce a SFR (Allen *et al.*, 1988). However, it should be noted that changing diastolic length also increases metabolic demand via the Feng effect (Gibbs *et al.*, 1967), so the observation of a SFR induced by diastolic length changes does not rule out a contribution via the metabolic pathway described here.

In conclusion, we have shown for the first time that elimination of cross-bridge cycling markedly reduces the stretch-dependent increase in the intracellular $Ca^{2+}$ transients that accompanies the SFR. We suggest this is linked to the metabolic consequences of stretch and cross-bridge cycling (i.e. proton production) via SL acid-equivalent efflux pathways that increase $[Na^+]_i$ and subsequently $[Ca^{2+}]_i$ via NCX. Since the SFR depended on the degree of SR $Ca^{2+}$ loading (in our experiments increased $[Ca^{2+}]_o$ was the *only* completely effective blocker of the SFR), these results may also help reconcile disparate reports and explanations for the SFR. We stress that this pathway may *not* explain the entire SFR in all preparations, but should be considered as a potentially important contributory factor in the SFR. In this regard, the metabolic link we have uncovered represents a novel positive feedback pathway that augments force under conditions of increased proton production (which also includes all sources of metabolic demand) and may provide a pathway for modulating force in disease states.

# Chapter 4. Contribution of Extra-Humoral Factors to the SFR

## 4.1. Chapter Overview

Myocytes account for only 30 to 35% of the total cell number in the adult rat heart, while the remaining 65 to 70% non-muscle cell types consists of endothelial cells, fibroblasts, pericytes, smooth muscle cells and macrophages (Nag, 1980). While studies have linked the SFR with the release of autocrine/paracrine factors such as angiotensin II (Ang II) and endothelin-1 (ET-1) (Alvarez *et al.*, 1999; Cingolani *et al.*, 2003; Pérez *et al.*, 2003), results from previous experiments (see Chapter 3) failed to demonstrate a linkage between Ang II and the SFR. This chapter outlines the identification process of paracrine/autocrine factors released with stretch using a bioassay system in conjunction with mass spectroscopy (MS). Furthermore, the effect of these substances on the SFR was also examined.

## 4.2. Bioassay System

In order to determine whether stretching cardiac muscles results in the release of paracrine/autocrine inotropic factors, a bioassay system was developed. The setup consists of two principal components: an 'upstream' whole heart in Langendorff configuration, and a 'downstream', isolated trabecula (as described in Chapter 2) superfused with the venous effluent obtained from the coronary circulation of the whole heart. The basic premise here is that the trabecula should exhibit an inotropic response in the presence of the coronary effluent obtained from the stretched whole heart if stretch does indeed release some positively inotropic factor.

Figure 4.1 illustrates the Langendorff apparatus configured to operate under constant-flow (Radnoti Langendorff System 120101BEZ, ADInstruments, NZ). The excised hearts of adult Wistar rats of either sex (average weight: 279.4 ± 7.6 g, $n$ = 13) were cannulated via the aorta and perfused under constant flow with oxygenated, non-recirculating HEPES-buffered Tyrode's solution (see Chapter 2). The flow rate was set by using a peristaltic pump (Masterflex 77521, ADInstruments, NZ), with an average coronary flow rate of 9.3 ± 0.1 ml per minute ($n$ = 13). Prior to cannulating the heart, Tyrode's solution was passed through the Langendorff apparatus and collected to serve as a 'blank' for subsequent MS analysis. Hearts were superfused with 1.5 mM $[Ca^{2+}]_o$ and maintained at 37 °C throughout the experiment. Furthermore, hearts were not electrically paced, and had an average intrinsic rate of 212 ± 8 beats per minute ($n$ = 13).

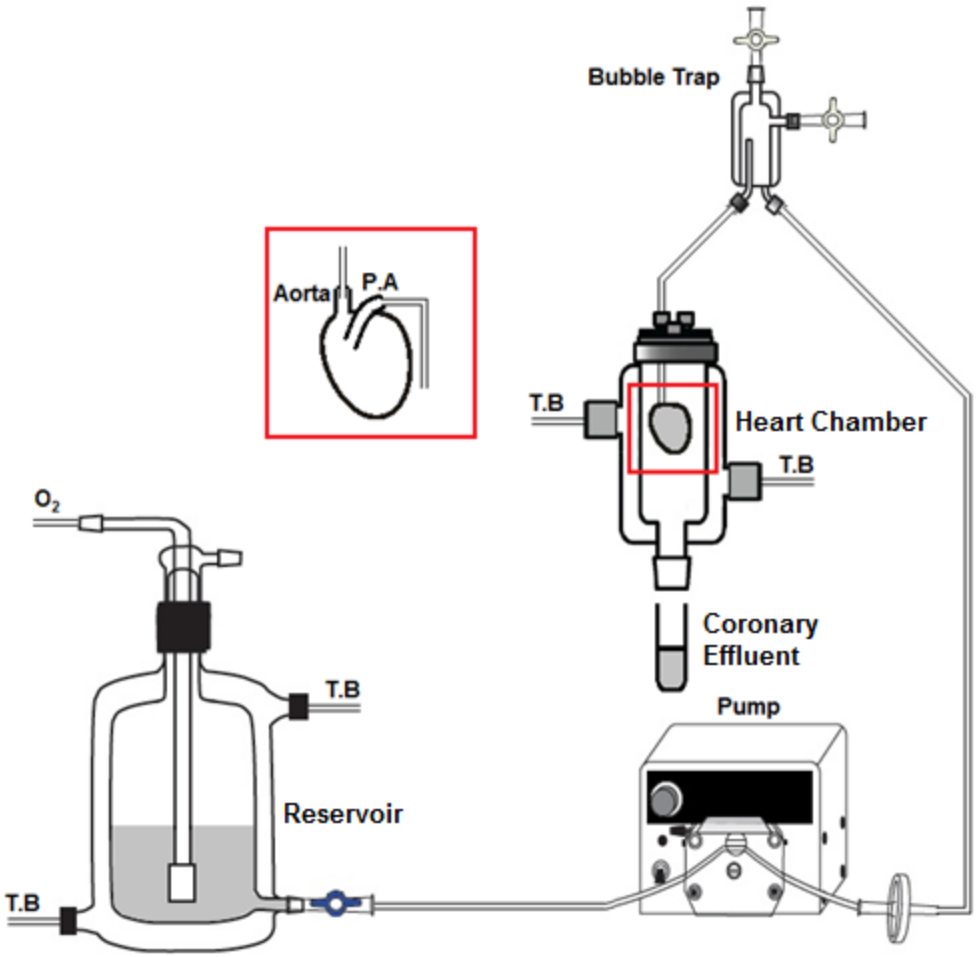


(Modified from ADInstruments, NZ)

Figure 4.1. Schematic diagram showing the Langendorff setup in constant-flow configuration. Oxygenated Tyrode's solution was delivered from a 1L reservoir via a peristaltic pump to the water jacketed heart chamber enclosing the cannulated whole heart. The reservoir, heart chamber and tubing were all insulated and maintained at 37 °C via a separate temperature bath (T.B). A small catheter was inserted into the RV via the pulmonary artery in order to collect the coronary effluent.

Once attached to the aortic cannula, a small incision was made in the left atrial appendage of each heart and a fluid-filled latex balloon (volume of 50 µl when deflated) inserted into the left ventricle through the mitral valve. The latex balloon was connected via a fluid-filled cannula to a pressure transducer (MLT844, ADInstruments, NZ) which was calibrated between 0 and 300 mmHg using a sphygmomanometer. Figure 4.2 shows the elastic hysteresis of the pressure-volume relationship for the latex balloon used. The balloon (size 4, ADInstruments, NZ) was of low compliance as indicated by the relatively large increase in recorded pressure following expansion. In order to measure left ventricular developed pressure (LVDP), the pressure generated by the balloon itself at a given volume (from Fig 4.2) was subtracted from the raw recorded value during experimentation.

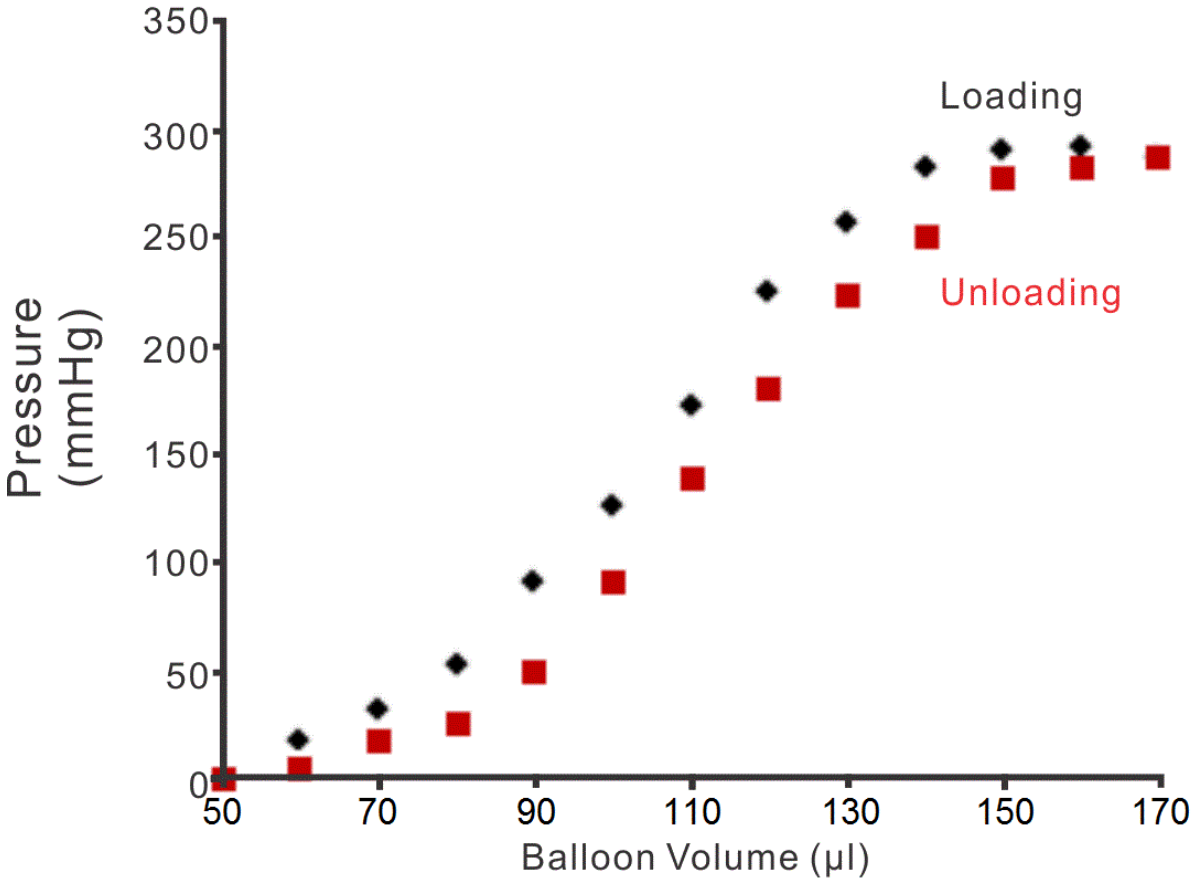


Figure 4.2. Elastic hysteresis of the latex balloon. In order to determine the elastic properties of the balloon, the volume of the fluid-filled balloon was increased in 10 µl increments from 0 to 120 µl. The balloon was submerged in water during inflation and deflation to mimic the intra-ventricular environment.

Once inserted into the LV, the initial volume of the balloon was adjusted to give a LVDP of 5 mmHg which served as baseline. Once the hearts were contracting at a steady pace, the balloon volume was gradually increased in order to determine the optimal volume, $V_o$, needed to achieve maximal ventricular developed pressure. That is, the point at which further increase in balloon volume does not lead to further increase in LV developed pressure. Figure 4.2 shows an exemplar recording illustrating how $V_o$ was determined in a typical isolated whole heart. A bolus of 10 µl of fluid was injected into the balloon while monitoring the increase in LVDP. This was repeated a number of times until LVDP no longer increased with balloon expansion. The mean ± SEM $V_o$ in this series of experiments was 103.1 ± 1.4 µl, $n$ = 13. Once $V_o$ was determined, balloon volume was returned to give 5 mmHg LVDP. As hearts were unpaced in these experiments, the pressure-time integral (PTI) was averaged from 5 consecutive beats and used as a uniform measure of contractile function. At $V_o$, hearts had an average PTI of 18.4 ± 0.2 mmHg.s ($n$ = 13). It is important to note that while the left ventricular volume of the rat is approximately 200 to 300 µl, the balloon volume at $V_o$ was only about 100 µl. This is likely to be due to the low-compliance balloon not being able to fully contort around the uneven contours of the ventricle. Nevertheless, increasing the balloon volume from 50 to 100 µl was able to increase the ventricular pressure by about 64% from baseline, a marked difference that is sufficient to produce a SFR.

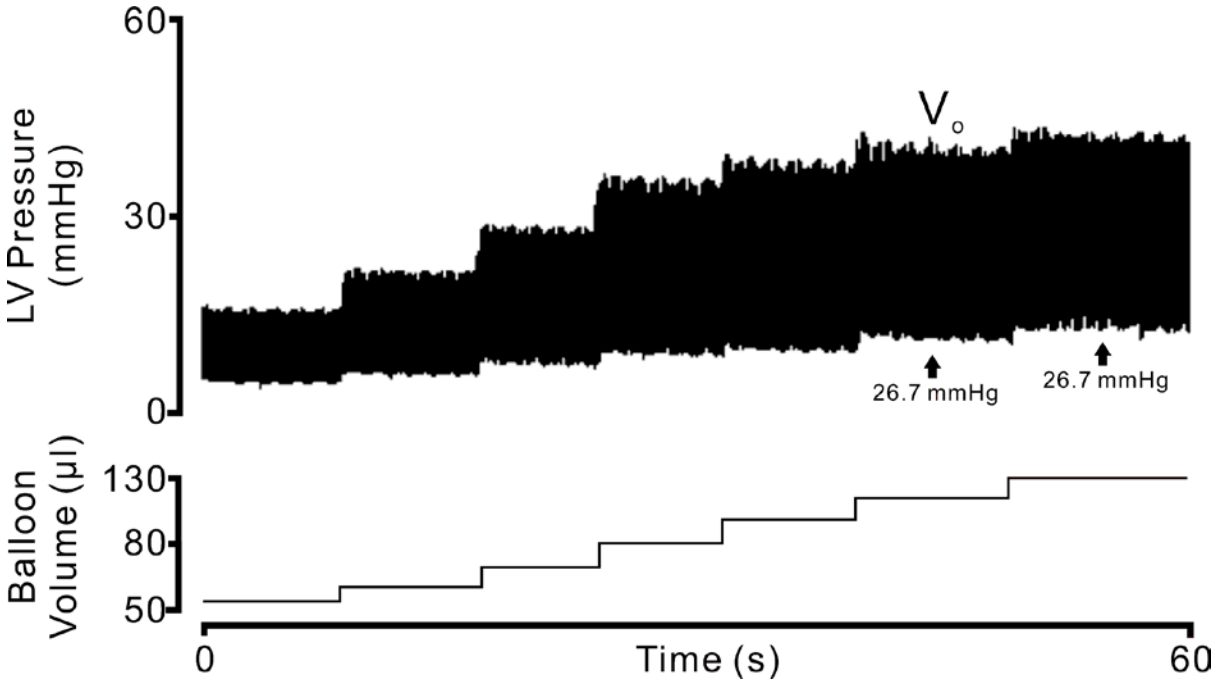


Figure 4.3. A representative recording of $V_o$ determination for an isolated whole heart. Increasing balloon volume in 10 µl increments was accompanied by increased LV pulse-pressure. $V_o$ denotes the point at which LV developed pressure no longer increased with increasing balloon volume.

Collection of coronary effluent was made from the RV via a catheter inserted through the pulmonary artery and collected through gravity. Note that the vena cavae were not tied off. However, the loss of coronary effluent by leakage from the vessels was minimal, presumably because the RV cannula acted as a siphon. Effluents were collected in duplicates, where one set was used to superfusate trabeculae on a separate set up, while the other was stored at -80 ºC prior to MS analysis. At the beginning of each intervention, 10 ml of effluent was collected at 5 mmHg LVDP, which served as the 'unstretched' control. This was followed by rapidly injecting the previously determined $V_o$ into the latex balloon for a period of 3 minutes, during which 10 ml of the 'stretched' effluent was collected immediately following the LV "stretch" protocol. To ensure that any released factor of interest was correlated with the SFR, and was not just a result of ventricular expansion itself, coronary effluents were collected only from hearts that exhibited a SFR. Figure 4.4 illustrates the stretch protocol used, the subsequent SFR that followed and the period during which the 'stretched' coronary effluent was collected. A rapid increase in ventricular volume gave rise to an immediate increase in developed pressure which was then followed by the SFR. As shown in figure 4.4, the magnitude of the SFR was defined as [(b – a)/a]*100, where "a" is the PTI of 5 beats immediately after balloon expansion, and "b" the PTI of 5 beats after 3 minutes at increased volume (i.e. "stretch"). At 37 °C and 1.5 mM $[Ca^{2+}]_o$, the mean ± SEM value (in mmHg.s) was 18.4 ± 0.2 for "a" and 23.76 ± 0.3 for "b". This translated to a SFR of 29.4 ± 2.1 % for isolated Langendorff hearts ($n$ = 13).

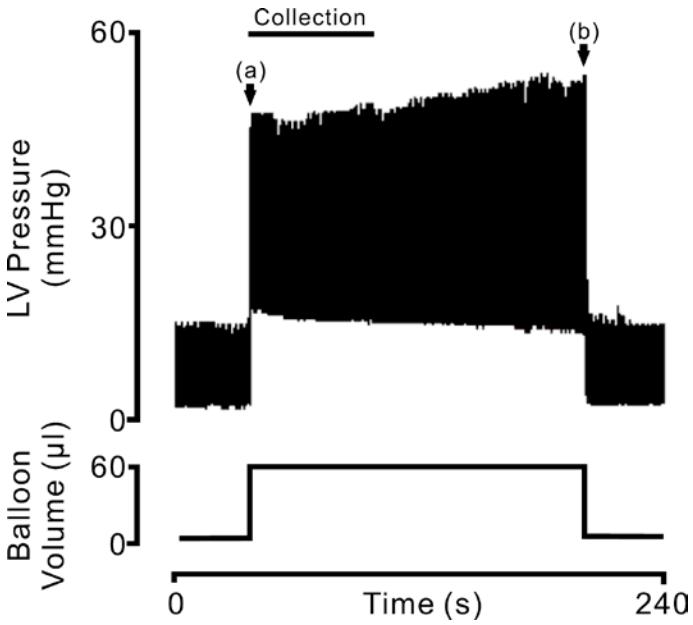


Figure 4.4. The SFR in a typical isolated whole heart preparation following an increase in LV volume (stretch). The SFR was expressed as [(b – a)/a]*100, where "a" is the developed pressure of the beat immediately after stretch, and "b" is the developed pressure of the beat after 3 minutes of stretch. The collection of the 'stretched' effluent (10 ml) was made immediately following stretch.

## 4.3. Inotropic Response of Trabeculae to Coronary Effluent Samples

Once collected, the coronary effluent samples were immediately used to superfuse an isolated RV trabecula held at optimal length, $L_o$. Figure 4.5A shows a representative force response of a trabecula that was first superfused with the 'unstretched' effluent and then the 'stretched' effluent. Upon changing the superfusate to the stretched effluent, the force of contraction increased over a period of several minutes. Figure 4.5B shows mean data from trabeculae subjected to this protocol. Switching from unstretched to stretched effluent saw a significant increase in mean stress from 15.4 ± 1.5 mN $mm^{-2}$ to 19.2 ± 1.9 mN $mm^{-2}$, an increase of 24.7 ± 3.7%, $p < 0.05$, $n = 13$. This inotropic effect was reversible, as when trabeculae were switched back into the unstretched effluent, the mean stress returned to 14.9 ± 1.7 mN $mm^{-2}$, $p < 0.01$, $n = 13$. Figure 4.5C shows examples of the $[Ca^{2+}]_i$ transient (as indicated by the 340/380 ratio) and twitch force from unstretched and stretch effluents. The mean $Ca^{2+}$ transient amplitude was 0.87 ± 0.04 in the unstretched effluent, while the average $Ca^{2+}$ transient amplitude was 0.94 ± 0.05 in the stretched effluent ($p < 0.05$, $n = 4$).

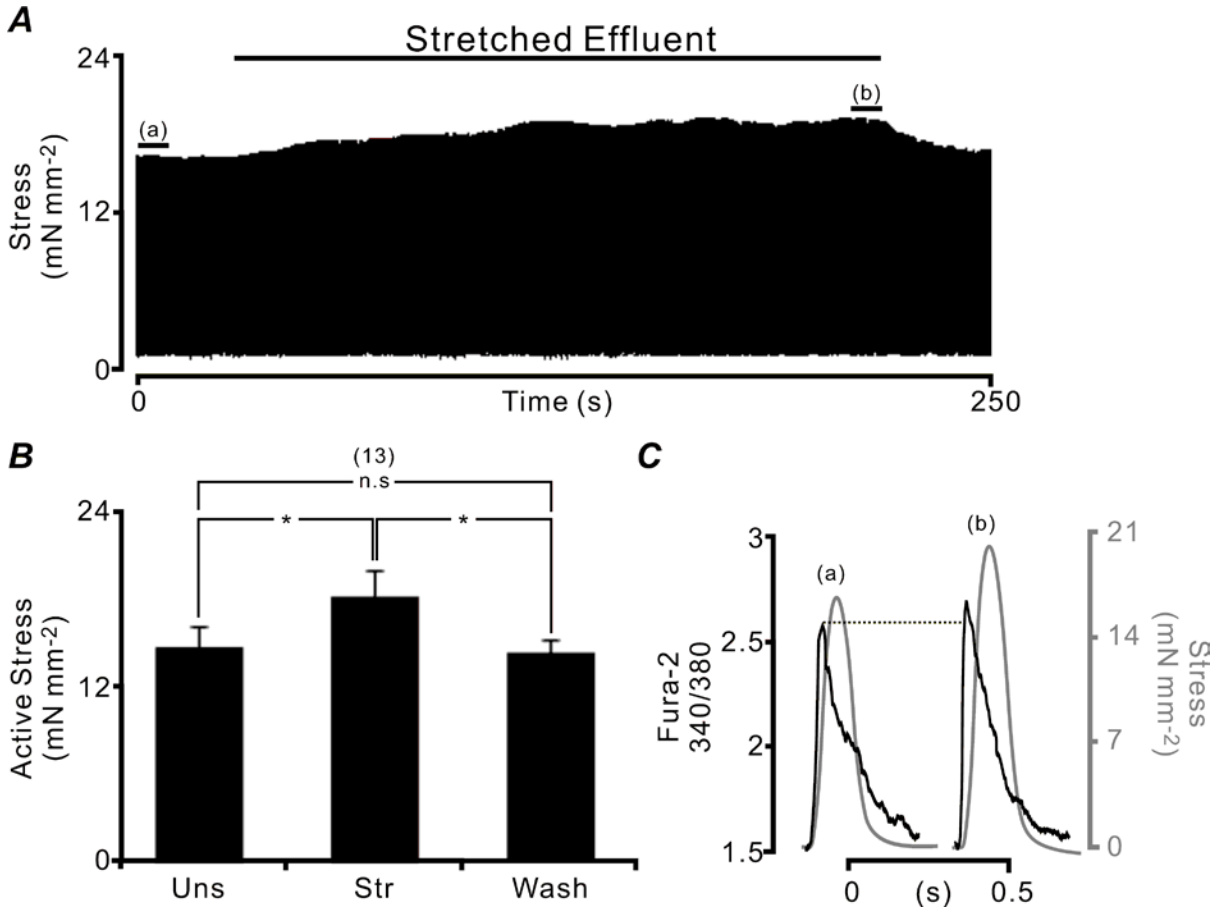


Figure 4.5. Inotropic effect of coronary effluent samples on rat RV trabeculae. A, a typical recording of stress from a trabecula held at fixed length and sequentially superfused with the 'unstretched' effluent (a), 'stretched' effluent (b) and finally back to the same 'unstretched' effluent. The 'stretched' effluent caused a gradual increase in stress 3 min. B, pooled active stress (Mean ± SEM) showing a significant difference between 'unstretched' (Uns) and the 'stretched' (Str) effluents, $*p < 0.05$, $n = 13$. C, an exemplar comparison of $Ca^{2+}$ transients between the 'unstretched' (a) and the 'stretched' (b) effluent, overlaid with their respective averaged twitch force.

Samples of ‘stretched’ and ‘unstretched’ effluents also underwent heat treatment to determine whether the factor of interest in the ‘stretched’ effluent was impaired by temperature denaturation. Effluent samples (10 ml) were pre-incubated at 100ºC for 20 minutes, cooled, oxygenated and used to superfuse the “downstream” trabecula. Figure 4.6 summarises the relative stress increase of trabeculae (%) in mean ± SEM under the control and heat-treated effluents. In control, the average increase in stress transitioning from the unstretched to the stretched effluent was 26.9 ± 1.4 %. This increase falls significantly to 21.1 ± 1.2 % in the heat-treated samples ($p < 0.05$, $n = 3$). Importantly, the heat treatment was unable to completely suppress the increase in stress, suggesting that peptides could not explain the observed inotropic response in the stretched effluent.

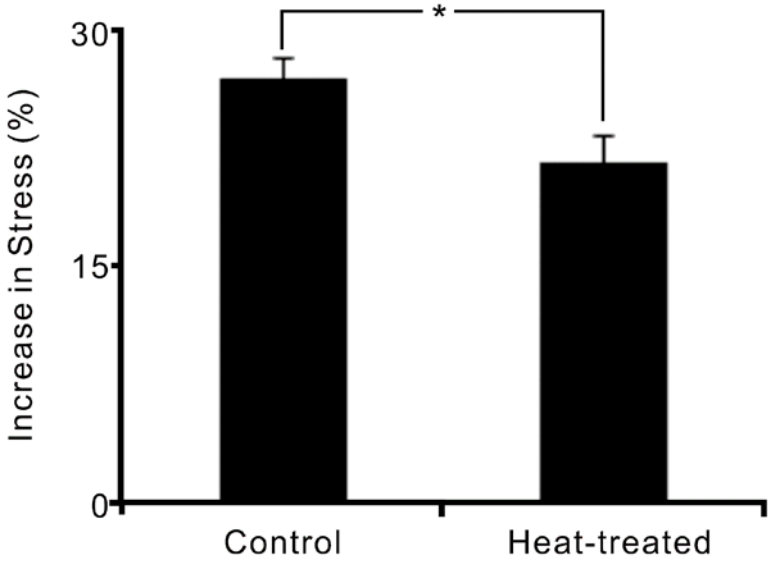


Figure 4.6. Effects of heat treatment (100ºC, 20 minutes) on the relative increase in stress when switching from the ‘unstretched’ effluent to the ‘stretched’ effluent (*$p < 0.032$, $n = 3$).

## 4.4. Identification of Extra-Humoral Substance via LC/MS

Collected coronary effluents underwent a series of treatments prior to LC/MS analysis. First, a separation process was required in order to minimise salts such as $Na^+$ from the samples. Aliquots (100 µl) of blank, unstretched and stretched effluents were diluted with 1% Formic acid (1:3 dilution) and subsequently passed through Ion Exchange Solid Phase Extraction (SPE) columns (Bond Elut Plexa, Agilent Technologies Inc., USA). The acidified samples were then washed with 500 µl of 5% methanol, followed by eluting with 500 µl of 100% methanol to yield a total volume of 1 ml. Next, samples were concentrated and preserved via lyophilisation. The freeze-drying process was carried out using a Labconco freeze dryer system (Model 7806020, Labconco, USA). The samples were dried at -40 ºC at a chamber pressure of 0.1 mbar for 24 hours. Lyophilised samples were diluted with 5% aqueous acetonitrile (ACN) and 0.1% formic acid and subsequently analysed using an LTQ FT ICR Hybrid Mass Spectrometer (Thermo Finnigan, San Jose, CA). Diluted samples (10 ul) were injected onto $C_{18}$ silica-based HPLC columns (Luna C18(2), Phenomenex Inc., USA). The samples were separated with a linear gradient of the solvents 5% ACN to 95% ACN with 0.1% formic acid ran for 80 min. The mass spectrometer operated in the positive-ion mode, with the mass range acquired between the mass-to-charge ratios of 80 and 1,200.

Ion chromatograms (displayed as relative abundance against retention time) and mass spectra (displayed as relative abundance against mass to charge ratio) from LC/MS runs ($n$ = 3) were generated as raw files in Xcalibur (Thermo Fisher Scientific Inc., USA). Quantitative and statistical analysis of the LCMS results were performed using SIEVE (Version 2.0, Thermo Fisher Scientific Inc., USA), a differential analysis software that compares the spectral data (molecular mass, retention time (RT) in the column and peak intensities) between two or more treatment groups. The general workflow of SIEVE can be described as follows:

**Chromographic Alignment**

↓

**Chromatogram Reconstruction and Statistics (Framing)**

↓

**Small Molecules and Protein/Peptide Identification**

Figure 4.7 illustrates the initial chromographic alignment process of the raw data files, whereby 2 or more chromatograms are aligned using an adaptive tile algorithm based on correlation derived from the full MS scan. Figure 4.8A details the framing process, in which individual peaks that were above a pre-set threshold (determined based on the blank solution) were re-ordered based on relative intensity. Figure 4.8B shows the framing process of an exemplar set of data. Here, 20 peaks were taken from the region marked by the black-bordered region, and were subsequently translated into frames. Each frame isdefined as a region in the m/z against retention-time plane. Importantly, each frame is also associated with a $p$ value denoting the statistical significance between the treatment groups.

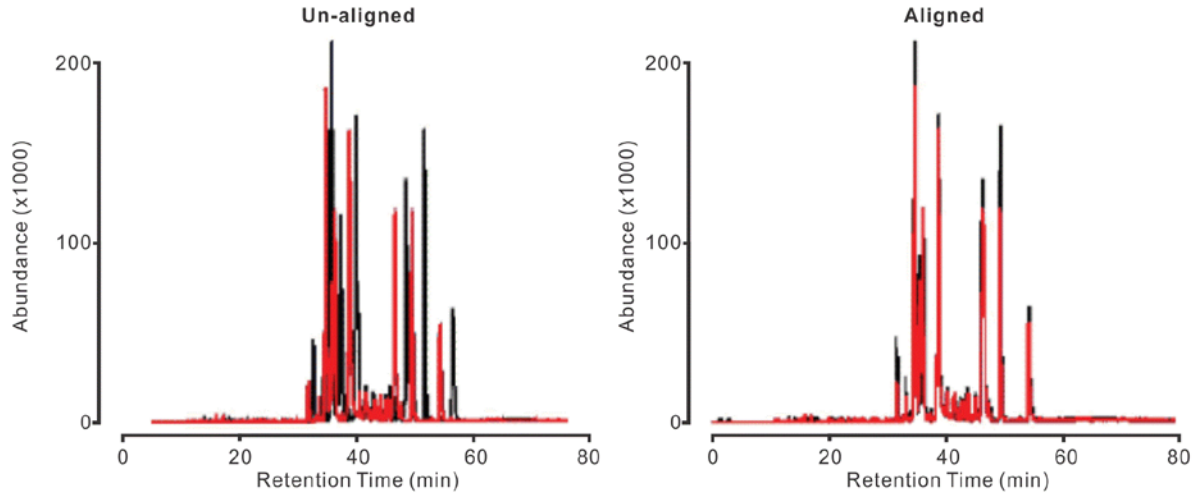


(Image modified from Sieve User Guide, Thermo Fisher Scientifc Inc.)

Figure 4.7. SIEVE chromographic alignment of two exemplar sets of data. Pairs of spectra from each raw file were separated into bins and a correlation matrix was constructed. The matrix were then sorted using a tiling algorithm and an alignment score calculated. For a detailed breakdown of the alignment process, refer to the SIEVE community portal at http://portal.thermo-brims.com.

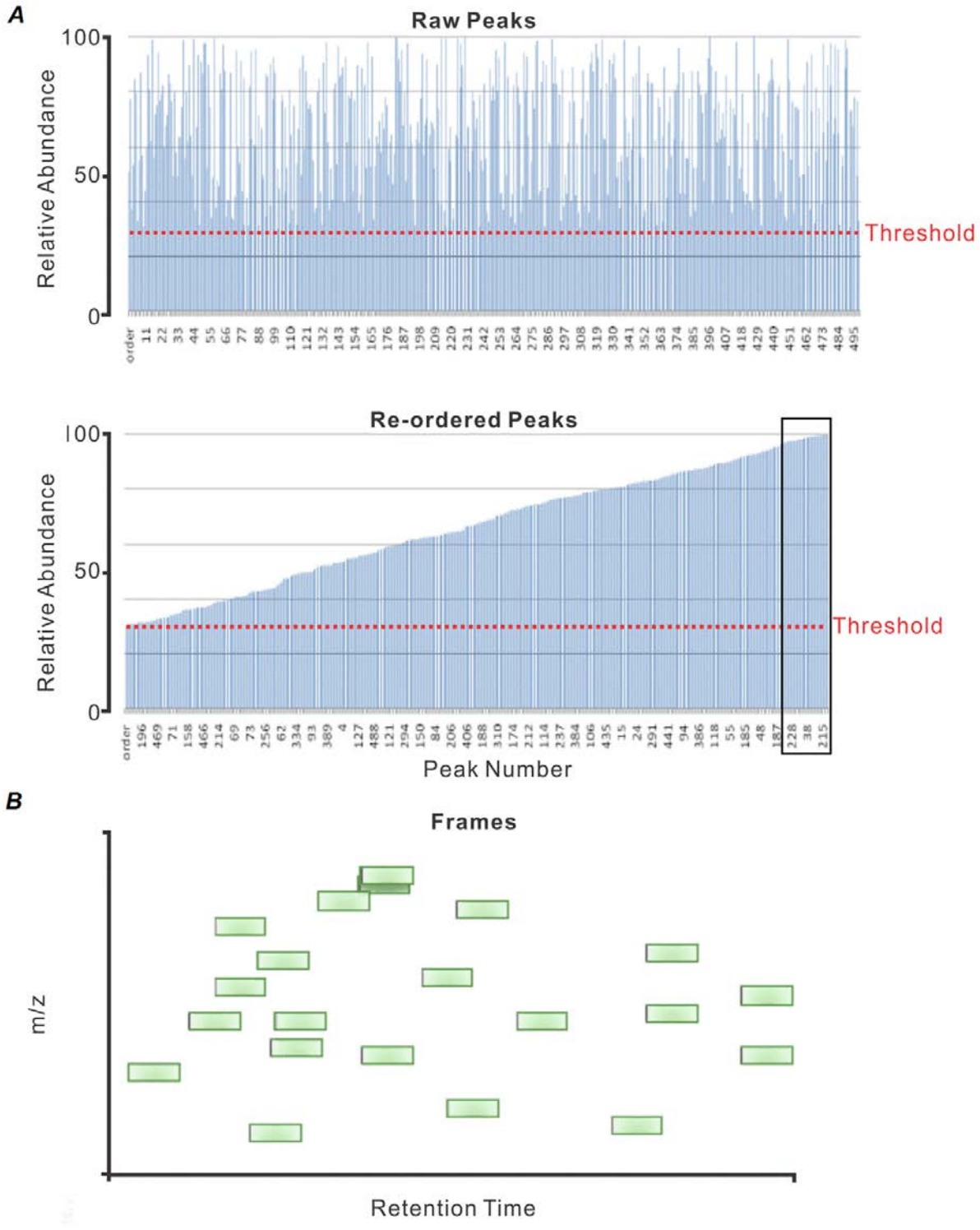


(Image modified from Sieve User Guide, Thermo Fisher Scientifc Inc.)

Figure 4.8. Re-organisation of raw peaks from MS runs and the subsequent framing of the peaks. A, all peaks from raw files were collected above a pre-determined threshold and were subsequently ordered by peak intensity. B, the largest peak is translated into a single frame, followed by the next highest peak and so on until all peaks become framed. Each frame has a number of characteristics associated with it, including m/z, retention time and statistical significance.

## 4.5. Increased concentrations of prostaglandin-related metabolites in the coronary effluent of stretched hearts

Initial qualitative results gathered from LC/MS runs are presented as ion chromatograms and mass spectra. Figure 4.9 shows an example of smoothed (Boxcar) Base Peak ion chromatograms of blank solution, 'unstretched' effluent and 'stretched' effluent from a typical LC/MS run from a single heart. In all 3 samples, a peak (a) was present at a retention time (RT) of approximately 40 min. There was also another peak (d) present at RT of ~60 min in both the unstretched and stretched samples, but this peak was absent in the blank. The most notable difference between the unstretched and the stretched effluent were the two peaks labelled (b) and (c) found between RT of 52 min and 56 min in the stretched sample.

Figure 4.10 show representative mass spectra (m/z range: 80 to 600, count: $2.14 \times 10^4$) of the blank, 'unstretched' and 'stretched' effluent from the same LC/MS run. There were a number of prominent peaks (m/z: 149.02, 179.60, 215.52, and 359.18) present in both the unstretched and the stretched sample, though all were present in greater relative abundance in effluent from 'stretched' heart sample. More importantly, the density of reported peaks was much higher in the stretched effluent compared to either the blank or the unstretched sample.

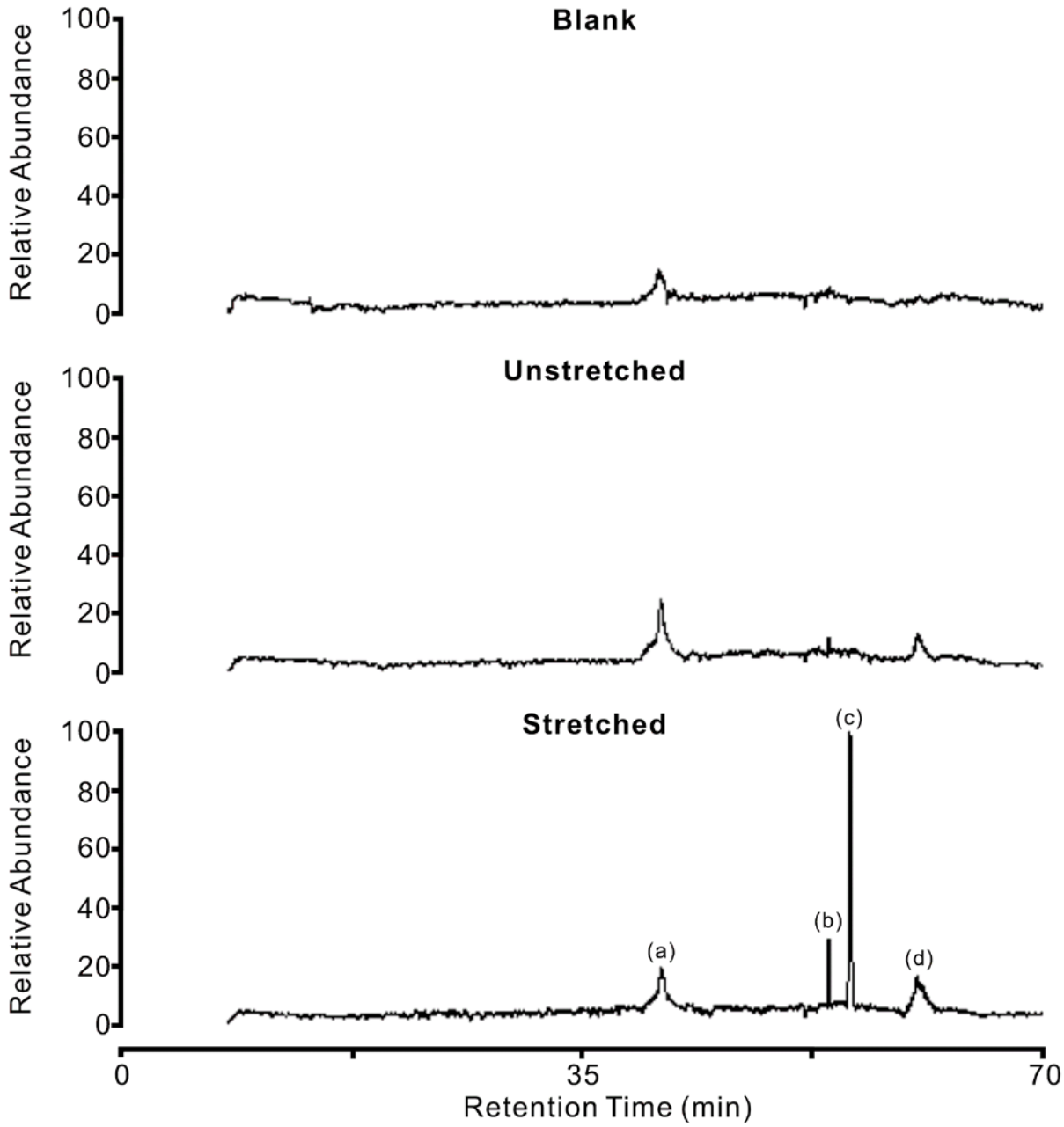


Figure 4.9. Representative Base Peak ion chromatographs showing qualitative difference between the blank, 'unstretched' and 'stretched' coronary effluent. Peak (a) was present in all three samples, while peak (d) was only present in the 'unstretched' and the 'stretched' sample. Peaks (b) and (c) was present only in the 'stretched' sample between RT of 52 and 56 min.

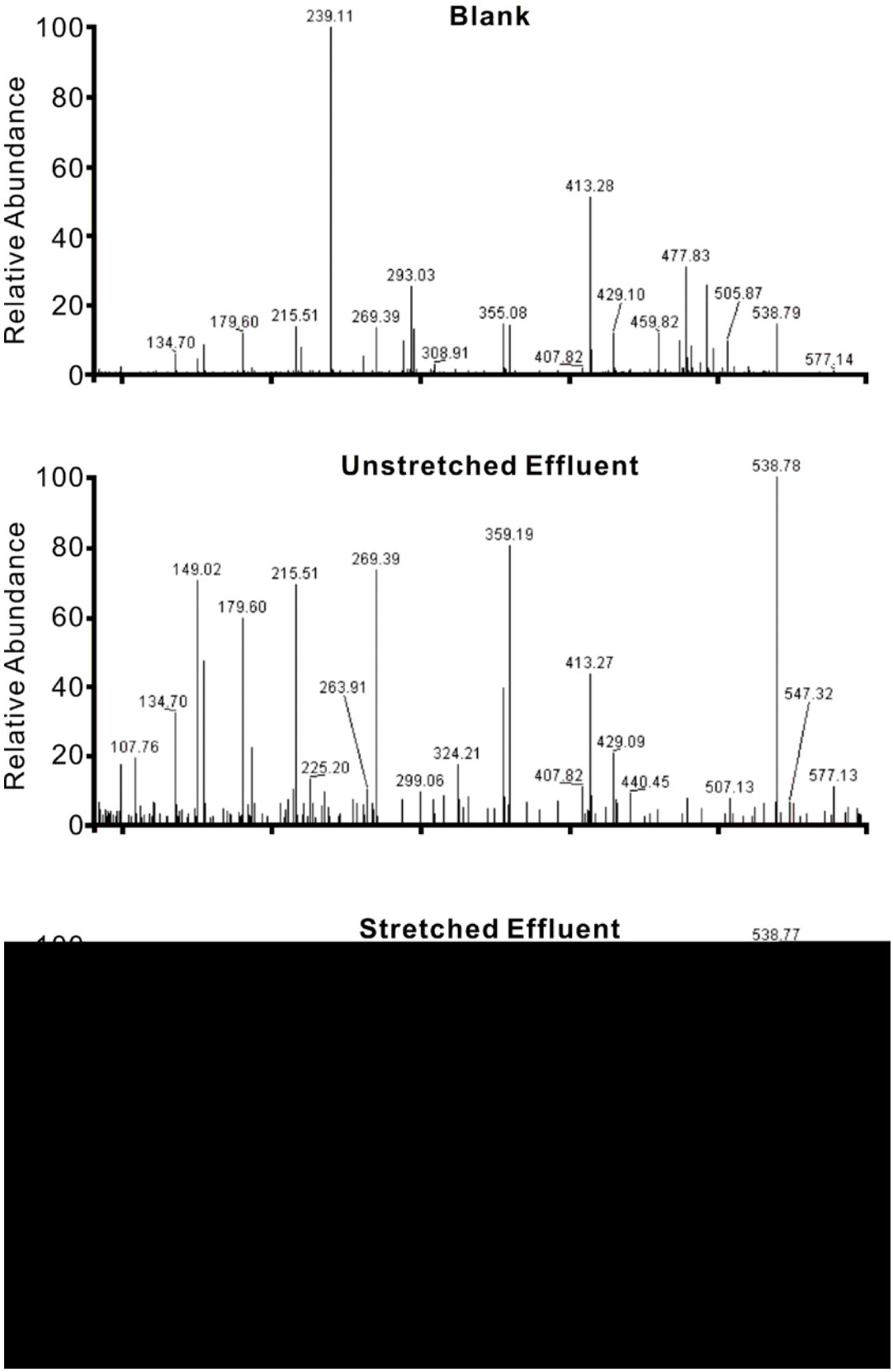


Figure 4.10. Representative mass spectra showing qualitative difference between the blank, unstretched and stretched coronary effluent. The overall density of peaks was much greater in the 'stretched' coronary effluent.

Following the initial alignment and framing process, frames that were differentially expressed between groups at a statistically significant level ($p < 0.05$) were searched against known databases. For small molecules, results were searched against the ChemSpider database (www.chemspider.com) to include adduct ions $H^+$, $Na^+$ and $NH_4^+$, while limiting the accurate mass window to 5 ppm. For protein and peptide identification, the analytical tool SEQUEST (Proteome Discoverer, Thermo Fisher Scientific Inc., USA) was used. Results were searched against the *Rattus norvegicus* protein sequence database with deamidation (N, Q) and oxidation (M) as variable side-chain modifications. Table 4.1 displays a list of small molecules that were differentially expressed on a significant level between the unstretched effluent and the stretched effluent ($p < 0.05$, n = 3). The table was ordered based on the compound intensity ratio between the unstretched and the stretched effluents, with a higher ratio value indicating a higher concentration of that particular compound in the stretched sample.

The majority of identified compounds were derivatives of the four families of eicosanoids: prostaglandins (PGs), prostacyclins, thromboxanes (TXs) and leukotrienes (for review, see (Wymann & Schneiter, 2008). Compounds showing the largest degree of difference (Ratio of 1.57) between the stretched and unstretched effluents were prostaglandin F2α and its metabolite 13,14-dihydro-15-keto PGF2α, as well as 11,15-Dihydroxy-9-oxoprost-13-en-1-oic acid (prostaglandin E1). Other prostaglandin-related compounds included (13E,15S)-15-Hydroxy-9-oxoprosta-8(12),13-dien-1-oic acid (prostaglandin B1) and 19-Hydroxy-PGE2. For leukotrienes, the level of leukotriene B4 and its derivative 20-trifluoromethyl-leukotriene B4 were found to be 34.5% and 20.4% higher in the stretched effluents, respectively. 6-Ketoprostaglandin E1, a metabolic product of prostacyclin (Panzenbeck *et al.*, 1988) and 11-Dehydro-thromboxane, a metabolite of thromboxane A2/B2 (Catella *et al.*, 1986) both expressed a ratio of 1.154.

| CSID | Compound Name | MW | m/z | RT | *p*-Value | Ratio |
|---|---|---|---|---|---|---|
| 4941255 | (2S)-2,3-dihydroxypropyl (9Z,12Z)-octadeca-9,12-dienoate | 354.524 | 355.282 | 59.986 | 0.010 | 1.570 |
| 4444144 | (5Z,9beta,11alpha,13E,15S)-9,11,15-Trihydroxyprosta-5,13-dien-1-oic acid | 354.481 | 355.282 | 59.986 | 0.010 | 1.570 |
| 4444438 | (9alpha,13E,15S)-9,15-Dihydroxy-11-oxoprost-13-en-1-oic acid | 354.481 | 355.282 | 59.986 | 0.010 | 1.570 |
| 209 | 11,15-Dihydroxy-9-oxoprost-13-en-1-oic acid | 354.481 | 355.282 | 59.986 | 0.010 | 1.570 |
| 4446166 | 13,14-dihydro-15-keto PGF2a | 354.481 | 355.282 | 59.986 | 0.010 | 1.570 |
| 10610 | Prostaglandin F2a | 354.481 | 355.282 | 59.986 | 0.010 | 1.570 |
| 13628109 | 5,8-tetradecadienoic acid | 224.339 | 225.196 | 60.927 | 0.034 | 1.361 |
| 4444132 | Leukotriene B4 | 336.466 | 337.258 | 53.740 | 0.033 | 1.345 |
| 4445196 | (13E,15S)-15-Hydroxy-9-oxoprosta-10,13-dien-1-oic acid | 336.466 | 337.258 | 53.740 | 0.033 | 1.345 |
| 4444076 | (13E,15S)-15-Hydroxy-9-oxoprosta-8(12),13-dien-1-oic acid | 336.466 | 337.258 | 53.740 | 0.033 | 1.345 |
| 4446167 | 20-hydroxy-PGF2a | 370.480 | 371.248 | 46.324 | 0.022 | 1.244 |
| 389698 | (9alpha,11alpha,15S)-9,11,15-Trihydroxy-6-oxoprost-13-en-1-oic acid | 370.480 | 371.248 | 46.324 | 0.022 | 1.244 |
| 4243 | 12(S)-HPETE | 336.465 | 354.263 | 53.780 | 0.022 | 1.243 |
| 4244 | 15(S)-HPETE | 336.465 | 354.263 | 53.780 | 0.022 | 1.243 |
| 389389 | (13S)-13-Hydroperoxy-9,11-octadecadienoic acid | 312.444 | 313.143 | 62.239 | 0.016 | 1.225 |
| 4446257 | 20-trifluoromethyl-leukotriene B4 | 390.437 | 391.284 | 61.045 | 0.013 | 1.204 |
| 1908 | 19-Hydroxy-PGE2 | 368.465 | 386.250 | 50.060 | 0.014 | 1.154 |
| 4241 | 6-Ketoprostaglandin E1 | 368.465 | 386.250 | 50.060 | 0.014 | 1.154 |
| 4242 | 11-Dehydro-thromboxane | 368.465 | 386.250 | 50.060 | 0.014 | 1.154 |

Table 4.1. A list of small molecules identified via the ChemSpider database. CSID is the ChemSpider ID number, MW is the molecular weight of the compound, m/z is the detected mass to charge ratio from LC/MS runs, RT is the chromatography retention time in minutes, *p*-Value is the significance level of the difference between the unstretched and the stretched samples and ratio is the compound's intensity difference between the unstretched and the stretched effluents (a higher ratio indicates a higher level of expression of a compound in the stretched sample). Results were compiled from LC/MS runs from 3 separate hearts.

## 4.6. Effects of Prostaglandin F2α on Force and $[Ca^{2+}]_i$

Preliminary MS results (Table 4.1) indicated that there were a number of factors present in the coronary effluents which could potentially contribute to the stretch-dependent inotropic response. Of the listed candidates, the relative abundance of prostaglandin F2α (PGF2α) and its metabolites exhibited the largest difference between the unstretched and stretched coronary effluent (57% higher in the stretched effluent, $p = 0.01$, n = 3). To date, the effects of PGF2α have been examined principally in reproductory (Momcilovic *et al.*, 1998; Dawood & Khan-Dawood, 2007), renal (Breyer & Breyer, 2000) and hepatic (Skouteris & Kaser, 1991) physiology. The role of PGF2α in cardiac function has only briefly been explored (Lai *et al.*, 1996; Mallat *et al.*, 1998), and its precise actions on multicellular preparations such as the cardiac trabeculae remain unclear.

We therefore examined the effects of PGF2α on contractile force and intracellular $Ca^{2+}$ in cardiac trabeculae (2 Hz stimulation, 1.5 mM $[Ca^{2+}]_o$, 37 ºC). Figure 4.11A shows a typical force recording from a trabecula held at $L_o$ in response to PGF2α (1 μM) added to the solution. PGF2α increased developed force gradually in a sigmoidal fashion before reaching a new steady state after a period of approximately 12 minutes. Figure 4.11B shows a dose-response curve for PGF2α obtained from 3 trabeculae over a range of 0.1 nM to 1 μM. For the concentration range examined, the dose-response curve was relatively linear. At 0.1 nM PGF2α, the average increase in stress was 27.4 ± 4.7% above control ($p < 0.05$, $n = 3$). With 1 μM PGF2α, the average increase in stress was 103.0 ± 11.3% above control ($p < 0.05$, $n = 3$). The 24.7% stress increase previously observed in trabeculae (figure 4.5) approximates to a PGF2α concentration of 0.04 nM (under the assumption that PGF2α was the sole contributing factor to the inotropic response).

Figure 4.11C (left) displays representative $Ca^{2+}$ transients between the control and PGF2α (1 μM) treated trabeculae, while the comparison of pooled data from 5 experiments are graphed on the right. On average, the magnitude of $Ca^{2+}$ transients (given by the 340/380 fura-2 ratio) increased significantly from 1.24 ± 0.18 in control to 1.46 ± 0.22 in 1 μM PGF2α ($p < 0.01$, $n = 5$). No difference was found in the time constant of decay of the $Ca^{2+}$ transients in the presence of PGF2α (0.26 ± 0.02 s) compared to control (0.25 ± 0.02 s), $p > 0.05$, $n = 5$).

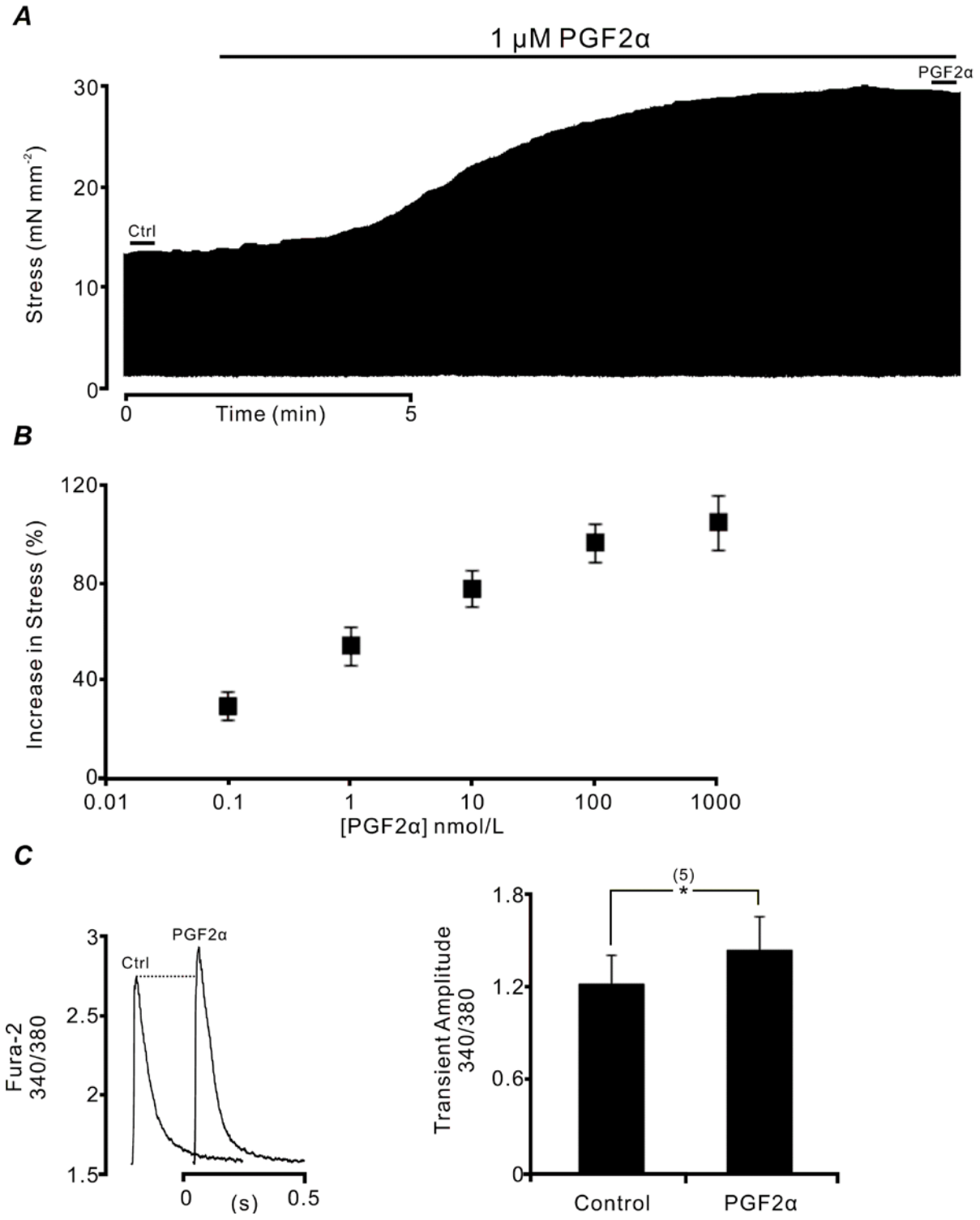


Figure 4.11. Effects of prostaglandin F2α on contractile force and intracellular $Ca^{2+}$ transients in rat trabeculae. A, representative force recording showing inotropic response following the application of 1 μM PGF2α. B, dose-response curve of PGF2α (n = 3). C, comparison of $Ca^{2+}$ transients between the control and 1 μM PGF2α treated trabeculae (*$p$ < 0.01, n = 5).

## 4.7. Addition of Prostaglandin E2 Does Not Increase Force in Trabeculae

Prostaglandin E2 (PGE2) is one of the more biologically active prostanoids whose physiological effects has been studied extensively (Dey *et al.*, 2006; Suzuki *et al.*, 2011; Castelino, 2012; Haversath *et al.*, 2012). The presence of PGE2 in 'stretched' effluent was reflected by its derivative 19-hydroxy-PGE2, which was found to be 15.4% higher than in 'unstretched' effluent (Table 4.1). To investigate whether PGE2 exhibited similar inotropic effects as PGF2α on the rat trabeculae, PGE2 (1 µM or 10 µM) was added to the superfusate under the same experimental conditions (2 Hz stimulation, 1.5 mM $[Ca^{2+}]_o$, 37 ºC) for a period of 15 minutes. Figure 4.12 shows the average stress in mean ± SEM between groups. Importantly, no significant differences in stress (in $mN.mm^{-2}$) were observed (control: 15.7 ± 0.6, 1 µM PGE2: 15.7 ± 0.7 and 10 µM PGE2: 15.5 ± 0.9, $p > 0.05$, n = 3).

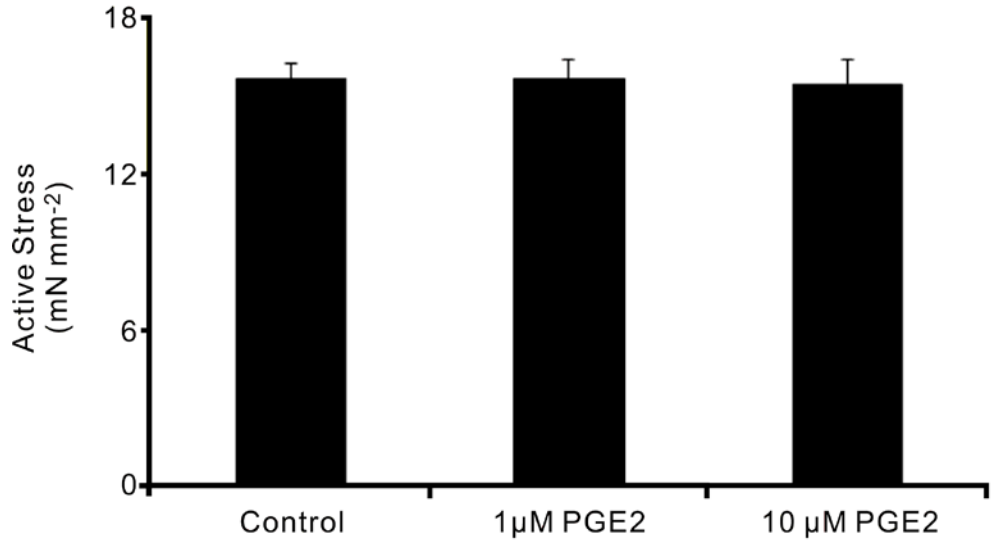


Figure 4.12. Application of either 1 µM or 10 µM PGE2 does not increase the force of contraction in rat trabeculae ($p > 0.05$, $n = 3$).

## 4.8. Effects of Arachidonic Acid on Force and $[Ca^{2+}]_i$

Arachidonic acid (AA) is a precursor in the synthesis of PGF2α via the enzyme cyclooxygenase (COX). At present, two metabolic products of AA, 12(S)-HPETE and 15(S)-HPETE, were found to be 24.3% greater in abundance in the stretched coronary effluent (Table 1). Furthermore, there is evidence to suggest that AA contributes to a number of cardiovascular functions (Bolton *et al.*, 1980; Lai *et al.*, 1996; Qiu & Quilley, 1999; Levick *et al.*, 2007). Consequently, the effects of AA on trabeculae force production and $Ca^{2+}$ transients were examined. Figure 4.13A shows a representative force recording of a trabecula held at $L_o$. The application of 10 µM of AA gave rise to a slow increase in the developed force, reaching steady-state after a period of around 12 minutes. On average, an increase of 132.5 ± 6.6% in force in the presence of 10 µM of AA was observed (n = 3). Figure 4.13B compares two exemplar $Ca^{2+}$ transients from a trabecula between control and in the presence of 10 µM AA, in which the magnitude of the $Ca^{2+}$ transients were much higher in the AA-treated samples. This increase was found to be significant, whereby the average Fura-2 340/380 ratio increased from 1.18 ± 0.27 in control to 1.28 ± 0.26 in AA, $p < 0.05$, n = 3). However, there was no significant difference in the time constant of decay of transients (in seconds) between the control and AA-treated groups (0.22 ± 0.03 in control compared with 0.22 ± 0.03 in AA, $p > 0.05$, $n = 3$).

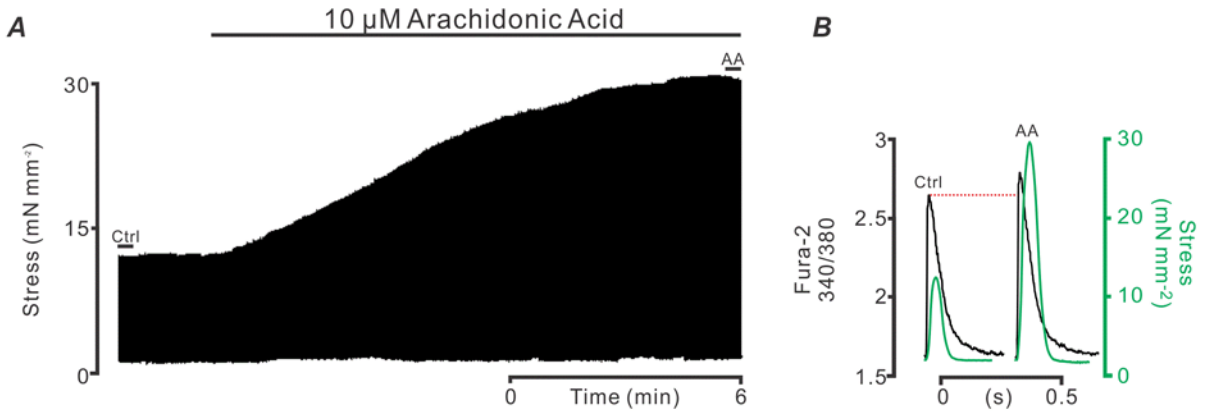


Figure 4.13. Effects of Arachidonic Acid on contractile force and intracellular $Ca^{2+}$ transients in rat trabeculae. A, representative force recording showing the positive inotropic effects of AA (10 µM) on a trabecula. B, shows two averaged $Ca^{2+}$ transients selected from control (Ctrl) and arachidonic acid-treated (AA) segments of the same trabecula, overlaid with their respective force trace.

## 4.9. Effects of Prostaglandin F2α, AA and Indomethacin on the SFR

The marked positive inotropic effects of both PGF2α and AA on the trabecula share a number of interesting similarities with the SFR. Namely, the time course (between 10 and 15 minutes) for the increase in force to reach steady-state (Alvarez *et al.*, 1999; Lewinski *et al.*, 2003), as well as the increase in the magnitude of intracellular $Ca^{2+}$ transients (figure 3.1). In order to determine whether stretch-mediated release of AA and the subsequent formation of PGF2α contributed the development of the SFR, the effects of both AA and PGF2α on the SFR were investigated. Previously, I have shown that the magnitude of the SFR was influenced by the degree of SR $Ca^{2+}$ content (figure 3.6). As such, if SFR was due to increased intracellular PGF2α or AA then in the presence of an already elevated intracellular PGF2α or AA, the SFR should be attenuated. Figure 4.14A shows representative recordings of the SFR in control and during exposure to 1 μM PGF2α for 20 minutes. Data from 4 trabeculae showed that the SFR was markedly blunted in the presence of PGF2α. Similar inhibition of the SFR was also observed in the presence of 10 μM AA, with the averaged data ± SEM illustrated in Figure 4.14B. The SFR was significantly reduced by the PGF2α treatment, decreasing from 33.3 ± 5.3% in control, to 10.3 ± 2.7% post treatment ($p < 0.01$ $n = 5$), and 10 μM AA was also able to reduce the SFR from 29.4 ± 5.4% in control, to 12.0 ± 1.4% post treatment ($p < 0.05$, $n = 3$).

The formation of PGF2α from AA is catalysed by cyclo-oxygenase (COX-1). If the SFR was abolished in the presence of a COX-inhibitor, it would indicate that AA alone is insufficient to produce the SFR. Here, a non-selective COX inhibitor indomethacin (500 μM) was used. Figure 4.14B summarises the data (expressed in Mean ± SEM), showing that the application indomethacin lead to a significant reduction in the SFR, decreasing the magnitude from 33.3 ± 5.3% in control, to just 18.3 ± 1.3% post treatment ($P < 0.01$, $n = 5$). Notably, this reduction was not 100%, suggesting that PGF2α only partly contribute to the SFR.

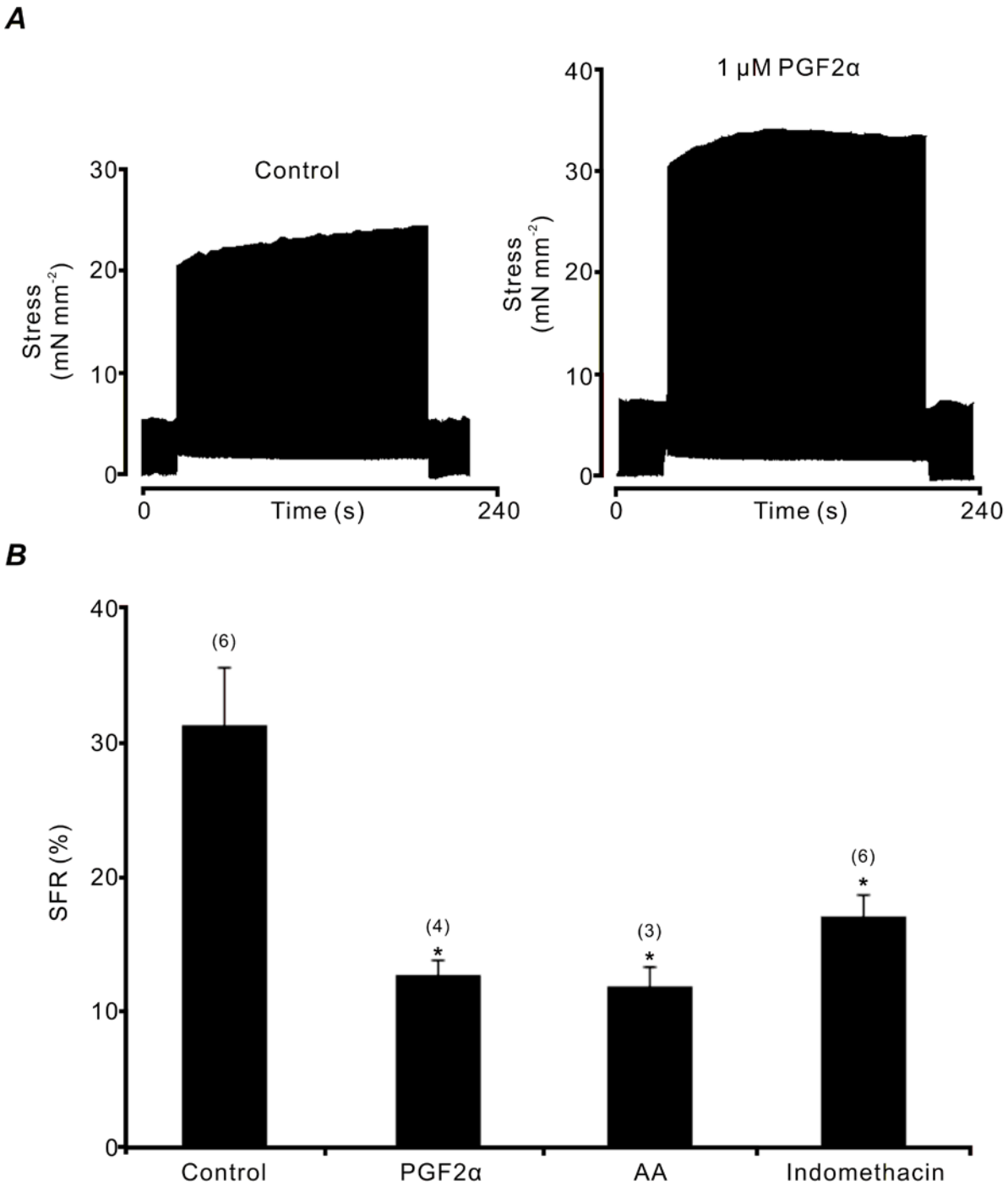


Figure 4.14. The effects of prostaglandin F2α, AA and indomethacin on the SFR. A, typical force recording comparing the magnitude of the SFR between control and PGF2α (1 μM). B, pooled data showing reduced SFR in the presence of either PGF2α (1 μM) or AA (10 μM). The application of indomethacin (500 μM) also lead to a significant reduction in the SFR, but was not able to fully block the response . *$p < 0.05$ between groups (ANOVA), with the number of trabeculae shown in brackets.

## 4.10. Absence of Angiotensin II in the Coronary Effluents

One mechanism thought to underlie the SFR involves stretch-mediated release of Angiotensin II (Ang II) and the subsequent activation of NHE and NCX (Alvarez *et al.*, 1999; Pérez *et al.*, 2001; Pérez *et al.*, 2003; Perez *et al.*, 2011). In order to determine whether Ang II was present in the coronary effluent when the whole heart was subjected to stretch, effluents were subjected to protein identification using the software SEQUEST described earlier (see section 4.5). Two separate blank solutions (HEPES-buffered Tyrode's solution) containing 1 µM and 10 µM Ang II were also put through the identification process to serve as positive control. Table 4.2 shows the results of SEQUEST identification process. A cross-correlation (Xcorr) value of at least 1.5 indicates a strong match between the peptide and the searched database. In both positive controls, 3 instances of angiotensinogen preproprotein (Ang II precursor) were reported at m/z of 523.77, 349.52 and 1046.54 with Xcorr values 1.51, 1.68 and 1.81, respectively. However, no traces of angiotensinogen preproprotein or any other peptide were found in either the unstretched or the stretched samples.

| **Positive Control (1 µM and 10 µM Ang II)** | | | |
|---|---|---|---|
| **Protein** | **m/z** | **RT** | **Xcorr** |
| angiotensinogen preproprotein | 523.77 | 34.92 | 1.51 |
| angiotensinogen preproprotein | 349.52 | 34.71 | 1.68 |
| angiotensinogen preproprotein | 1046.54 | 34.72 | 1.81 |
| **Effluent (Unstretched heart)** | | | |
| **Protein** | **m/z** | **RT** | **Xcorr** |
| angiotensinogen preproprotein | n/a | n/a | n/a |
| **Effluent (Stretched heart)** | | | |
| **Protein** | **m/z** | **RT** | **Xcorr** |
| angiotensinogen preproprotein | n/a | n/a | n/a |

Table 4.2. Protein/peptide identification of coronary effluents using SEQUEST. 1 µM and 10 µM Ang II were added to blank solutions to serve as positive control. No peptides were found in either the unstretched or the stretched coronary effluents.

## 4.11. Chapter Summary and Discussion

In the previous chapter, the inotropic state of the cardiac trabeculae and $HCO_3^-$ transport were identified as being part of an integral component in the development of the SFR. It should be noted that it was almost impossible to completely abolish the SFR via pharmacological means, and that the only way to fully remove the SFR was by raising the SR $Ca^{2+}$ content. As a consequence, we concluded that the mechanism underlying the SFR was multifactorial. In this study, several important findings were made. First, when the coronary effluent from a stretched, Langendorff-perfused whole heart was used to superfuse an isolated trabecula held at a fixed length, an inotropic response was observed (figure 4.5). Secondly, the increase in force was accompanied by an increase in the magnitude of $[Ca^{2+}]_i$ transient, a characteristic typical of the SFR. Thirdly, these inotropic substances are most likely to be prostaglandins, in particular, PGF2α. Finally, angiotensin II was not present in coronary effluent of stretched hearts.

### 4.11.1. Coronary effluent of stretched hearts contains inotropic factors

When isolated trabeculae were superfused with the coronary effluent collected from the stretched whole hearts, both force and $[Ca^{2+}]_i$ increased. Importantly, the magnitude of these changes closely mirrored that of the SFR. For example, the average increase in LV developed pressure during the SFR (over a period of 3 minutes) in the Langendorff-perfused heart was 29.4 ± 2.1%, compared with an average force increase of 24.7 ± 3.7% in the trabecula ($n$ = 13, $p > 0.05$). Similarly, the overall increase in $[Ca^{2+}]_i$ during the SFR was 9.2 ± 1.8%, $n$ = 6, while the increase in $[Ca^{2+}]_i$ in the presence of stretched effluent was 8.0 ± 2.1%, $n$ = 4 ($p > 0.05$). The significance of this particular observation is that the regulation of the SFR may not just be limited to intrinsic autocrine/paracrine signalling pathways within the myocyte itself. Instead, it is highly plausible that non-muscle cells surrounding the cardiac myocytes also contribute to this stretch-mediated response. For example, there is evidence to suggest that stretch leads to increased nitric oxide (NO) release from endothelial cells, a process mediated by stretch-activated channels and transient receptor potential vanilloid type 1 (TRPV1) receptor (Torres-Narvaez *et al.*, 2012). An important observation given that

previous studies have reported intrinsic release of NO associated with the SFR in cardiac myocytes (Petroff *et al.*, 2001). Other studies have reported the release of vasoactive peptide endothelin-1 (ET-1) from cultured human endothelial cells in response to increased pressure (Hishikawa *et al.*, 1995). Notably, the pressure-induced increase in ET-1 was unaffected in the presence of either nifedipine (dihydropyridine calcium channel blocker), or gadolinium (stretch-activated channel inhibitor), but was significantly reduced when a phospholipase C inhibitor was applied (Hishikawa *et al.*, 1995). With ET-1 being one of the principal components in the proposed Ang II-mediated pathway underlying the SFR (Alvarez *et al.*, 1999; Pérez *et al.*, 2001; Pérez *et al.*, 2003; Perez *et al.*, 2011), the release of ET-1 from endothelial cells could further contribute to the response. There are also evidence supporting the possibility of other vasoactive autocoids such as prostacyclin (Quadt *et al.*, 1982; Frangos *et al.*, 1985) and prostaglandin H2 (Saito *et al.*, 2003) being released from the endothelium as a result of increased shear stress due to coronary flow. For example, infusion of prostacyclin appeared to increase ventricular contractility in perfused guinea pig hearts (Allan & Levi, 1980), a response likely to be mediated by the prolongation of the action potential in conjunction with enhanced cAMP-mediated phosphorylation of L-type $Ca^{2+}$ channels (Alloatti *et al.*, 1991). The synthesis of these metabolites can also be mediated by bradykinin and Ang II (Needleman *et al.*, 1975).

The aim of investigating the effect of heat treatment (figure 4.6) was that if the inotropic substance of interest was a protein/peptide (as is the case for both Ang II and ET-1), heating and the subsequent denaturing of these biologically active compounds should eliminate the inotropic response. Here, heating the coronary effluents to 100 ºC for a period of 20 minutes was able to significantly reduce, but not completely abolish the inotropic response. This suggests that while protein/peptides are likely to be a contributing factor, there must also be other components present that mediate the SFR. Previous experiments show that a portion of the SFR can be attributed to increased cross-bridge cycling and subsequent acid extrusion (Shen *et al.*, 2013), though this does not rule out the possibility of additional extrinsic pathways. The SEQUEST analysis showed no protein/peptide present in the effluent (Table 4.2). However, this does not rule out the possibility of stretch-mediated release of protein/peptides, since coronary effluents were collected only from the first minute of the stretch and may not have provided sufficient time for larger molecules to diffuse into the coronary circulation.

### 4.11.2. The role of PGF2α in the regulation force and $[Ca^{2+}]_i$

Prostaglandins (PGs) are products of arachidonic acid metabolism (figure 4.15) and are primarily synthesized and released from endothelial cells and fibroblast-like cells in rats (Linssen *et al.*, 1993). A number of different mechanical and chemical factors have been shown to trigger the formation of PGs. In the cardiac tissue, these can include ischemic reperfusion (Karmazyn, 1989), addition of $Ca^{2+}$ ionophore A23187 (Okahara *et al.*, 1980), increased exogenous AA (Gerritsen, 1987) and acute pressure overload (Mentz *et al.*, 1988). Based on current LC/MS analysis in conjunction with bioassay results, there is strong evidence to suggest that PGF2α is one of the principal inotropic compounds released with stretch in Langendorff-perfused hearts.

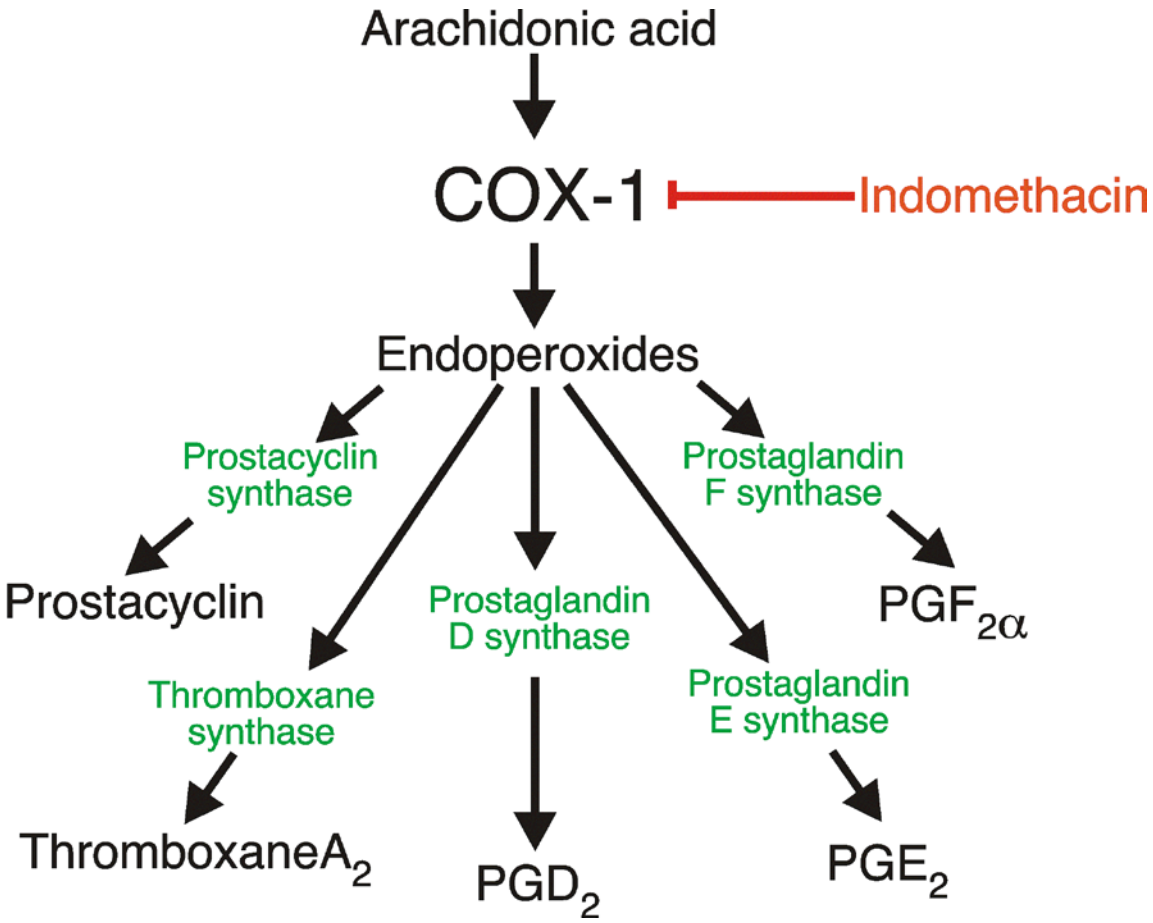


Modified from (Tang & Vanhoutte, 2009)

Figure 4.15. Synthesis of different prostaglandins from arachidonic acid via COX-1. Indomethacin is a non-selective inhibitor of COX.

In this study, the inotropic effect of PGF2α on rat cardiac trabeculae approximately translates to a maximum concentration of 0.04 nM present in the collected coronary effluent, although the actual amount released endogenously is likely to be higher, as PGF2α typically exerts its effects in an autocrine/paracrine manner (Chan *et al.*, 1998). The increase in contractile force upon the addition of PGF2α was accompanied by a parallel increase in the magnitude of $[Ca^{2+}]_i$ transient. It is possible that the increase in $[Ca^{2+}]_i$ is due to the activation of prostaglandin F receptors (FP), a G protein-coupled receptor which when activated, leads to the activation of protein kinase C (PKC) and the subsequent accumulation of inositol 1,4,5-trisphosphate ($IP_3$) and diacylglycerol (DAG) (Otani *et al.*, 1988; Abramovitz *et al.*, 1994). Importantly, both $IP_3$ (for reviews, see (Kockskamper *et al.*, 2008c; Berridge, 2009)) and DAG (Harteneck & Gollasch, 2011) are known to partake in the regulation of intracellular $Ca^{2+}$. A previous study by Yew *et al.* (1998) observed a similar positive inotropic effect of PGF2α on cardiac myocytes. However, the increased cell shortening was not due to increased $[Ca^{2+}]_i$, but was rather attributed to a PKC- and NHE-mediated sensitisation of myofilaments to $Ca^{2+}$. If PGF2α promoted the activation of PKC, one might be expected to see a faster time constant of decay of $Ca^{2+}$ transients due to the phosphorylation of phospholamban (Koss & Kranias, 1996; Yamamura *et al.*, 2005). Evidently, this was not the case in the rat cardiac trabeculae as the time constant of decay did not change in PGF2α-treated preparations. One study showed that the PGF2α-mediated inotropic response in mice atrial tissue was due to increased prolongation of the action potential (Tanaka *et al.*, 2001). Conversely, the addition of PGE2 did not significantly alter the action potential duration (Tanaka *et al.*, 2003). Therefore, the enhanced $Ca^{2+}$ influx as a result of increased action potential duration could serve as an explanation to our current results.

Arachidonic acid gave rise to a similar positive inotropic response on the trabecula, albeit at a concentration that was an order of magnitude greater than the response we measured when PGF2α was applied to trabeculae. The increased contractile response could be attributed to its ability to modulate intracellular $Ca^{2+}$ handling through the modification of $Ca^{2+}$ (Huang *et al.*, 1992) and $K^+$ (Damron *et al.*, 1993) currents, as well as enhanced SR $Ca^{2+}$ release (Dettbarn & Palade, 1993). In the presence of indomethacin (data not shown), the positive inotropic response was greatly diminished, but could not be fully abolished. This suggests that the effect of AA is both direct (mediated by itself) and indirect (mediated by its metabolites such as PGF2α). This may also explain why a higher concentration was required to achieve a

similar degree of force increase, since not all of its metabolites would exert positive inotropy (as is the case for PGE2 presently observed).

### 4.11.3. PGF2α, Arachidonic Acid and the Slow Force Response

In rat hearts, the positive inotropic response of PGF2α shares many similarities with the SFR; the magnitude of the force increase, the duration over which this increase occurs and the corresponding increase in $[Ca^{2+}]_i$. Current results suggest that PGF2α plays an important part to the development of the SFR, since in the presence of an already elevated concentration of PGF2α, SFR became attenuated. Similarly, the addition of exogenous arachidonic acid prior to stretching reduced the magnitude of the SFR. The partial inhibition of the SFR in the presence of indomethacin supports that idea of a stretch-mediated release of PGF2α. However, the inability to completely abolish the SFR suggests that PGF2α contributes only a part of the total SFR.

In summary, LC/MS analysis of coronary effluent from stretched hearts provided direct evidence of stretch-dependent release of PGF2α in rat myocardium. The positive inotropic response of PGF2α was associated with increased $[Ca^{2+}]_i$ transient amplitude. Functionally, PGF2α has been shown to stimulate hypertrophic growth of cardiac myocytes (Lai *et al.*, 1996; Jiang *et al.*, 2007; Hara *et al.*, 2008) and induce ventricular arrhythmias (Rao *et al.*, 1989). Further investigation into its mechanism of action in response to acute stretch might therefore provide valuable insights underlying these pathophysiological conditions.

# Chapter 5. Thesis Summary

## 5.1. Summary

In this thesis, cellular and extra-humoral mechanisms contributing to the SFR were explored in isolated cardiac muscle preparations obtained from adult Wistar rats. Contractile force, intracellular [$Ca^{2+}$] and intracellular pH were investigated at physiological temperature (37 ºC) in order to better understand the mechanisms that contribute to the stretch-dependent increase in $[Ca^{2+}]_i$ observed during the SFR.

Experiments outlined in Chapter 3 showed that the magnitude of the SFR was dependent upon SR $Ca^{2+}$ load, as alterations to the SR content through rate (frequency) or extracellular $Ca^{2+}$ directly influenced the SFR. An increase in the amplitude of the $Ca^{2+}$ transients during the SFR suggests an accompanying change in SR $Ca^{2+}$ release, since the SR is the major source of $Ca^{2+}$ during the transient. This study investigated the SFR under experimental conditions that altered SR $Ca^{2+}$ release and/or load. It was found that the magnitude of the SFR was inversely related to the concentration of extracellular $Ca^{2+}$, and completely abolished when $[Ca^{2+}]_o$ was increased to 3 mM. Furthermore, it was unlikely that the absence of the SFR at high $[Ca^{2+}]_o$ is due to saturation of the contractile machinery since a short burst of paired-pulse stimulation during the SFR was able to increase force substantially at both low and high $[Ca^{2+}]_o$.

The SR $Ca^{2+}$ content is largely unaffected by increases in $[Ca^{2+}]_o$ (Bers, 1987; Trafford *et al.*, 2001), with the increase in contractility with increasing $[Ca^{2+}]_o$ the result of increased driving force for $Ca^{2+}$ entry via L-type $Ca^{2+}$ channels. This, in turn, produces a greater trigger for SR $Ca^{2+}$ release via CICR (assuming the trigger were less than maximal) as well as providing an increased contribution to the $Ca^{2+}$ transient. L-type calcium channels show saturation in their single channel conductance (with $K_d$ ~ 1.7 mM (Guia *et al.*, 2001)) and their ability to trigger SR release also depends on the local $Ca^{2+}$-dependence of ryanodine receptor (RyR) activation. Since the latter also shows saturation (and may even decline at high local $Ca^{2+}$ concentrations - see Laver and Honen 2008 fig. 7B (Laver & Honen, 2008)), we would expect the relative increase in SR $Ca^{2+}$ release to decline with increasing $[Ca^{2+}]_o$, eventually showing almost no $[Ca^{2+}]_o$ dependence at high $[Ca^{2+}]_o$ - as observed. When $[Ca^{2+}]_o$ is decreased, SR load

decreases (Diaz *et al.*, 1997; Trafford *et al.*, 2001), which will alter the relative contribution between $[Ca^{2+}]_o$ influx via L-type Ca channels (and NCX) and SR release. The latter will decrease faster (due to the steep load dependence of SR release (Shannon *et al.*, 2000; Eisner *et al.*, 2005)) than the sarcolemmal component of the SFR. Together, these factors would seem capable of explaining both the biphasic rate dependence of the SFR as well as the monotonic SR load dependence of the SFR, but also recapitulate the idea that the SFR must depend on sarcolemmal $Ca^{2+}$ homeostasis, with the SR playing a modulatory role.

There is strong evidence to suggest that the increase in intracellular $[Ca^{2+}]$ accompanying the SFR is due to increased intracellular $[Na^+]$ accumulation via activation of NHE and NCX (Alvarez *et al.*, 1999; Cingolani *et al.*, 2003; White, 2004; Kockskamper *et al.*, 2008b; Perez *et al.*, 2011). Results presented in Chapter 3 not only confirmed the role of both NHE as well as NCX in the development of the SFR, but also showed the effects of cross-bridge cycling and $HCO_3^-$ transport on the stretch-mediated phenomenon. When cross-bridges were inhibited using either BDM or blebbistatin, the increase in $Ca^{2+}$ transient associated with the SFR was also reduced, suggestive of a metabolic demand-dependent pathway underlying the SFR. While NHE and $Na^+$-independent $Cl^-$-$HCO_3^-$ exchanger (CBE) have been implicated in the SFR (Alvarez *et al.*, 1999; Pérez *et al.*, 2001; Cingolani *et al.*, 2003; Lewinski *et al.*, 2003; White, 2004), present results show that the increased metabolic demand and the subsequent development of the SFR is also facilitated by $HCO_3^-$ transporters. It should be noted that, although the change in pH is less in $HCO_3^-$-buffered solutions, the increased rate of $H^+$ production associated with the immediate inotropic response to stretch presumably leads to increased sodium and bicarbonate entry via the $Na^+$-$HCO3^-$ co-transporter (for review see (Vaughan-Jones *et al.*, 2006)). Again, this mechanism leads to increased $Na^+$ influx which stimulates NCX-mediated $Ca^{2+}$ entry in response to increased metabolic demand.

One possible mechanism that is thought to precede the activation of NHE during the SFR involves stretch-mediated release of Ang II/ET-1 (Alvarez *et al.*, 1999; Pérez *et al.*, 2001; Pérez *et al.*, 2003; Perez *et al.*, 2011). However, current results showed that neither losartan nor BQ-123 were able to modulate the SFR. Moreover, LC/MS analysis revealed that neither Ang II nor ET-1 were present in the coronary effluent collected from stretched Langendorff-perfused whole hearts. While these results suggest that Ang II is unlikely to be the underlying factor in the SFR in the current study, its role cannot be completely ruled out. Studies have shown that Ang II mediates stretch-induced cardiac hypertrophy through the induction of several immediate-early genes such as c-fos and c-jun (Sadoshima & Izumo, 1993;

Sadoshima *et al.*, 1993). More importantly, the maximal expression of these immediate-early genes typically takes 30 to 60 minutes post induction (Zheng *et al.*, 1994; Cullinan *et al.*, 1995). Given the 3-minute stretch protocol used in the current study, the contribution of Ang II to the total SFR appears to be negligible.

When isolated trabeculae were superfused with the coronary effluent collected from the stretched whole hearts, both force and $Ca^{2+}$ transients increased. LC/MS analysis in conjunction with bio-assay results pointed to PGF2α as being one of the major components underlying the inotropic response. Moreover, there appeared to be a clear linkage between PGF2α and stretch, since the magnitude of the SFR was significantly reduced in the presence of either indomethacin or an already elevated concentration of PGF2α. The effects of PGF2α are primarily modulated by protein kinase C (PKC). Activation of PKC leads to increased $IP_3$ and DAG production which could explain the increased $Ca^{2+}$ transients (Kockskamper *et al.*, 2008c; Harteneck & Gollasch, 2011). Arachidonic acid, the precursor to PGF2α, also had a similar inotropic response on the trabecula. However, it is unclear at this stage whether the inotropic effects of AA are predominantly through the synthesis of PGF2α, as AA itself has been shown to regulate intracellular $Ca^{2+}$ handling (Huang *et al.*, 1992; Dettbarn & Palade, 1993).

## 5.2. Conclusions

Ultimately, the SFR can be modulated by a number of intrinsic and extrinsic factors. Intrinsically, the elimination of cross-bridge cycling was able to significantly prevent the stretch-dependent increase in $Ca^{2+}$ transients. Experiments showed increased metabolic demand as a result of increased cross-bridge cycling, which leads to $Na^+$-dependent proton extrusion to increase $Na^+$ and subsequently $Ca^{2+}$ via NCX. The magnitude of SFR was also rate-dependent, which means the extent of SR $Ca^{2+}$ load directly contribute towards the response. Extrinsically, coronary effluent obtained from stretched whole hearts had an inotropic effect on a separate isolated rat trabecula. The ‘factor’ responsible for the increased inotropic response was PGF2α, and the inhibition of its synthesis using indomethacin was able to significantly reduce the SFR. However, the mechanism by which PGF2α increases intracellular $Ca^{2+}$ warrants further investigation. One aspect of the bio-assay experiments that

was not carried out was analysis of coronary effluent from whole hearts that did not have a SFR. It may be that commencing the Langendorff perfusion of these hearts was delayed for some reason during the dissection procedure, causing them to be $Ca^{2+}$ overloaded (see section 3.4). Because the MS analysis was costly, and time consuming, I decided to focus only on collecting coronary effluent from "healthy" hearts, as determined by their robust SFR.

This thesis shows that there are a number of different mechanisms contributing to the SFR, and that no one particular pathway fully accounted for it. Indeed, the only intervention that was able to fully abolish the SFR in the current study was high $[Ca^{2+}]_o$. Given the multiple pathways involved, it should be expected that the SFR serves as an important means of regulating cardiac contractility on a beat to beat basis. From a pathophysiological perspective, PGF2α pathway may be involved in the very early steps along the way to hypertrophy when stretch is sustained.

# Bibliography


Abramovitz M, Boie Y, Nguyen T, Rushmore TH, Bayne MA, Metters KM, Slipetz DM & Grygorczyk R. (1994). Cloning and expression of a cDNA for the human prostanoid FP receptor. *Journal of Biological Chemistry* **269,** 2632-2636.

Allan G & Levi R. (1980). The cardiac effects of prostaglandins and their modification by the prostaglandin antagonist N-0164. *Journal of Pharmacology and Experimental Therapeutics* **214,** 45-49.

Allen DG & Kentish JC. (1985). The cellular basis of the length-tension relation in cardiac muscle. *Journal of molecular and cellular cardiology* **17,** 821-840.

Allen DG & Kurihara S. (1982). The effects of muscle length on intracellular calcium transients in the mammalian cardiac muscle. *Journal of Physiology* **407,** 489-503.

Allen DG, Nichols CG & Smith GL. (1988). The effects of changes in muscle length during diastole on the calcium transient in ferrent ventricular muscle. *Journal of Physiology* **406,** 359-370.

Alloatti G, Serazzi L & Levi RC. (1991). Prostaglandin I2 (PGI2) enhances calcium current in guinea-pig ventricular heart cells. *Journal of molecular and cellular cardiology* **23,** 851-860.

Alvarez BV, Pérez NG, Ennis IL, Hurtado MC & Cingolani HE. (1999). Mechanisms Underlying the Increase in Force and $Ca^{2+}$ Transient That Follow Stretch of Cardiac Muscle: A Possible Explanation of the Anrep Effect. *Circulation research* **85,** 716-722.

Arai M, Yoguchi A, Iso T, Takahashi T, Imai S, Murata K & Suzuki T. (1995). Endothelin-1 and its binding sites are upregulated in pressure overload cardiac hypertrophy. *American Journal of Physiology - Heart and Circulatory Physiology* **268,** H2084-H2091.

Backx PH, Gao WD, Azan-Backx MD & Marban E. (1994). Mechanism of force inhibition by 2,3-butanedione monoxime in rat cardiac muscle: roles of $[Ca^{2+}]_i$ and cross-bridge kinetics. *Journal of Physiology* **476,** 487-500.

Bailey K. (1946). Tropomyosin: a new asymmetric protein component of muscle. *Nature* **157,** 368.

Balligand JL, Feron O & Dessy C. (2009). eNOS Activation by Physical Forces: From Short-Term Regulation of Contraction to Chronic Remodeling of Cardiovascular Tissues. *Physiological reviews* **89,** 481-534.

Bassani JW, Yuan W & Bers DM. (1995). Fractional SR $Ca^{2+}$ release is regulated by trigger $Ca^{2+}$ and SR $Ca^{2+}$ content in cardiac myocytes. *American Journal of Physiology - Cell Physiology* **268,** C1313-C1319.

Bassani RA, Gilioli R, Oliveira ES & Hoehr NF. (2012). Blood calcium levels in immature rats: influence of extracellular calcium concentration on myocardial calcium handling. *Experimental animals / Japanese Association for Laboratory Animal Science* **61,** 399-405.

Baudet S, E, Noireaud J & Marec H. (1996). Alterations in the force-frequency relationship by tert-butylbenzohydroquinone, a putative SR $Ca^{2+}$ pump inhibitor, in rabbit and rat ventricular muscle. *British journal of pharmacology* **117,** 258-267.

Berridge MJ. (2009). Inositol trisphosphate and calcium signalling mechanisms. *Biochimica et Biophysica Acta - Molecular Cell Research* **1793,** 933-940.

Bers DM. (1987). Ryanodine and the calcium content of cardiac SR assessed by caffeine and rapid cooling contractures. *American Journal of Physiology - Cell Physiology* **253,** C408-C415.

Bers DM. (2002). Cardiac excitation-contraction coupling. *Nature* **415,** 198-205.

Bers DM. (2004). Macromolecular complexes regulating cardiac ryanodine receptor function. *Journal of molecular and cellular cardiology* **37,** 417-429.

Bers DM, Barry WH & Despa S. (2003). Intracellular $Na^{+}$ regulation in cardiac myocytes. *Cardiovascular research* **57,** 897-912.

Blaustein MP & Lederer WJ. (1999). Sodium/calcium exchange: its physiological implications. *Physiological reviews* **79,** 763-854.

Bluhm WF & Lew WY. (1995). Sarcoplasmic reticulum in cardiac length dependent activation in rabbits. *American Journal of Physiology* **269,** H965-H972.

Bolton HS, Chanderbhan R, Bryant RW, Bailey JM, Weglicki WB & Vahouny GV. (1980). Prostaglandin synthesis by adult heart myocytes. *Journal of molecular and cellular cardiology* **12,** 1287-1298.

Boron WF & De Weer P. (1976). Active proton transport stimulated by $CO_2/HCO_3^-$, blocked by cyanide. *Nature* **259,** 240-241.

Bountra C, Kaila K & Vaughan-Jones RD. (1988). Effect of repetitive activity upon intracellular pH, sodium and contraction in sheep cardiac Purkinje fibres. *Journal of Physiology* **398,** 341-360.

Bowman CL, Gottlieb PA, Suchyna TM, Murphy YK & Sachs F. (2007). Mechanosensitive ion channels and the peptide inhibitor GsMTx-4: history, properties, mechanisms and pharmacology. *Toxicon* **49,** 249-270.

Brette F & Orchard C. (2003). T-Tubule Function in Mammalian Cardiac Myocytes. *Circulation research* **92,** 1182-1192.

Breyer MD & Breyer RM. (2000). Prostaglandin receptors: their role in regulating renal function. *Current Opinion in Nephrology and Hypertension* **9,** 23-29.

Calaghan SC & White E. (2001). Contribution of angiotensin II, endothelin 1 and the endothelium to the slow inotropic response to stretch in ferret papillary muscle. *Pflugers Archiv (European Journal of Physiology)* **441,** 514-520.

Caldiz CI, Díaz RG, Nolly MB, Chiappe de Cingolani GE, Ennis IL, Cingolani HE & Pérez NG. (2011). Mineralocorticoid receptor activation is crucial in the signalling pathway leading to the Anrep effect. *Journal of Physiology* **589,** 6051-6061.

Caldiz CI, Garciarena CD, Dulce RA, Novaretto LP, Yeves AM, Ennis IL, Cingolani HE, Cingolani GC & Perez NG. (2007). Mitochondrial reactive oxygen species activate the slow force response to stretch in feline myocardium. *Journal of Physiology* **584,** 895-905.

Carraro-Lacroix LR, Girardi AC & Malnic G. (2009). Long-term regulation of vacuolar $H(^{+})$-ATPase by angiotensin II in proximal tubule cells. *Pflugers Archiv : European journal of physiology* **458,** 969-979.

Castelino FV. (2012). Lipids and eicosanoids in fibrosis: emerging targets for therapy. *Current opinion in rheumatology* **24,** 649-655.

Catella F, Healy D, Lawson JA & FitzGerald GA. (1986). 11-Dehydrothromboxane B2: a quantitative index of thromboxane A2 formation in the human circulation. *Proceedings of the National Academy of Sciences of the United States of America* **83,** 5861-5865.

Caulfield, Borg, 364–372. & 364–372. (1979). The collagen network of the heart.

Chan BS, Satriano JA, Pucci M & Schuster VL. (1998). Mechanism of prostaglandin E2 transport across the plasma membrane of HeLa cells and Xenopus oocytes expressing the prostaglandin transporter "PGT". *The Journal of biological chemistry* **273,** 6689-6697.

Cho WK, Mennone A & Boyer JL. (1998). Intracellular pH regulation in bombesin-stimulated secretion in isolated bile duct units from rat liver. *The American journal of physiology* **275,** G1028-1036.

Choi HS & Eisner DA. (1999a). The effects of inhibition of the sarcolemmal Ca-ATPase on systolic calcium fluxes and intracellular calcium concentration in rat ventricular myocytes. *Pflugers Archiv : European journal of physiology* **437,** 966-971.

Choi HS & Eisner DA. (1999b). The role of sarcolemmal $Ca^{2}$+-ATPase in the regulation of resting calcium concentration in rat ventricular myocytes. *J Physiol* **515 ( Pt 1),** 109-118.

Cingolani HE, Alvarez BV, Ennis IL & Hurtado MC. (1998). Stretch-Induced Alkalinization of Feline Papillary Muscle : An Autocrine-Paracrine System. *Circulation research* **83,** 775-780.

Cingolani HE, Chiappe GE, Ennis IL, Morgan PG, Alvarez BV, Casey JR, Dulce RA, Pérez NG & Hurtado MC. (2003). Influence of $Na^{+}$-Independent Cl--$HCO_3^{-}$ Exchange on the Slow Force Response to Myocardial Stretch. *Circulation research* **93,** 1082-1088.

Cingolani HE, Ennis IL, Aiello EA & Perez NG. (2011). Role of autocrine/paracrine mechanisms in response to myocardial strain. *Pflugers Archiv : European journal of physiology* **462,** 29-38.

Cingolani HE, Perez NG, Cingolani OH & Ennis IL. (2013). The Anrep effect: 100 years later. *American journal of physiology Heart and circulatory physiology* **304,** H175-182.

Cooper DM, Mons N & Karpen JW. (1995). Adenylate cyclases and the interaction between calcium and cAMP signaling. *Nature* **374,** 421-424.

Corson MA, James NL, Latta SE, Nerem RM, Berk BC & Harrison DG. (1996). Phosphorylation of endothelial nitric oxide synthase in response to fluid shear stress. *Circulation research* **79,** 984-991.

Crespo LM, Grantham CJ & Cannell MB. (1990). Kinetics, stoichiometry and role of the Na-Ca exchange mechanism in isolated cardiac myocytes. *Nature* **345,** 618-621.

Cullinan WE, Herman JP, Battaglia DF, Akil H & Watson SJ. (1995). Pattern and time course of immediate early gene expression in rat brain following acute stress. *Neuroscience* **64,** 477-505.

Damron DS, Van Wagoner DR, Moravec CS & Bond M. (1993). Arachidonic acid and endothelin potentiate $Ca^{2}$+ transients in rat cardiac myocytes via inhibition of distinct $K^{+}$ channels. *The Journal of biological chemistry* **268,** 27335-27344.

Davidson SM. (2010). Endothelial mitochondria and heart disease. *Cardiovascular research* **88,** 58-66.

Davies PF. (1995). Flow-mediated endothelial mechanotransduction. *Physiological reviews* **75,** 519-560.

Dawood MY & Khan-Dawood FS. (2007). Differential suppression of menstrual fluid prostaglandin F2a, prostaglandin E2, 6-keto prostaglandin F1a and thromboxane B2 by suprofen in women with primary dysmenorrhea. *Prostaglandins & other lipid mediators* **83,** 146-153.

De Giusti VC, Garciarena CD & Aiello EA. (2009). Role of reactive oxygen species (ROS) in angiotensin II-induced stimulation of the cardiac $Na^+/HCO_3^-$ cotransport. *Journal of molecular and cellular cardiology* **47,** 716-722.

Despa S, Brette F, Orchard CH & Bers DM. (2003). Na/Ca Exchange and Na/K-ATPase Function Are Equally Concentrated in Transverse Tubules of Rat Ventricular Myocytes. *Biophysical Journal* **85,** 3388-3396.

Dettbarn C & Palade P. (1993). Arachidonic acid-induced $Ca^{2+}$ release from isolated sarcoplasmic reticulum. *Biochemical pharmacology* **45,** 1301-1309.

Dey I, Lejeune M & Chadee K. (2006). Prostaglandin E2 receptor distribution and function in the gastrointestinal tract. *British journal of pharmacology* **149,** 611-623.

Di Virgilio F, Fasolato C & Steinberg TH. (1988). Inhibitors of membrane transport system for organic anions block fura-2 excretion from PC12 and N2A cells. *The Biochemical journal* **256,** 959-963.

Diaz ME, Trafford AW, O'Neill SC & Eisner DA. (1997). Measurement of sarcoplasmic reticulum $Ca^{2+}$ content and sarcolemmal $Ca^{2+}$ fluxes in isolated rat ventricular myocytes during spontaneous $Ca^{2+}$ release. *Journal of Physiology* **501,** 3-16.

Dimmeler S, Fleming I, Fisslthaler B, Hermann C, Busse R & Zeiher AM. (1999). Activation of nitric oxide synthase in endothelial cells by Akt-dependent phosphorylation. *Nature* **399,** 601-605.

Ebashi S, Ebashi F & Kodama A. (1967). Troponin as the $Ca^{2+}$-receptive Protein in the Contractile System. *Journal of Biochemistry* **62,** 137-138.

Eisner DA, Diaz ME, Li Y, O'Neill SC & Trafford AW. (2005). Stability and instability of regulation of intracellular calcium. *Experimental Physiology* **90,** 3-12.

Endo M. (1977). Calcium release from the sarcoplasmic reticulum. *Physiological reviews* **57,** 71-108.

Endoh M. (2004). Force-frequency relationship in intact mammalian ventricular myocardium: physiological and pathophysiological relevance. *European journal of pharmacology* **500,** 73-86.

Ervasti JM. (2003). Costameres: the Achilles' Heel of Herculean Muscle. *Journal of Biological Chemistry* **278,** 13591-13594.

Fabiato A. (1983). Calcium-induced release of calcium from the cardiac sarcoplasmic reticulum. *The American journal of physiology* **245,** C1-14.

Fanchaouy M, Polakova E, Jung C, Ogrodnik J, Shirokova N & Niggli E. (2009). Pathways of abnormal stress-induced $Ca^{2+}$ influx into dystrophic mdx cardiomyocytes. *Cell Calcium* **46,** 114-121.

Farman G, Tachampa K, Mateja R, Cazorla O, Lacampagne A & Tombe P. (2008). Blebbistatin: use as inhibitor of muscle contraction. *Pflugers Archiv (European Journal of Physiology)* **455,** 995-1005.

Fawcett DW & McNutt NS. (1969). The ultrastructure of the cat myocardium. I. Ventricular papillary muscle. *J Cell Biol* **42,** 1-45.

Feolde E, Vigne P & Frelin C. (1993). Angiotensin II receptor subtypes and biological responses in the rat heart. *Journal of molecular and cellular cardiology* **25,** 1359-1367.

Fishman AP. (1982). Endothelium: a distributed organ of diverse capabilities. *Annals of the New York Academy of Sciences* **401,** 1-8.

Frangos JA, Eskin SG, McIntire LV & Ives CL. (1985). Flow effects on prostacyclin production by cultured human endothelial cells. *Science* **227,** 1477-1479.

Frank KF, Balck B, Erdmann E & Schwinger RH. (2003). Sarcoplasmic reticulum $Ca^{2+}$-ATPase modulates cardiac contraction and relaxation. *Cardiovascular research* **57,** 20-27.

Franzini-Armstrong C, Protasi F & Ramesh V. (1998). Comparative Ultrastructure of $Ca^{2+}$ Release Units in Skeletal and Cardiac Muscle. *Annals of the New York Academy of Sciences* **853,** 20-30.

Garcia-Cardena G, Fan R, Shah V, Sorrentino R, Cirino G, Papapetropoulos A & Sessa WC. (1998). Dynamic activation of endothelial nitric oxide synthase by Hsp90. *Nature* **392,** 821-824.

Gerritsen ME. (1987). Eicosanoid production by the coronary microvascular endothelium. *Federation proceedings* **46,** 47-53.

Gibbs CL, Mommaerts WF & Ricchiuti NV. (1967). Energetics of cardiac contractions. *J Physiol* **191,** 25-46.

Gordon AM, Homsher E & Regnier M. (2000). Regulation of Contraction in Striated Muscle. *Physiological reviews* **80,** 853-924.

Greenbaum RA, Ho SY, Gibson DG, Becker AE & Anderson RH. (1981). Left ventricular fibre architecture in man. *British heart journal* **45,** 248-263.

Guia A, Stern MD, Lakatta EG & Josephson IR. (2001). Ion Concentration-Dependence of Rat Cardiac Unitary L-Type Calcium Channel Conductance. *Biophysical Journal* **80,** 2742-2750.

Hanley PJ & Loiselle DS. (1998). Mechanisms of force inhibition by halothane and isoflurane in intact rat cardiac muscle. *Journal of Physiology* **506,** 231-244.

Hansen DE, Stacy GP, Taylor LK, Jobe RL, Wang Z, Denton PK & Alexander J. (1995). Calcium- and sodium-dependent modulation of stretch-induced arrhythmias in isolated canine ventricles. *American Journal of Physiology - Heart and Circulatory Physiology* **268,** H1803-H1813.

Hanson J & Huxley HE. (1953). Structural basis of the cross-striations in muscle. *Nature* **172,** 530-532.

Hanson J & Lowy J. (1963). The structure of F-actin and of actin filaments isolated from muscle. *Journal of Molecular Biology* **6,** 46-IN45.

Hara S, Arai M, Tomaru K, Doi H, Koitabashi N, Iso T, Watanabe A, Tanaka T, Maeno T, Suga T, Yokoyama T & Kurabayashi M. (2008). Prostaglandin F2alpha Inhibits SERCA2 Gene Transcription Through an Induction of Egr-1 in Cultured Neonatal Rat Cardiac Myocytes. *International heart journal* **49,** 329-342.

Harteneck C & Gollasch M. (2011). Pharmacological modulation of diacylglycerol-sensitive TRPC3/6/7 channels. *Current pharmaceutical biotechnology* **12,** 35-41.

Haversath M, Catelas I, Li X, Tassemeier T & Jager M. (2012). PGE(2) and BMP-2 in bone and cartilage metabolism: 2 intertwining pathways. *Canadian journal of physiology and pharmacology* **90,** 1434-1445.

Hilal-Dandan R & Brunton LL. (1995). Transmembrane mechanochemical coupling in cardiac myocytes: novel activation of Gi by hyposmotic swelling. *American Journal of Physiology* **269,** H798-H804.

Hishikawa K, Nakaki T, Marumo T, Suzuki H, Kato R & Saruta T. (1995). Pressure enhances endothelin-1 release from cultured human endothelial cells. *Hypertension* **25,** 449-452.

Holtzer A & Lowey S. (1959). The Molecular Weight, Size and Shape of the Myosin Molecule. *Journal of the American Chemical Society* **81,** 1370-1377.

Hongo K, White E, Guennec JY & Orchard CH. (1996). Changes in $[Ca^{2+}]_i$, $[Na^{+}]_i$ and $Ca^{2+}$ current in isolated rat ventricular myocytes following an increase in cell length. *Journal of Physiology* **491,** 609-619.

Hove-Madsen L & Bers DM. (1993). Sarcoplasmic reticulum $Ca^{2+}$ uptake and thapsigargin sensitivity in permeabilized rabbit and rat ventricular myocytes. *Circulation research* **73,** 820-828.

Huang JM, Xian H & Bacaner M. (1992). Long-chain fatty acids activate calcium channels in ventricular myocytes. *Proceedings of the National Academy of Sciences of the United States of America* **89,** 6452-6456.

Huxley A & Niedergerke R. (1954). Structural changes in muscle during contraction; interference microscopy of living muscle fibres. *Nature* **173,** 971-973.

Huxley H & Hanson J. (1954). Changes in the Cross-Striations of Muscle during Contraction and Stretch and their Structural Interpretation. *Nature* **173,** 973-976.

Iribe G, Ward CW, Camelliti P, Bollensdorff C, Mason F, Burton RA, Garny A, Morphew MK, Hoenger A, Lederer WJ & Kohl P. (2009). Axial Stretch of Rat Single Ventricular Cardiomyocytes Causes an Acute and Transient Increase in $Ca^{2+}$ Spark Rate. *Circulation research* **104,** 787-795.

Iwamoto T, Inoue Y, Ito K, Sakaue T, Kita S & Katsuragi T. (2004). The exchanger inhibitory peptide region-dependent inhibition of $Na^{+}/Ca^{2+}$ exchange by SN-6 [2-[4-(4-nitrobenzyloxy)benzyl]thiazolidine-4-carboxylic acid ethyl ester], a novel benzyloxyphenyl derivative. *Molecular pharmacology* **66,** 45-55.

Jiang Q-s, Huang X-n, Yang G-z, Jiang X-y & Zhou Q-x. (2007). Inhibitory effect of ginsenoside Rb1 on calcineurin signal pathway in cardiomyocyte hypertrophy induced by prostaglandin F2[alpha]. *Acta Pharmacol Sin* **28,** 1149-1154.

Jorgensen AO, Shen AC, Arnold W, McPherson PS & Campbell KP. (1993). The $Ca^{2+}$-release channel/ryanodine receptor is localized in junctional and corbular sarcoplasmic reticulum in cardiac muscle. *Journal of Cell Biology* **120,** 969-980.

Kabbara AA & Stephenson DG. (1997). Effects of 2,5-di-tert-butylhydroquinone on rat cardiac muscle contractility. *American Journal of Physiology - Heart and Circulatory Physiology* **272,** H1001-H1010.

Kagiyama S, Eguchi S, Frank GD, Inagami T, Zhang YC & Phillips MI. (2002). Angiotensin II-induced cardiac hypertrophy and hypertension are attenuated by epidermal growth factor receptor antisense. *Circulation* **106,** 909-912.

Kamkin A, Kiseleva I & Isenberg G. (2003). Ion selectivity of stretch-activated cation currents in mouse ventricular myocytes. *Pflugers Archiv (European Journal of Physiology)* **446,** 220-231.

Karmazyn M. (1989). Synthesis and relevance of cardiac eicosanoids with particular emphasis on ischemia and reperfusion. *Canadian journal of physiology and pharmacology* **67,** 912-921.

Kassiri Z, Myers R, Kaprielian R, Banijamali HS & Backx PH. (2000). Rate-dependent changes of twitch force duration in rat cardiac trabeculae: a property of the contractile system. *Journal of Physiology* **524,** 221-231.

Katz AM. (1966). Purification and Properties of a Tropomyosin-containing Protein Fraction That Sensitizes Reconstituted Actomyosin to Calcium-binding Agents. *Journal of Biological Chemistry* **241,** 1522-1529.

Katz AM. (2001). Physiology of the heart. **XVI,** 718.

Kentish JC. (1999). A Role for the Sarcolemmal $Na^+/H^+$ Exchanger in the Slow Force Response to Myocardial Stretch. *Circulation research* **85,** 658-660.

Kentish JC & Wrzosek A. (1998). Changes in force and cytosolic $Ca^{2+}$ concentration after length changes in isolated rat ventricular trabeculae. *Journal of Physiology* **506,** 431-444.

Khandoudi N, Albadine J, Robert P, Krief S, Berrebi-Bertrand I, Martin X, Bevensee MO, Boron WF & Bril A. (2001). Inhibition of the cardiac electrogenic sodium bicarbonate cotransporter reduces ischemic injury. *Cardiovascular research* **52,** 387-396.

Kim D & Smith TW. (1988). Cellular mechanisms underlying calcium-proton interactions in cultured chick ventricular cells. *J Physiol* **398,** 391-410.

Kimura J, Noma A & Irisawa H. (1986). Na-Ca exchange current in mammalian heart cells. *Nature* **319,** 596-597.

Kimura S, Zhang GX, Nishiyama A, Shokoji T, Yao L, Fan YY, Rahman M & Abe Y. (2005). Mitochondrial-derived reactive oxygen species and vascular MAP kinases. *Hypertension* **45,** 438-444.

King AJ & Taylor DE. (1968). The inotropic action of paired pulse stimulation in the normal and failing heart: an experimental study. *Cardiovascular research* **2,** 122-129.

Kockskamper J, Khafaga M, Grimm M, Elgner A, Walther S, Kockskamper A, von Lewinski D, Post H, Grossmann M, Dorge H, Gottlieb PA, Sachs F, Eschenhagen T, Schondube FA & Pieske B. (2008a). Angiotensin II and myosin light-chain phosphorylation contribute to the stretch-induced slow force response in human atrial myocardium. *Cardiovascular research* **79,** 642-651.

Kockskamper J, von Lewinski D, Khafaga M, Elgner A, Grimm M, Eschenhagen T, Gottlieb PA, Sachs F & Pieske B. (2008b). The slow force response to stretch in atrial and ventricular myocardium from human heart: functional relevance and subcellular mechanisms. *Progress in biophysics and molecular biology* **97,** 250-267.

Kockskamper J, Zima AV, Roderick HL, Pieske B, Blatter LA & Bootman MD. (2008c). Emerging roles of inositol 1,4,5-trisphosphate signaling in cardiac myocytes. *Journal of molecular and cellular cardiology* **45,** 128-147.

Koss KL & Kranias EG. (1996). Phospholamban: a prominent regulator of myocardial contractility. *Circulation research* **79,** 1059-1063.

Kresh J & Chopra A. (2011). Intercellular and extracellular mechanotransduction in cardiac myocytes. *Pflugers Archiv (European Journal of Physiology)***,** 1-13.

Lai J, Jin H, Yang R, Winer J, Li W, Yen R, King KL, Zeigler F, Ko A, Cheng J, Bunting S & Paoni NF. (1996). Prostaglandin F2 alpha induces cardiac myocyte hypertrophy in vitro and cardiac growth in vivo. *American Journal of Physiology - Heart and Circulatory Physiology* **271,** H2197-H2208.

Laver DR & Honen BN. (2008). Luminal $Mg^{2+}$, A Key Factor Controlling RYR2-mediated $Ca^{2+}$ Release: Cytoplasmic and Luminal Regulation Modeled in a Tetrameric Channel. *Journal of General Physiology* **132,** 429-446.

Layland J & Kentish JC. (1999). Positive force- and $[Ca^{2+}]_i$-frequency relationships in rat ventricular trabeculae at physiological frequencies. *American Journal of Physiology - Heart and Circulatory Physiology* **276,** H9-H18.

Lee E, Peng J, Radke M, Gotthardt M & Granzier HL. (2010). Calcium sensitivity and the Frank-Starling mechanism of the heart are increased in titin N2B region-deficient mice. *Journal of molecular and cellular cardiology* **49,** 449-458.

LeGrice IJ, Smaill BH, Chai LZ, Edgar SG, Gavin JB & Hunter PJ. (1995). Laminar structure of the heart: ventricular myocyte arrangement and connective tissue architecture in the dog. *American journal of physiology* **269,** H571-582.

Levick SP, Loch DC, Taylor SM & Janicki JS. (2007). Arachidonic Acid Metabolism as a Potential Mediator of Cardiac Fibrosis Associated with Inflammation. *Journal of Immunology* **178,** 641-646.

Levin KR & Page E. (1980). Quantitative studies on plasmalemmal folds and caveolae of rabbit ventricular myocardial cells. *Circulation research* **46,** 244-255.

Lewinski D, Stumme B, Fialka F, Luers C & Pieske B. (2004). Functional Relevance of the Stretch-Dependent Slow Force Response in Failing Human Myocardium. *Circulation research* **94,** 1392-1398.

Lewinski D, Stumme B, Maier LS, Luers C, Bers DM & Pieske B. (2003). Stretch-dependent slow force response in isolated rabbit myocardium is $Na^+$ dependent. *Cardiovascular research* **57,** 1052-1061.

Li Z, Matsuoka S, Hryshko LV, Nicoll DA, Bersohn MM, Burke EP, Lifton RP & Philipson KD. (1994). Cloning of the NCX2 isoform of the plasma membrane $Na^+$-$Ca^{2+}$ exchanger. *Journal of Biological Chemistry* **269,** 17434-17439.

Linssen MC, Engels W, Lemmens PJ, Heijnen VV, Van Bilsen M, Reneman RS & van der Vusse GJ. (1993). Production of arachidonic acid metabolites in adult rat cardiac myocytes, endothelial cells, and fibroblast-like cells. *The American journal of physiology* **264,** H973-982.

Luers C, Fialka F, Elgner A, Zhu D, Kockskämper J, von Lewinski D & Pieske B. (2005). Stretch-dependent modulation of $[Na^+]_i$, $[Ca^{2+}]_i$, and $pH_i$ in rabbit myocardium–a mechanism for the slow force response. *Cardiovascular research* **68,** 454-463.

Luo CH & Rudy Y. (1994). A dynamic model of the cardiac ventricular action potential. I. Simulations of ionic currents and concentration changes. *Circulation research* **74,** 1071-1096.

Mallat Z, Philip I, Lebret M, Chatel D, Maclouf J & Tedgui A. (1998). Elevated Levels of 8-iso-Prostaglandin F2α in Pericardial Fluid of Patients With Heart Failure : A Potential Role for In Vivo Oxidant Stress in Ventricular Dilatation and Progression to Heart Failure. *Circulation* **97,** 1536-1539.

Maroto R, Raso A, Wood TG, Kurosky A, Martinac B & Hamill OP. (2005). TRPC1 forms the stretch-activated cation channels in vertebrate cells. *Nature Cell Biology* **7**.

Mentz P, Pawelski KE, Giessler C, Mest HJ, Mannes F & Rotzoll S. (1988). Myocardial biosynthesis of prostacyclin and the influence of cardiac loading and drugs. *Biomedica biochimica acta* **47,** S244-247.

Mika D, Leroy J, Vandecasteele G & Fischmeister R. (2012). PDEs create local domains of cAMP signaling. *Journal of molecular and cellular cardiology* **52,** 323-329.

Momcilovic D, Archbald LF, Walters A, Tran T, Kelbert D, Risco C & Thatcher WW. (1998). Reproductive performance of lactating dairy cows treated with gonadotrophin-releasing hormone (GnRH) and/or prostaglandin F2a (PGF2a) for synchronization of estrus and ovulation. *Theriogenology* **50,** 1131-1139.

Monasky MM, Biesiadecki BJ & Janssen PM. (2010). Increased phosphorylation of tropomyosin, troponin I, and myosin light chain-2 after stretch in rabbit ventricular myocardium under physiological conditions. *Journal of molecular and cellular cardiology* **48,** 1023-1028.

Nag AC. (1980). Study of non-muscle cells of the adult mammalian heart: a fine structural analysis and distribution. *Cytobios* **28,** 41-61.

Needleman P, Marshall GR & Sobel BE. (1975). Hormone interactions in the isolated rabbit heart. Synthesis and coronary vasomotor effects of prostaglandins, angiotensin, and bradykinin. *Circulation research* **37,** 802-808.

Nicoll DA, Longoni S & Philipson KD. (1990). Molecular cloning and functional expression of the cardiac sarcolemmal $Na^{+}$-$Ca^{2+}$ exchanger. *Science* **250,** 562-565.

Nicoll DA, Quednau BD, Qui Z, Xia Y, Lusis AJ & Philipson KD. (1996). Cloning of a Third Mammalian $Na^{+}$-$Ca^{2+}$ Exchanger, NCX3. *Journal of Biological Chemistry* **271,** 24914-24921.

Okahara T, Abe Y, Imanishi M, Miura K & Yamamoto K. (1980). Effects of calcium ionophore, A23187, on prostaglandin E2 and renin release in dogs. *Japanese circulation journal* **44,** 394-399.

Orchard C & Brette F. (2008). t-tubules and sarcoplasmic reticulum function in cardiac ventricular myocytes. *Cardiovascular research* **77,** 237-244.

Orchard CH & Kentish JC. (1990). Effects of changes of pH on the contractile function of cardiac muscle. *American Journal of Physiology* **258,** C967-C981.

Orchard CH, Pásek M & Brette F. (2009). The role of mammalian cardiac t-tubules in excitation-contraction coupling: experimental and computational approaches. *Experimental Physiology* **94,** 509-519.

Otani H, Otani H & Das DK. (1988). Positive inotropic effect and phosphoinositide breakdown mediated by arachidonic acid and prostaglandin F2 alpha. *Journal of Pharmacology and Experimental Therapeutics* **244,** 844-851.

Page E, McCallister LP & Power B. (1971). Sterological measurements of cardiac ultrastructures implicated in excitation-contraction coupling. *Proceedings of the National Academy of Sciences of the United States of America* **68,** 1465-1466.

Page E & Surdyk-Droske M. (1979). Distribution, surface density, and membrane area of diadic junctional contacts between plasma membrane and terminal cisterns in mammalian ventricle. *Circulation research* **45,** 260-267.

Panzenbeck MJ, Hintze TH & Kaley G. (1988). 6-Keto-prostaglandin E1 is a potent coronary vasodilator and stimulates a vagal reflex in dogs. *Journal of Pharmacology and Experimental Therapeutics* **244,** 814-819.

Parker KK & Ingber DE. (2007). Extracellular matrix, mechanotransduction and structural hierarchies in heart tissue engineering. *Philosophical Transactions of the Royal Society of London Series B, Biological Sciences* **362,** 1267-1279.

Parmley WW & Chuck L. (1973). Length-dependent changes in myocardial contractile state. *American Journal of Physiology* **224,** 1195-1199.

Pérez NG, Hurtado MC & Cingolani HE. (2001). Reverse Mode of the $Na^{+}$-$Ca^{2+}$ Exchange After Myocardial Stretch : Underlying Mechanism of the Slow Force Response. *Circulation research* **88,** 376-382.

Perez NG, Nolly MB, Roldan MC, Villa-Abrille MC, Cingolani E, Portiansky EL, Alvarez BV, Ennis IL & Cingolani HE. (2011). Silencing of NHE-1 blunts the slow force response to myocardial stretch. *Journal of Applied Physiology* **111,** 874-880.

Pérez NG, Villa-Abrille MC, Aiello EA, Dulce RA, Cingolani HE & Hurtado MC. (2003). A low dose of angiotensin II increases inotropism through activation of reverse $Na^{+}/Ca^{2+}$ exchange by endothelin release. *Cardiovascular research* **60,** 589-597.

Petroff MG, Kim SH, Pepe S, Dessy C, Marban E, Balligand J & Sollott SJ. (2001). Endogenous nitric oxide mechanisms mediate the stretch dependence of $Ca^{2+}$ release in cardiomyocytes. *Nature Cell Biology* **3,** 867-873.

Pitts BJ. (1979). Stoichiometry of sodium-calcium exchange in cardiac sarcolemmal vesicles. Coupling to the sodium pump. *The Journal of biological chemistry* **254,** 6232-6235.

Prosser BL, Khairallah RJ, Ziman AP, Ward CW & Lederer WJ. (2013). X-ROS signaling in the heart and skeletal muscle: Stretch-dependent local ROS regulates $[Ca^{2+}]_i$. *Journal of molecular and cellular cardiology* **58,** 172-181.

Qiu Y & Quilley J. (1999). Vascular effects of arachidonic acid in the rat perfused heart: role of the endothelium, cyclooxygenase, cytochrome P450, and $K^{+}$ channels. *Journal of Lipid Research* **40,** 2177-2184.

Quadt JF, Voss R & ten Hoor F. (1982). Prostacyclin production of the isolated pulsatingly perfused rat aorta. *Journal of pharmacological methods* **7,** 263-270.

Raman S, Kelley MA & Janssen PM. (2006). Effect of muscle dimensions on trabecular contractile performance under physiological conditions. *Pflugers Archiv : European journal of physiology* **451,** 625-630.

Rao TS, Seth SD, Manchanda SC & Nayar U. (1989). Contrastive effects of prostaglandin F2 alpha on normal cardiac rhythm and ouabain-induced cardiac arrhythmias in cats: possible neural basis. *Archives internationales de pharmacodynamie et de therapie* **302,** 128-144.

Rink TJ, Tsien RY & Pozzan T. (1982). Cytoplasmic pH and free $Mg^{2+}$ in lymphocytes. *Journal of Cell Biology* **95,** 189-196.

Rothstein EC, Byron KL, Reed RE, Fliegel L & Lucchesi PA. (2002). $H_2O_2^-$induced $Ca^{2+}$ overload in NRVM involves ERK1/2 MAP kinases: role for an NHE-1-dependent pathway. *American Journal of Physiology - Heart and Circulatory Physiology* **283,** H598-H605.

Rousseau E & Meissner G. (1989). Single cardiac sarcoplasmic reticulum $Ca^{2+}$-release channel: activation by caffeine. *American Journal of Physiology - Heart and Circulatory Physiology* **256,** H328-H333.

Ruoslahti E. (1991). Integrins. *Journal of Clinical Investigation* **87,** 1-5.

Russo LA, Rannels R, Laslow KS & Rannels DE. (1989). Stretch-related changes in lung cAMP after partial pneumonectomy. *American Journal of Physiology* **257,** E261-E268.

Ruwhof C & Laarse A. (2000). Mechanical stress-induced cardiac hypertrophy: mechanisms and signal transduction pathways. *Cardiovascular research* **47,** 23-37.

Sadoshima J & Izumo S. (1993). Molecular characterization of angiotensin II--induced hypertrophy of cardiac myocytes and hyperplasia of cardiac fibroblasts. Critical role of the AT1 receptor subtype. *Circulation research* **73,** 413-423.

Sadoshima J, Xu Y, Slayter HS & Izumo S. (1993). Autocrine release of angiotensin II mediates stretch-induced hypertrophy of cardiac myocytes in vitro. *Cell* **75,** 977-984.

Saito M, Tanabe Y, Kudo I & Nakayama K. (2003). Endothelium-derived prostaglandin H2 evokes the stretch-induced contraction of rabbit pulmonary artery. *European journal of pharmacology* **467,** 151-161.

Samarel AM. (2005). Costameres, focal adhesions, and cardiomyocyte mechanotransduction. *American Journal of Physiology - Heart and Circulatory Physiology* **289,** H2291-H2301.

Sandow A. (1952). Excitation-Contraction Coupling in Muscular Response. *Yale Journal of Biology and Medicine* **25,** 176-201.

Scheibe RJ, Gros G, Parkkila S, Waheed A, Grubb JH, Shah GN, Sly WS & Wetzel P. (2006). Expression of membrane-bound carbonic anhydrases IV, IX, and XIV in the mouse heart. *The journal of histochemistry and cytochemistry : official journal of the Histochemistry Society* **54,** 1379-1391.

Schiaffino S & Reggiani C. (1996). Molecular diversity of myofibrillar proteins: gene regulation and functional significance. *Physiological reviews* **76,** 371-423.

Schouten VJ & Keurs HE. (1986). The force-frequency relationship in rat myocardium. The influence of muscle dimensions. *Pflugers Archiv : European journal of physiology* **407,** 14-17.

Shannon TR, Ginsburg KS & Bers DM. (2000). Potentiation of Fractional Sarcoplasmic Reticulum Calcium Release by Total and Free Intra-Sarcoplasmic Reticulum Calcium Concentration. *Biophysical Journal* **78,** 334-343.

Shen X, Cannell MB & Ward M-L. (2013). Effect of SR load and pH regulatory mechanisms on stretch-dependent $Ca^{2+}$ entry during the slow force response. *Journal of molecular and cellular cardiology*.

Sitsapesan R & Williams AJ. (1990). Mechanisms of caffeine activation of single calcium-release channels of sheep cardiac sarcoplasmic reticulum. *Journal of Physiology* **423,** 425-439.

Skouteris GG & Kaser MR. (1991). Prostaglandins E2 and F2a mediate the increase in c-myc expression induced by EGF in primary rat hepatocyte cultures. *Biochemical and Biophysical Research Communications* **178,** 1240-1246.

Soeller C & Cannell MB. (1999). Examination of the Transverse Tubular System in Living Cardiac Rat Myocytes by 2-Photon Microscopy and Digital Image Processing Techniques. *Circulation research* **84,** 266-275.

Sommer JR & Johnson EA. (1970). Comparative ultrastructure of cardiac cell membrane specializations. A review. *American Journal of Cardiology* **25,** 184-194.

Spassova MA, Hewavitharana T, Xu W, Soboloff J & Gill DL. (2006). A common mechanism underlies the stretch activation and receptor activation of TRPC6 channels. *Proceedings of the National Academy of Sciences of the United States of America* **103,** 16586-16591.

Spencer CI & Berlin JR. (1995). Control of sarcoplasmic reticulum calcium release during calcium loading in isolated rat ventricular myocytes. *Journal of Physiology* **488,** 267-279.

Stoyanovsky D, Murphy T, Anno PR, Kim YM & Salama G. (1997). Nitric oxide activates skeletal and cardiac ryanodine receptors. *Cell Calcium* **21,** 19-29.

Suzuki J, Ogawa M, Watanabe R, Takayama K, Hirata Y, Nagai R & Isobe M. (2011). Roles of prostaglandin E2 in cardiovascular diseases. *International heart journal* **52,** 266-269.

Swift F, Strømme TA, Amundsen B, Sejersted OM & Sjaastad I. (2006). Slow diffusion of $K^+$ in the T tubules of rat cardiomyocytes. *Journal of Applied Physiology* **101,** 1170-1176.

Tada M, Yabuki M & Toyofuku T. (1998). Molecular Regulation of Phospholamban Function and Gene Expressiona. *Annals of the New York Academy of Sciences* **853,** 116-129.

Takahashi A, Camacho P, Lechleiter JD & Herman B. (1999). Measurement of intracellular calcium. *Physiological reviews* **79,** 1089-1125.

Tanaka H, Nishimaru K, Kobayashi M, Matsuda T, Tanaka Y & Shigenobu K. (2001). Acetylcholine-induced positive inotropy mediated by prostaglandin released from endocardial endothelium in mouse left atrium. *Naunyn-Schmiedeberg's archives of pharmacology* **363,** 577-582.

Tanaka H, Nishimaru K, Makuta R, Hirayama W, Kawamura T, Matsuda T, Tanaka Y, Kawanishi T & Shigenobu K. (2003). Possible involvement of prostaglandins F(2alpha) and D(2) in acetylcholine-induced positive inotropy in isolated mouse left atria. *Pharmacology* **67,** 157-162.

Tang EHC & Vanhoutte PM. (2009). Prostanoids and reactive oxygen species: Team players in endothelium-dependent contractions. *Pharmacology & Therapeutics* **122,** 140-149.

Taylor CJ, Nicola PA, Wang S, Barrand MA & Hladky SB. (2006). Transporters involved in regulation of intracellular pH in primary cultured rat brain endothelial cells. *J Physiol* **576,** 769-785.

Thomas JA, Buchsbaum RN, Zimniak A & Racker E. (1979). Intracellular pH measurements in Ehrlich ascites tumor cells utilizing spectroscopic probes generated in situ. *Biochemistry* **18,** 2210-2218.

Todaka K, Ogino K, Gu AG & Burkhoff D. (1998). Effect of ventricular stretch on contractile strength, calcium transient, and cAMP in intact canine hearts. *American Journal of Physiology* **43,** H990-H1000.

Torres-Narvaez JC, Mondragon Ldel V, Varela Lopez E, Perez-Torres I, Diaz Juarez JA, Suarez J & Hernandez GP. (2012). Role of the transient receptor potential vanilloid type 1 receptor and stretch-activated ion channels in nitric oxide release from endothelial cells of the aorta and heart in rats. *Experimental and clinical cardiology* **17,** 89-94.

Trafford AW, Díaz ME & Eisner DA. (2001). Coordinated control of cell $Ca^{2+}$ loading and triggered release from the sarcoplasmic reticulum underlies the rapid inotropic response to increased L-type $Ca^{2+}$ current. *Circulation research* **88,** 195-201.

Tucci PJ, Bregagnollo EA, Spadaro J, Cicogna AC & Ribeiro MC. (1984). Length dependence of activation studied in the isovolumic blood-perfused dog heart. *Circulation research* **55,** 59-66.

Vaughan-Jones RD, Spitzer KW & Swietach P. (2009). Intracellular pH regulation in heart. *Journal of molecular and cellular cardiology* **46,** 318-331.

Vaughan-Jones RD, Villafuerte FC, Swietach P, Yamamoto T, Rossini A & Spitzer KW. (2006). pH-Regulated $Na^+$ Influx into the Mammalian Ventricular Myocyte: The Relative Role of $Na^+$-$H^+$ Exchange and $Na^+$-$HCO_3^-$ Co-Transport. *Journal of Cardiovascular Electrophysiology* **17,** S134-S140.

Villa-Abrille MC, Caldiz CI, Ennis IL, Nolly MB, Casarini MJ, Cingolani GE, Cingolani HE & Perez NG. (2010). The Anrep effect requires transactivation of the epidermal growth factor receptor. *Journal of Physiology* **588,** 1579-1590.

Virgilio F, Steinberg TH & Silverstein SC. (1989). Organic-anion transport inhibitors to facilitate measurement of cytosolic free $Ca^{2+}$ with fura-2. *Methods in Cell Biology* **31,** 453-462.

Wallert MA & Frohlich O. (1989). $Na^+$-$H^+$ exchange in isolated myocytes from adult rat heart. *The American journal of physiology* **257,** C207-213.

Ward M, Pope AJ, Loiselle DS & Cannell MB. (2003). Reduced contraction strength with increased intracellular [$Ca^{2+}$] in left ventricular trabeculae from failing rat hearts. *Journal of Physiology* **546,** 537-550.

Ward M, Williams IA, Chu Y, Cooper PJ, Ju Y & Allen DG. (2008). Stretch-activated channels in the heart: Contributions to length-dependence and to cardiomyopathy. *Progress in biophysics and molecular biology* **97,** 232-249.

Ward ML, Crossman DJ, Loiselle DS & Cannell MB. (2010). Non-steady-state calcium handling in failing hearts from the spontaneously hypertensive rat. *Pflugers Archiv : European journal of physiology* **460,** 991-1001.

Watson PA. (1990). Direct stimulation of adenylate cyclase by mechanical forces in S49 mouse lymphoma cells during hyposmotic swelling. *Journal of Biological Chemistry* **265,** 6569-6575.

White E. (2004). Activation of $Na^+$-$H^+$ exchange and stretch-activated channels underlies the slow inotropic response to stretch in myocytes and muscle from the rat heart. *Journal of Physiology* **559,** 205-214.

White E, Boyett MR & Orchard CH. (1995). The effects of mechanical loading and changes of length on single guinea-pig ventricular myocytes. *Journal of Physiology* **482,** 93-107.

WHO. (2011). Mortality and Global Health Estimates. World Health Organisation.

Wymann MP & Schneiter R. (2008). Lipid signalling in disease. *Nat Rev Mol Cell Biol* **9,** 162-176.

Yamamura K, Steenbergen C & Murphy E. (2005). Protein kinase C and preconditioning: role of the sarcoplasmic reticulum. *American journal of physiology Heart and circulatory physiology* **289,** H2484-2490.

Yamazaki T, Komuro I, Kudoh S, Zou Y, Shiojima I, Hiroi Y, Mizuno T, Maemura K, Kurihara H, R A, Takano H & Yazaki Y. (1996). Endothelin-1 is involved in mechanical stress-induced cardiomyocyte hypertrophy. *Journal of Biological Chemistry* **271,** 3221-3228.

Yanagisawa M, Kurihara H, Kimura S, Tomobe Y, Kobayashi M, Mitsui Y, Yazaki Y, Goto K & Masaki T. (1988). A novel potent vasoconstrictor peptide produced by vascular endothelial cells. *Nature* **332,** 411-415.

Yeung EW & Allen DG. (2004). Stretch-activated channels in stretch-induced muscle damage: role in muscular dystrophy. *Clinical and experimental pharmacology & physiology* **31,** 551-556.

Yew SF, Reeves KA & Woodward B. (1998). Effects of prostaglandin F2 alpha on intracellular pH, intracellular calcium, cell shortening and L-type calcium currents in rat myocytes. *Cardiovascular research* **40,** 538-545.

Youm B, Han J, Kim N, Zhang YH, Kim E, Joo H, Hun LC, Joon KS, Cha KA & Earm YE. (2006). Role of stretch-activated channels on the stretch-induced changes of rat atrial myocytes. *Progress in biophysics and molecular biology* **90,** 186-206.

Zamir E, Srinivasan V, Perucchio R & Taber L. (2003). Mechanical Asymmetry in the Embryonic Chick Heart During Looping. *Annals of Biomedical Engineering* **31,** 1327-1336.

Zhai P, Galeotti J, Liu J, Holle E, Yu X, Wagner T & Sadoshima J. (2006). An angiotensin II type 1 receptor mutant lacking epidermal growth factor receptor transactivation does not induce angiotensin II-mediated cardiac hypertrophy. *Circulation research* **99,** 528-536.

Zheng JS, Boluyt MO, O'Neill L, Crow MT & Lakatta EG. (1994). Extracellular ATP induces immediate-early gene expression but not cellular hypertrophy in neonatal cardiac myocytes. *Circulation research* **74,** 1034-1041.